Gain-Distributed Feedback Filters

by

Mohammad Jalal Khan

Submitted to the Department of Electrical Engineering and Computer Science
in partial fulfillment of the requirements for the degree of

Master of Engineering in Electrical Engineering and Computer Science

at the

MASSACHUSETTS INSTITUTE OF TECHNOLOGY

May 1996

Author .....
Department of Electrical Engineering and Computer Science
March 6, 1996

Certified by .....
Hermann A. Haus
Institute Professor
Thesis Supervisor

Accepted by .....
Frederic. R. Morgenthaler
Chairman, Departmental Committee on Graduate Theses

Gain-Distributed Feedback Filters

by

Mohammad Jalal Khan

Submitted to the Department of Electrical Engineering and Computer Science
on March 6, 1996, in partial fulfillment of the
requirements for the degree of
Master of Engineering in Electrical Engineering and
Computer Science

Abstract

Gain Distributed Feedback (GDFB) structures are used to form a novel type of channel dropping filter which possesses several unique and desirable features. GDFB channel dropping filters allow transparent detection of selected channels and provide better suppression of undesired resonances than passive filters. Equivalent circuits of GDFB filters are developed. A general scheme to assemble the equivalent circuits of an arbitrary number of coupled GDFB resonators is devised. This technique is a very powerful tool to analyse and design higher-order filters. Optical gain in semiconductors is reviewed and its relation to the injected current density through the device is discussed. A simple gain grating design is discussed and is used as an example to illustrate the spurious effect of index coupling and net travelling wave gain (or dc gain) on the performance of the device. Techniques to minimize these effects are explored.

Thesis Supervisor: Hermann A. Haus
Title: Institute Professor

Acknowledgments

I am deeply indebted to Prof. Hermann Haus for his years of support and guidance. His unique intuition, uncanny insight and remarkable personality have been a continual source of motivation for me. Without his help and direction this thesis would not have been possible.

I would like to thank Jay Damask who I have enjoyed working with over the past couple of years. Jay has been extremely helpful and encouraging, taking out many hours at length to discuss my project with me. Jay's sound advice, and his keen and penetrating questions have helped to indentify the strengths and weaknesses of my work, giving it an improved shape. I am looking forward to continued collaboration with him in the future.

I would like to thank everyone in the Optics Group with whom I have had the opportunity to interact and learn. Particularly, I would like to mention my office mate Charles Yu, with whom I have had many interesting and "philosophical" conversations. I would like to thank Jerry Chen for teaching me how to use his Beam Propagation Program. Constantine Tziligakis and I have been "co-victims" of some of the more brutal classes at MIT and my discussions with him always proved to be helpful. My special thanks to Cindy Kopf whose latex'ing repertoire was greatly appreciated.

I am specially thankful to my numerous friends for making my life at MIT very enjoyable and memorable. Since a complete list would be a thesis in itself, I appologize for mentioning only a few names. To Asad Naqvi, Asim Khwaja, Farhan Rana, Agha Mirza, Ahmad Shah, and Yassir Elley I owe a truly wonderful time at MIT and many indelible memories. Their support and friendship has been invaluable and will always be treasured by me. Asif Shakeel's spontaneity and sense of humor were always welcomed and I thank him for everything, particulary introducing me to sculling. Samir Nayfeh and Ammar al-Nahwi, deserve special thanks for devising the necessary soccer digressions and for helping to create a "balance" between work and play.

Most of all I am grateful to my family whose unconditional support and endless

prayers have made it possible for me to achieve all that I have. Their love, their sacrifices, and their trust in my abilities, more than my own, has been a constant driving force in my life. My feelings and sense of gratitude for them cannot be encompassed by words and I only hope that I can give them the sort of happiness that they have given to me.

Mohammad Jalal Khan.

Contents

List of Figures

List of Tables

Chapter 1

Introduction

1.1 Motivation

The invention of the laser in 1960 [1] and the development of low-loss fibers in the 70's [2, 3] sparked a flurry of research in the field of optical fiber transmission technology paving the way for viable optical communication systems. As early as 1978, development of the Trans-Atlantic Telephone cable system (TAT-8) based on the SL single-mode fiber-based lightwave system had started [4]. The TAT-8 cable system, connecting the European and North American continents was in service by 1988. Also, during the late 80's several high-speed terrestrial single-mode optical fiber systems operating above 1 Gb/s were developed. These included AT&T's FT series G 1.5 Gb/s, Fujitsu's 1.6 Gb/s transmission system, NEC's 1.12 and 1.6 Gb/s systems and many others [4]. More recently a 10 Gb/s channel is being developed by AT&T, ready to be deployed in New York. At the very high bit-rate end, a project between MIT and Lincoln Laboratories is attempting to provide a 100 Gb/s optical link between the campus and Lincoln Laboratories. The transition to higher and higher data rates is driven by the increased demand for high speed telecommunications. With applications like high-definition TV, videobroadcasting, supercomputers with high resolution graphic terminals, etc. the need for higher data transmission rates has continued to increase. In recent years, research has been focussed on providing low cost solutions for this increased demand using existing fiber systems. Among the techniques being

considered are Time Division Multiplexing (TDM) and Wavelength-Division Multiplexing (WDM). TDM techniques increase the capacity of a communication link by using higher transmission speeds. This technique is, however, limited at the opto-electronic interface by the speed of the digital processing circuitry. Even with GaAs digital IC's, the maximum date rate is probably going to be limited to about 2 Gb/s [1].

1.1.1 Wavelength-Division Multiplexing

An alternative approach to increase the transmission rate at small additional costs involves exploiting the large bandwidths of optical fibers and optical integrated circuits (OICs) [5]. By multiplexing several signals at different wavelengths and transmitting them across the same fiber, the transmission rate can be increased linearly with the number of data channels [6]. This process, called wavelength-division multiplexing (WDM), allows the optimal use of the fiber bandwidth making it possible to upgrade systems without installing new fibers. The key components of a WDM system are a multiplexer, to combine signals at different wavelengths for transmission down the fiber, and a de-multiplexer to resolve the signals at the receiving end. De-multiplexers can primarily be divided into two main classes: full-spectral resolvers and channel-dropping filters (CDFs). In the first class the multiplexed signal is simultaneously resolved into all its different wavelength components. Devices of this type include integrated diffraction gratings which reflect the various wavelength components into different directions [6]. These can then be collected by separate fibers dedicated for specific wavelengths. Channel-dropping filters, on the other hand, allow a single data channel to be filtered out from the multiplexed signal. Among the devices in this class are planar optical waveguide filters [6] and distributed feedback filters [7, 8, 9, 10, 11]

The two classes of de-multiplexers offer their own advantages. Full-spectral resolvers are fast as they simultaneously de-multiplex all the data channels. However, if the signal needs to be transmitted further, the signals have to be multiplexed again. Channel-dropping filters, on the other hand, while sacrificing speed allow a single channel to be detected leaving the other channels unaffected. They can be cascaded

to perform desirable filtering operations. This allows greater freedom to a system designer.

An "ideal" filter is one that allows data on a specific channel to be detected without disturbing the ongoing signal. Moreover, an "ideal" filter should be tunable enabling it to detect the different data channels, with the ability to turn the filter on or off as needed. The first property of such an "ideal" filter requires an active device since it is not possible to transparently detect a channel in passive devices without violating the energy conservation principle. The tunability of the filter while a desirable property can be sacrificed by using an array of filters with their center frequency placed at the different channels, accompanied by the ability to pass the signal to the appropriate filter. The ability to turn the filter on or off is a flexibility that system designer would like to have, although this requirement too may be circumvented by shunting the signal via an alternate route with no filter.

Gain Distributed Feedback (GDFB) channel-dropping filters are a class of filters which possess some of the properties of the "ideal" filter [9, 12]. Since these structures have gain they allow a channel to be detected with little distortion of the ongoing signal. Moreover, it is possible to tune the center frequency of these filter across a finite frequency range. GDFB resonators or gain-gratings are made by forming alternate regions of gain and loss along a waveguide. These regions cause coupling between the counter-propagating waves leading to an energy storage cavity. By evanescently coupling such a resonator to a signal bus, it is possible to form a CDF. GDFB structures are interesting devices with applications in practical optical communication systems and are the topic of this thesis.

1.2 Thesis Objective

This thesis attempts to provide a comprehensive theoretical treatment of gain distributed feedback (GDFB) structures. Prior familiarity with DFB structures is not presupposed and the material presented in this thesis is mostly self-contained. It is intended that this thesis will be a valuable reference for researchers interested in de-

signing and fabricating GDFB filters and for those interested in learning about these devices.

An understanding of waveguides and waveguide couplers is essential for the study of distributed feedback structures. For this reason, chapter 2 provides a brief overview of waveguides and coupling between them. The properties of guided solution needed to derive the equations describing DFB structures are highlighted. The coupled-mode equations describing waveguide couplers are reviewed and an expression for the coupling parameter is derived.

In chapter 3 the coupled-mode equations describing the waves in a GDFB resonator, (also known as gain grating) made by a periodic gain variation along the length of a waveguide, are derived using perturbation theory. The coupled-mode equations are solved and the threshold condition for lasing is derived. The filter characteristics of a gain grating below threshold are discussed thoroughly. The chapter concludes by deriving an equivalent circuit for a symmetric GDFB resonator. This circuit, we will see, forms the basic element of the equivalent circuits of GDFB structures discussed in the following chapters.

Having discussed an isolated GDFB resonator, chapter 4 turns to consider how two evanescently coupled GDFB resonators interact. The filter characteristics of this second-order system are explored by developing an equivalent circuit for the coupled resonators. This circuit is related to the equivalent circuits of isolated GDFB resonators and helps to clarify how these resonators exchange power. Moreover, chapter 4 gives us the tools to assemble the equivalent circuit of an arbitrary number of coupled resonators.

Gain distributed feedback resonators when coupled to a signal waveguide form channel-dropping filters which are the topic of the next two chapters. Chapter 5 discusses the case of a single GDFB resonator coupled to a bus which forms a first-order CDF. Chapter 6 deals with higher-order or multi-pole CDFs. The case of a second-order CDF is discussed in detail and a general scheme to solve a n^{th}-order CDF is explained.

The performance of GDFB filters relies heavily on the ability to precisely control

the gain/loss in these structures. Consequently, chapter 7 is devoted to the study of optical gain, produced by current injection, in semiconductors. A scheme to relate the injected current to the material gain is discussed. The chapter discusses the distinction between material and modal gain and concludes by discussing a double heterojunction structure which can be used in making gain gratings.

Practically fabricated gain gratings do not possess the features of an ideal gain gratings. Chapter 8 discusses two important non-idealities that have to be dealt with when fabricating these structures, namely the presence of net d.c modal gain and index coupling in gain gratings. The behavior of these non-ideal gratings is explored and schemes to minimize the spurious effects are discussed.

Chapter 2

Waveguides and Waveguide Couplers

Integrated optics technology has focussed on developing microscopic optical circuits on appropriate solid-state substrates to enable signal processing of optical signals. Waveguides and waveguide couplers are used to provide guidance and distribution of the optical waves in these circuits. Filters may then be used to separate out the various frequency components of a signal, as in a WDM communication system. The intent of this chapter is to lay the foundations for understanding Gain Distributed Feedback (GDFB) structures and their application in channel-dropping filters. To this end, a brief overview of waveguides and waveguide couplers is provided. This review is not intended to be exhaustive and will be used to refresh some basics and to introduce the notation to be used.

The chapter will discuss the properties of guided modes in waveguides. By solving the case of a symmetric slab structure insight into guiding structures and the conditions for guidance is developed. We shall see that such structures can support one or more discrete guided modes and a continuum of radiation modes which are orthogonal to each other. The modes of an optical waveguide form a complete set, a property which will be assumed without proof. If two or more waveguides are fabricated close to one another, transfer of electromagnetic energy can occur between them. The guides exchange power as the radiation propagates along them. Such structures are

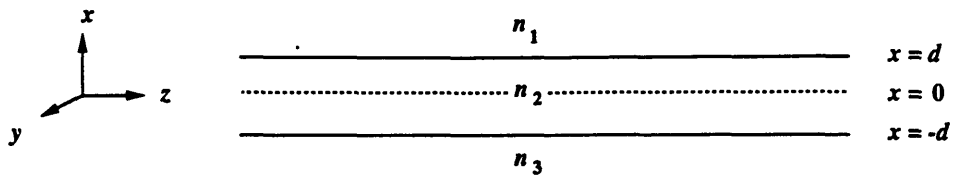

Figure 2-1: Planar waveguide

known as waveguide couplers and have many applications including use as switches [13] and broad-band filters [14] and in channel dropping filters [9]. The equations describing a waveguide coupler are derived. This chapter, thus, reviews two basic optical components that are pervasive in optical networks and integrated optics. Knowledge of these devices is essential for understanding DFB structures which is the topic of the subsequent chapters.

2.1 Waveguides

Figure (2-1) shows a planar dielectric slab structure comprised of three regions of refractive index n_i. As we will see, such a structure acts as a waveguide, confining the field in the x-direction and guiding it along the z-direction. The central region is called the core and the adjacent regions are known as the cladding. The planar guide has no variation along the y-direction. Practical guides, however, wish to confine the fields in both transverse dimension x and y and thus have index or effective index variations in the y-direction as well (fig. (2-4)). Finding the mode profiles in these structures is mathematically challenging and tends to obscure the properties of guided modes. For this reason, we will only consider planar structures. The electric field, $\mathbf{E}$, in any one of the three regions must obey the wave equation

$$\nabla^2\mathbf{E} = \mu_o\epsilon_o {n_i}^2 \frac{\partial^2}{\partial t^2}\mathbf{E}$$

where $i = 1, 2$ or 3. Since there is no variation along the y-direction, we postulate solutions of the form [15]

$$\mathbf{E}(\mathbf{r}) = E(x)e^{-j\beta z} \tag{2.1}$$

Substituting this into the above equation and explicitly writing out the results for the three regions, we find

$$\begin{aligned}
\frac{\partial^2 E(x)}{\partial x^2} + ({k_o}^2 {n_1}^2 - \beta^2)E(x) &= 0 && (2.2)\\
\frac{\partial^2 E(x)}{\partial x^2} + ({k_o}^2 {n_2}^2 - \beta^2)E(x) &= 0 && (2.3)\\
\frac{\partial^2 E(x)}{\partial x^2} + ({k_o}^2 {n_3}^2 - \beta^2)E(x) &= 0 && (2.4)
\end{aligned}$$

where $k_o = \omega\sqrt{\mu_o \epsilon_o}$ is the free space propagation constant. For the modes to be guided, the electromagnetic energy must be confined in the x-direction while propagating in the z-direction.[16] The assumed form of the solution presupposes a forward propagating wave. For the mode to be confined in the transverse dimension, we require that $E(x)$ should tend to zero as $x \to \pm\infty$. This requirement imposes a condition on the propagation constant β and the consequently on the refractive indices, namely

$$\begin{aligned}
\beta &< k_o n_2\\
\beta &> k_o n_1 \qquad (2.5)\\
\beta &> k_o n_3
\end{aligned}$$

which is only possible if $n_2 > n_1$ and $n_2 > n_3$.

Use of (2.2), (2.3) and (2.4) reveals that a wave which obeys (2.5) decays exponentially in regions 1 and 3 and is sinusoidal in region 2, thus satisfying the original constraint for guided modes. Having derived the conditions for the modes to be guided, we turn to solve for the electric field distribution in the guide. We consider the case of a symmetric dielectric slab for which $n_1 = n_3$ and $n_2 > n_1$. The symmetric structure yields itself to a simple mathematical analysis and is a good case to study

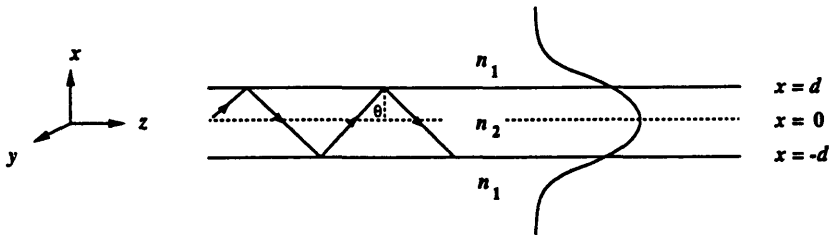

Figure 2-2: Symmetric Planar Waveguide

the properties of guided modes.

Since $n_2 > n_1$, it is possible for waves in region 2, or the core, to undergo total internal reflection at the interface of regions 1/2 and 2/3 if the waves strike these interfaces at angles larger than the critical angle, θ_c. This results in an electric field distribution which has a standing wave pattern in the x-direction while propagating in the z-direction. Since total internal reflection is occuring at the core boundaries, the field dies out exponentially in regions 1 and 3. Therefore, this structure can support guided modes. This discussion seems to suggest that total internal reflection which is responsible for wave guidance, occurs for all angles, θ, larger than the critical angle. This would lead to a continuum of guided modes, corresponding to the uncountably infinite values of angles, θ, that exist in the range $\theta_c < \theta < 90°$. We will see, however, that the continuity of the **E** and **H** fields imposes restrictions on which values of θ can exist, leading to a discrete set of guided modes.

The symmetry of the structure leads us to expect symmetric and antisymmetric solutions. For a TE distribution, hence, the solutions must be of the form [16]:

$$\mathbf{E}(\mathbf{r}) = \hat{y}\mathcal{E}_y(x)e^{-j\beta z} = \hat{y}B\left\{\begin{array}{c}\sin kx\\ \cos kx\end{array}\right\}e^{-j\beta z} \quad |x| \leq d \tag{2.6}$$

$$\mathbf{E}(\mathbf{r}) = \hat{y}\mathcal{E}_y(x)e^{-j\beta z} = \hat{y}Ae^{-\alpha x - j\beta z} \quad x \geq d \tag{2.7}$$

$$\mathbf{E}(\mathbf{r}) = \hat{y}\mathcal{E}_y(x)e^{-j\beta z} = \hat{y}\left\{\begin{array}{c}-\\ +\end{array}\right\}Ae^{\alpha x - j\beta z} \quad x \leq -d \tag{2.8}$$

where A and B are the complex amplitudes of the field and are related by the boundary conditions. The top and the bottom line of the brace refer to the symmetric and

antisymmetric solutions. The magnetic fields, $\mathbf{H}$ can be found by using Faraday's law. We find that

$$\mathbf{H(r)} = (\hat{x}\mathcal{H}_x(x) + \hat{z}\mathcal{H}_z(x)) = \frac{\beta}{\omega\mu_o}\left(-\hat{x}\beta\left\{\begin{array}{c}\sin kx\\ \cos kx\end{array}\right\}\right.$$
$$\left. - \hat{z}jk\left\{\begin{array}{c}-\cos kx\\ \sin kx\end{array}\right\}\right) e^{-j\beta z} \tag{2.9}$$

$$\mathbf{H(r)} = (\hat{x}\mathcal{H}_x(x) + \hat{z}\mathcal{H}_z(x)) = -\frac{A}{\omega\mu_o}(\hat{x}\beta + \hat{z}j\alpha)\, e^{-\alpha x - j\beta z} \tag{2.10}$$

$$\mathbf{H(r)} = (\hat{x}\mathcal{H}_x(x) + \hat{z}\mathcal{H}_z(x)) = -\frac{A}{\omega\mu_o}\left\{\begin{array}{c}-\\ +\end{array}\right\}(-\hat{x}\beta + \hat{z}j\alpha)\, e^{\alpha x - j\beta z} \tag{2.11}$$

Substitution of (2.6) in (2.2) and (2.3) leads to

$$\beta^2 - \alpha^2 = {k_o}^2{n_1}^2 \tag{2.12}$$

$$\beta^2 + k^2 = {k_o}^2{n_2}^2 \tag{2.13}$$

which is simply a restatement of the dispersion relationship applied to regions 1 and 2. The boundary conditions at the interfaces ($x = \pm d$) are that the tangential components of $\mathbf{E}$ and $\mathbf{H}$ must be continuous. For the symmetric solutions, the continuity of E_y and H_z at $x = d$ leads to the constraint that

$$Ae^{-\alpha d} = B\cos kd \tag{2.14}$$

$$\alpha Ae^{-\alpha d} = kB\sin kd \tag{2.15}$$

which simplifies to

$$\frac{\alpha}{k} = \tan kd \tag{2.16}$$

For antisymmetric solutions, continuity of the tangential components of $\mathbf{E}$ and $\mathbf{H}$ leads to

$$\frac{\alpha}{k} = -\cot kd. \tag{2.17}$$

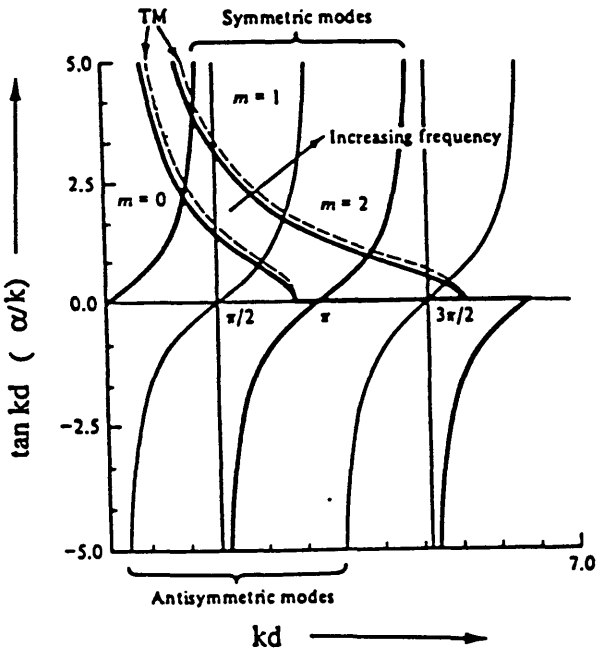

Figure 2-3: Graphical solution of (2.23) and (2.24). Construction of TM modes shown dashed for $\epsilon_2/\epsilon_1 = 1.1$. (Courtesy of [16]).

Subtracting (2.12) from (2.13), we get

$$k^2 + \alpha^2 = k_o{}^2(n_2{}^2 - n_1{}^2) \tag{2.18}$$

Eqs. (2.16) and (2.18) can be solved simultaneously for α and k to yield allowable guided modes of this structure. This is illustrated best by a graphical solution. As can be seen from fig. (2-3), α and k take on discrete values corresponding to the discrete modes which this waveguide can support. Use of (2.12) and (2.13), enables us to find the allowable values of β. $\beta = k_o n_2 \sin\theta$ and consequently θ can only take on discrete values, rather than the entire continuous range $\theta > \theta_c$ as was asserted earlier. For a given width, d, of the core, this structure can support one or more guided modes, determined by the number of intersections in fig. (2-3). These modes are represented by E_y^m, where

$$E_y^m(x,z) = \mathcal{E}_y^m(x)e^{-j\beta_m z}$$

β_m, and $\mathcal{E}_y^m(x)$ are the propagation constant and the transverse field distribution, respectively, of the m^{th} mode.

So far we have found the conditions that α, k and β must obey for guided modes to exist. In fact, we started off by assuming guided modes, (2.6) and use of the boundary conditions led to the constraints on α, β and k. These, however, are not the only solutions that exist to the slab problem. Consider the case when $\beta < k_o n_1$. Since $\beta = k_o n_2 \sin\theta$, this translates to the situation when $\theta < \theta_c$. The angle of incidence is less than the critical angle and the waves striking off the core boundaries are partially transmitted into the substrate carrying power with them. Such solutions are members of a set of solutions called the radiation modes. Radiation modes, unlike the guided modes, form a continuous set. We will not go into an analysis of radiation modes. The interested reader is referred to [17]. However, we refer to these modes for the sake of completeness. We have solved for guided modes for the case of a T.E distribution. The analysis of the T.M is very similar is, therefore, not attempted.

A very important property of the modes of a waveguide is that they form a complete set. [17] Thus an arbitrary T.E distribution, E, in the waveguide can be expanded as a superposition of these modes as follows:

$$E = \sum_m a_m \mathcal{E}_y^m(x) e^{-j\beta_m z} + b_m \mathcal{E}_y^m(x) e^{j\beta_m z} \tag{2.19}$$

where the first term represents the m^{th} mode travelling in the $+z$ direction and the second term corresponds to the m^{th} mode propagating in the opposite direction. a_m and b_m represent the projection of the electric field distribution in the guide on the m^{th} forward and backward travelling eigenmode of the waveguide, respectively. Another very important and general property of these modes is that they are orthogonal to each other. For the planar structure this translates into [15]

$$\int_{-\infty}^{\infty} \mathcal{E}_y^m(x) \mathcal{E}_y^l(x) dx = 2\frac{\omega\mu}{\beta_m}\delta_{l,m} \tag{2.20}$$

The factor of $2\omega\mu/\beta_m$ is conveniently chosen so as to normalize the power in the m^{th}

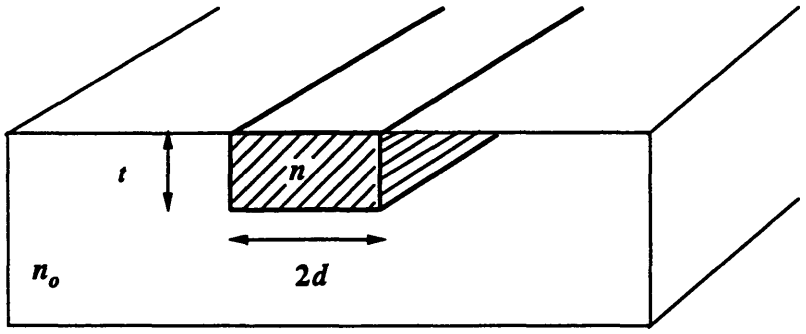

Figure 2-4: Optical waveguide

mode to unity. That is,

$$\frac{1}{2}\int_{-\infty}^{\infty} E_y^m H_y^{*m} dx = \frac{\beta_m}{2\omega\mu}\int_{-\infty}^{\infty}\left[\mathcal{E}_y^m(x)\right]^2 dx = 1$$

Orthogonality of modes can be easily demonstrated by substituting for $\mathcal{E}_y^m(x)$ and $\mathcal{E}_y^l(x)$ from (2.6). It is, however, a general property of guided modes in a lossless medium and can be derived from power conservation and the reciprocity theorm [7]. Thus, we see that modes of a guiding structure form a complete orthonormal set of functions allowing any distribution to be expanded as a superposition of them. This is the crucial property of modes which will be used in deriving the coupling-of-modes equations for distributed feedback structures in the following chapter. We now turn to coupling of energy between adjacent waveguides.

2.2 Waveguide Couplers [18, 19]

Consider the dielectric waveguide structure shown in fig. (2-4) . This structure is in some sense similar to the dielectric slab discussed in the previous section. It differs, however, in that it is finite in both the x and y directions. No attempt will be made to solve this structure analytically and the interested reader is refered to the vast literature available on this topic [17, 20]. However, based on the analysis of the symmetric slab of the previous section, we expect that this structure supports one or more guided modes. Furthermore, as in the previous section, we expect the modes

to be mainly confined to the region of greater refractive index, n, and to die out exponentially in the surrounding regions of lower index, n_o. Thus, the electric field distribution of TE mode is of the form [15]

$$E = a(z)\mathcal{E}(x,y) \tag{2.21}$$

and obeys the wave equation

$$a(z)\nabla_T^2\mathcal{E}(x,y) - (\beta^2 - \omega^2\mu\epsilon_o\, n_i)a(z)\mathcal{E}(x,y) = 0$$

where $\mathcal{E}(x,y)$ is the field distribution in the transverse dimension and $a(z)$ is the amplitude in the z-direction. We have assumed here that the waveguide of fig (2-4) is single moded. This greatly simplifies the notation and for simplicity we will assume that all our guides are single moded. Extension to the case of a multi-moded guide is not too difficult. As in (2.6), the variation in the z-direction is $a(z) \propto e^{-j\beta z}$ where β is the propagation constant along the z-direction. It is constrained by the boundary condition on the tangential components of the field and obeys equations similar to (2.12) and (2.13). $a(z)$ represents the fact that we have a forward propagating modes which maintains its transverse distribution, $\mathcal{E}(x,y)$ as it moves along the guide. Ignoring the transverse distribution, we can write a differential equation for $a(z)$ [7]:

$$\frac{da(z)}{dz} = -j\beta a(z) \tag{2.22}$$

Let us now suppose that we fabricate another guide next to the first one and separated from it by a distance, D as shown in fig. (2-5). If D is very large, the exponential tails of the electric field distribution do not "see" the other guide and we expect the modes will not interact with each other. In this case, the modes in the two guides can be solved for separately are described by the following equations:

$$\frac{da_1}{dz} = -j\beta_1 a_1 \qquad \text{Guide 1} \tag{2.23}$$

$$\frac{da_2}{dz} = -j\beta_2 a_2 \qquad \text{Guide 2} \tag{2.24}$$

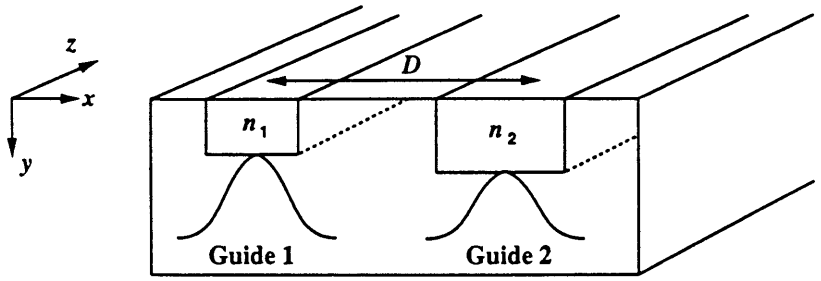

Figure 2-5: Coupled Waveguides

If, however, the separation, D, is such that the transverse mode profiles of the two guides begin to overlap, we expect the modes to interact. If this overlap is small, the modes will couple weakly and in this case we may treat the presence of the other guide as a perturbation to the first one. The weak coupling, then, justifies the assumption that the transverse mode profiles in guides 1 and 2 remain essentially unchanged with the total electric field given by [21]

$$E = a_1(z)\mathcal{E}_1(x,y) + a_2(z)\mathcal{E}_2(x,y) \tag{2.25}$$

$a_1(z)$ and $a_2(z)$ are, however, no longer described by equations (2.23) and (2.24). We will see shortly how coupling modifies these equations.

Weak coupling implies that we may evaluate the power in the two waves disregarding the coupling. Thus, using the normalization condition, we find that the power in the mode of the coupled structure is given by $|a_1|^2 + |a_2|^2$. For weak coupling the system is power orthogonal (i.e there are no cross terms of the form $a_1^* a_2$ etc. in the power expression). [21] This is the type of coupling we will be concerned with. When the mode overlap becomes large or the coupling is strong, the system is no longer power orthogonal and is described by the more general non-orthogonal coupled mode theory [18, 21] which will not be discussed.

To see how $a_1(z)$ and $a_2(z)$ are modified due to weak coupling, let us conduct a simple thought experiment. Suppose we excite a mode in one of the guides, say guide

1, at $z = 0$ but not in guide 2 (i.e $a_2(0) = 0$). The exponential tails of the electric field distribution in guide 1 extends across guide 2. They act as a source of excitation for guide 2 and are capable of transferring power to it, provided the propagation constants β_1 and β_2 of the two guides do not differ by too much. If $\beta_1 \gg \beta_2$ (or vice versa), the field in guide 1 will not be able to effectively transfer power and thus excite a mode in guide 2. The situation is akin to driving a RLC circuit far away from its resonance. Effective power transfer cannot be accomplished in this case. On the other hand, if $\beta_1 \simeq \beta_2$, we expect energy to be transferred from guide 1 to guide 2 as the modes propagate along the guides as a result of the exponentially decaying field coupling power from one guide to the other. Once a mode has been excited in guide 2, the roles of the two waveguides are reversed and the excitation in guide 2 couples back to guide 1. We, therefore, expect that as the modes propagate, along z, there will be a "sloshing" of power between guides 1 and 2. As stated earlier the transverse mode profiles are assumed to be unaffected in this weak coupling regime and we concern ourselves with a_1 and a_2. Since a_1 is affected by a_2 and vice versa, we postulate that the new equations describing the wave amplitudes are [7]:

$$\frac{da_1}{dz} = -j\beta a_1 - j\mu_{12} a_2 \tag{2.26}$$

$$\frac{da_2}{dz} = -j\beta a_2 - j\mu_{21} a_2 \tag{2.27}$$

where μ_{12} and μ_{21} are the coupling coefficients describing how a_1 and a_2 affect each other.

Although, we have modified the equations in a rather adhoc fashion, we will see that these new equations correctly describe the behavior of the system expected from the previous arguments. More formally, it can be shown that the coupled mode equations can be derived from a variational principle for the propagation constant which assumes that the electric field distribution for the composite structure is given by a linear superposition of the uncoupled modes as in (2.25) [21]. For the power to be conserved as the modes propagate along the guides, a constraint is imposed on μ_{12} and μ_{21} so that they are not independent of each other. Since the modes are

propagating in the same direction, conservation of power requires

$$\frac{d}{dz}\left(|a_1|^2 + |a_2|^2\right) = 0 \tag{2.28}$$

$$j\left(\mu_{12}^* - \mu_{21}\right) a_1 a_2^* + j\left(\mu_{21}^* - \mu_{12}\right) a_1^* a_2 = 0 \tag{2.29}$$

Since the phases of a_1 and a_2 are arbitrary, the above equation is satisfied if

$$\mu_{12} = \mu_{21}^* \equiv \mu \tag{2.30}$$

Using the above relations, we can rewrite the coupled-mode equations as

$$\frac{da_1}{dz} = j\beta_1 a_1 - j\mu a_2 \tag{2.31}$$

$$\frac{da_2}{dz} = j\beta_2 a_2 - j\mu^* a_1 \tag{2.32}$$

For an assumed dependence of $\exp(-j\beta z)$, we find that the determinantal equation is

$$-\left(\beta_1 - \beta\right)\left(\beta_2 - \beta\right) + |\mu|^2 = 0$$

which has the solution

$$\beta = \frac{\beta_1 + \beta_2}{2} \pm \sqrt{\left(\frac{\beta_1 - \beta_2}{2}\right)^2 + |\mu|^2}$$

If we assume that the mode profiles at $z = 0$ are $a_1(0)$ and $a_2(0) = 0$, we find that $a_1(z)$ and $a_2(z)$ are given by

$$a_1(z) = \left[a_1(0)\left(\cos\beta_o z + j\frac{\beta_2 - \beta_1}{2\beta_o}\sin\beta_o z\right)\right] e^{-j\,[(\beta_1+\beta_2)/2]z} \tag{2.33}$$

$$a_2(z) = \left[-j\frac{\mu^*}{\beta_o} a_1(0)\sin\beta_o z\right] e^{-j\,[(\beta_1+\beta_2)/2]z} \tag{2.34}$$

where

$$\beta_o = \sqrt{\left(\frac{\beta_1 - \beta_2}{2}\right)^2 + |\mu|^2}$$

If $\beta_1 \gg \beta_2$ or $\beta_2 \gg \beta_1$, so that $|\beta_1 - \beta_2| \gg |\mu|$, we find that $\beta_o \approx (\beta_1 - \beta_2)/2$. Substituting this in the above expression and bearing in mind that $|\beta_o| \gg \mu$, we get

$$a_1(z) \simeq a_1(0)e^{-j\beta_1 z} \tag{2.35}$$

$$a_2(z) \simeq 0 \tag{2.36}$$

Thus, as expected from the qualitative reasoning if β_1 is very different from β_2, we are unable to excite a mode in guide 2 and the mode in guide 1 propagates undisturbed with its characteristic constant, β_1 along the guide as though guide 2 were absent. However, if $\beta_1 \simeq \beta_2$ so that $\beta_o \simeq |\mu|$, we find that

$$a_1(z) \simeq [a_1(0)\cos\beta_o z]\, e^{-j[(\beta_1+\beta_2)/2]z} \tag{2.37}$$

$$a_2(z) \simeq \left[-j\frac{\mu^*}{|\mu|}a_1(0)\sin\beta_o z\right] e^{-j[(\beta_1+\beta_2)/2]z} \tag{2.38}$$

The above expressions clearly show that the power oscillates between the two guides as we had expected. Moreover, for $\beta_1 = \beta_2$, complete power transfer is possible between the two guides with the transfer length, $l_t = \pi/(2\mu)$. If β_1 not equal to β_2, the transfer of power between the guides is incomplete and the maximum fraction of power transferred, F, given by

$$F = \left(\frac{|a_2|^2}{|a_1|^2 + |a_2|^2}\right)\Bigg|_{\beta_o l=\pi/2} = \frac{1}{1 + \left(\frac{\beta_2-\beta_1}{2|\mu|}\right)^2} \tag{2.39}$$

The coupled-mode equations, therefore, correctly describe the behavior of the system we had speculated based on physical arguments. This does not, however, constitute a proof of the coupled-mode equation and readers who would like a more rigorous development are referred to ref. [21].

2.2.1 Coupling Coefficient, μ

Thus far, we have assumed that the coupling coefficient, μ, is a known quantity. We will see now that μ can be calculated using a physically appealing argument [7].

Recall that the field in the coupled structure is given by

$$E = a_1(z)\mathcal{E}_1(x,y) + a_2(z)\mathcal{E}_2(x,y)$$

The rate of change of power per unit length along guide 2 can be found easily by using the coupled mode equations. It is given by

$$\begin{aligned} \frac{d}{dz}|a_2|^2 &= a_2\frac{da_2^*}{dz} + a_2^*\frac{da_2}{dz} \\ &= j\mu a_1^* a_2 - j\mu^* a_1 a_2^* \end{aligned} \tag{2.40}$$

We know that this power is supplied to guide 2 by the polarization current produced in this guide due to that part of the field of mode 1 which overlaps with guide 2. Mode 1 finds a perturbation $\epsilon_1 - \epsilon_2$ and drives a polarization current $j\omega P_{12}$ through it, given by [18]

$$j\omega P_{12} = j\omega\left(\epsilon_1 - \epsilon_2\right) a_1\mathcal{E}_1(x,y) \tag{2.41}$$

The power fed into mode 2 per unit length is given by

$$-\frac{1}{4}\left[\int E_y^*.\left(j\omega P_{12}\right) da + cc\right]$$

which simplifies to

$$-\frac{1}{4}\left[\int a_1 a_2^*\mathcal{E}_2^*\mathcal{E}_1\left(\epsilon_1 - \epsilon_2\right) da + cc\right]$$

Comparing the above expression with (2.40), we find that the coupling coefficient is given by

$$\mu = \frac{1}{4}\int \omega\,\Delta\epsilon\,\mathcal{E}_1^*(x,y)\,\mathcal{E}_2(x,y)da \tag{2.42}$$

where $\Delta\epsilon \equiv \epsilon_1 - \epsilon_2$ and the integration is performed over the cross section of guide 2.

We have reviewed waveguides and the coupling between them. In the following chapter we treat distributed feedback structures freely employing the results derived in this chapter.

Chapter 3

Distributed Feedback Gain Gratings

In the previous chapter we saw that a dielectric waveguide can support TE and TM guided modes. These modes are orthogonal to each other and if excited in an ideal waveguide without imperfections, propagate along the guide undisturbed with their characteristic group velocities and propagation constants, β_m, without interacting with one another. However, practical waveguides are not without imperfections. The imperfections can be in the form of index inhomogeneities, rough surfaces, non-uniform widths of the guide, etc. These imperfections can result in the guided modes of a waveguide interacting and exchanging power with each other [17]. Thus, it is possible for energy from one mode of the guide to couple to another mode propagating in the same guide. In many cases this is not desirable. For example, if guided modes couple power to the continuum radiation modes, it results in waveguide losses. However, coupling between modes is not always an undesired effect. In fact, in some structures perturbations are intentionally introduced in the guide so as to couple modes. One class of such devices are the distributed feedback (DFB) structures.

DFB structures are produced by periodic perturbations in the complex refractive index [22] along the length of the guiding structure as shown in fig. (3-1). If the periodic variations are purely real, we have a passive index grating. Passive index gratings are used as mirrors and if side-coupled to another waveguide, behave as a

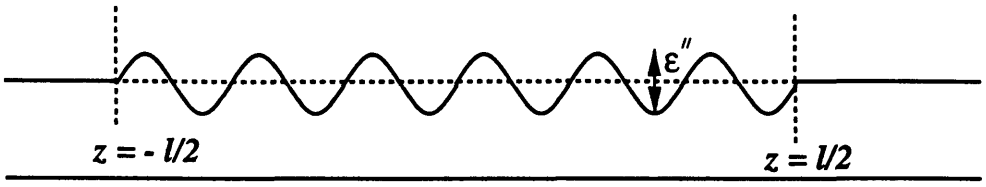

Figure 3-1: Gain grating

filters [10, 23]. A passive index grating can perform useful filtering functions [24]. If, however, the perturbation is purely imaginary, or in other words, we have periodic gain/loss variations along the guide, the resulting structure is a gain grating belonging to the larger class of GDFB structures. Gain gratings, although harder to fabricate, have certain distinct advantages over passive gratings for use as filters. As we will see, distributed feedback structures (index and gain) couple power between the forward and backward travelling waves of the same mode, when appropriately designed. The equations describing the behavior of the optical modes in the DFB grating will be derived using perturbation theory. We will focus on gain gratings, which are produced by periodic variations of the gain along the guide. Gain gratings have the essential ingredients for lasing, namely feedback and gain. The oscillation condition will be derived and the behavior of the gain grating will be thoroughly explored. The chapter will end by deriving an equivalent ciruit for a gain grating, which as we will see is a very convenient way of understanding these structures.

3.1 Coupled Mode Equations [15]

Consider the guiding structure shown in fig. (3-1). It is similar to the planar dielectric waveguide of the previous chapter. However, unlike the previous waveguide, this structure has gain and loss variations along its length which are represented schematically by the sinosoidal variations on the top surface of the guide. If the gain variations are small, we may use perturbation theory to analyse this structure. Before

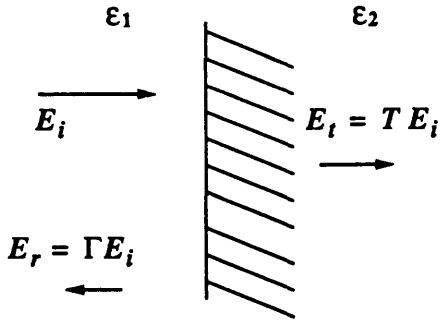

Figure 3-2: Reflection from a gain boundary

we proceed with this approach, however, let us gain some insight into this structure by considering what happens to an optical wave at the boundary of two media with different gains. Fig. (3-2) shows a normally incident wave at a boundary between two media with dielectric constants ϵ_1 and ϵ_2 respectively. Continuity of the tangential fields yields the familiar expression for the reflectivity, Γ:

$$\Gamma = \frac{\sqrt{\epsilon_1} - \sqrt{\epsilon_2}}{\sqrt{\epsilon_1} + \sqrt{\epsilon_2}} \tag{3.1}$$

Let us assume that the real part of the dielectric constant for the two media is the same , i.e $\Re\{\epsilon_1\} = \Re\{\epsilon_2\} \equiv \epsilon'$ and is much larger than the imaginary part. The imaginary parts of the dielectric constants for the two regions are unequal which corresponds to these regions having different gain. $\Im\{\epsilon_1\} \equiv \epsilon_1''$ and $\Im\{\epsilon_2\} \equiv \epsilon_2''$. In this case, we have that

$$\Gamma \simeq j\frac{\epsilon_1'' - \epsilon_2''}{4\epsilon'} \tag{3.2}$$

Thus, we see that the wave is reflected when it encounters a boundary between media which have different gain. Returning to the gain grating, we recall that an ideal gain grating alternates region of gain and loss along the guide with no dc. gain value as shown schematically in fig. (3-1). From the previous discussion, we expect the optical waves to be reflected at each of the gain/loss boundary. If the waves have the appropriate wavelength, the reflected waves could add in phase leading to a wavelength dependent resonant behavior. Based on this simplistic approach, we

expect a coupling between the forwards and backward propagating waves in a gain grating. To quantify this coupling between the counter-propagating waves of the optical mode, we resort to perturbation theory. The approach used to derive the coupled-mode equations is similar to that of ref. [25]

The electric field in the gain grating obeys the wave equation

$$\nabla^2 \mathbf{E} = \mu_o \epsilon_o \frac{\partial^2 \mathbf{E}}{\partial t^2} + \mu_o \frac{\partial^2 \mathbf{P}_{\text{tot}}}{\partial t^2} \tag{3.3}$$

It is convenient to separate the total polarization density, $\mathbf{P}_{\text{tot}}$, into two parts, namely the polarization of the unperturbed waveguide corresponding to the dashed lines and the polarization produced due to the perturbation, P_{pert}. Thus,

$$\mathbf{P}_{\text{tot}} = \mathbf{P}_{\text{o}} + \mathbf{P}_{\text{pert}} \tag{3.4}$$

where

$$\mathbf{P}_{\text{o}} = \epsilon_o \chi_e \mathbf{E}(\mathbf{r}, t) = [\epsilon(r) - \epsilon_o]\mathbf{E}(\mathbf{r}, t) \tag{3.5}$$

and $\epsilon(r)$ is the dielectric constant of the unperturbed waveguide.

As stated in the previous chapter, the modes of the unperturbed waveguide form a complete orthonormal set allowing any distribution to be expanded as a superposition of them. The orthonormal set consists of all the guided modes, TE and TM and the continuum of radiation modes. However, we will assume that the electric field distribution in the perturbed structure has no projection on the radiation modes. For well designed systems this is a valid assumption since we are dealing with guided modes which do not lose power to radiation modes, but couple only to other discrete modes. To be specific, we treat the case of a TE distribution. Extension to an arbitrary guided distribution is straightforward but unnecessarily complicates the notation and thus will not be attempted.

According to the previous discussion, we can write the electric field E_y in the

perturbed structure as a superposition of the modes of the unperturbed guide, i.e [25]

$$E_y(r,t) = \frac{1}{2}\sum_m A'_m(z)\mathcal{E}_y^m(x)e^{j(\omega t-\beta_m z)} + B'_m(z)\mathcal{E}_y^m(x)e^{j(\omega t+\beta_m z)} + c.c \qquad (3.6)$$

where as in (2.19) the first term represents the m^{th} mode travelling in the + z direction and the second term represents same mode travelling in the − z direction. Notice, however, unlike in eq. (2.19), the weighting coefficients A'_m and B'_m are functions of z. This is because the perturbation itself is a function of z and thus requires that the coefficients, which represent the projection of the field in the perturbed structure on the unperturbed modes, to be z-dependent as well. Recall that $\mathcal{E}_y^m(x)e^{j(\omega t\pm\beta_m z)}$ are solutions of the unperturbed waveguide and hence obey the following equation:

$$\frac{\partial^2\mathcal{E}_y^m(x)}{\partial t^2} - {\beta_m}^2\mathcal{E}_y^m(x) = -\omega^2\mu_o\epsilon(r)\mathcal{E}_y^m(x) \qquad (3.7)$$

where we have used the fact that $\frac{\partial}{\partial y} = 0$ for the planar waveguide. Using (3.4) and (3.5), we can rewrite (3.3) as

$$\nabla^2\mathbf{E} - \mu_o\epsilon_o\frac{\partial^2\mathbf{E}}{\partial^2 t^2} = \mu_o\frac{\partial^2\mathbf{P}_{\text{pert}}}{\partial t^2}$$

Substituting the expression for the electric field distribution, (3.6), in the above equation, we find

$$\begin{aligned} e^{j\omega t}\{ & \sum_m \tfrac{A'_m}{2}(\tfrac{\partial^2}{\partial x^2} - {\beta_m}^2 + \omega^2\mu_o\epsilon(r))\mathcal{E}_y^m(x)e^{-j\beta_m z} \\ + & \sum_m \tfrac{B'_m}{2}(\tfrac{\partial^2}{\partial x^2} - {\beta_m}^2 + \omega^2\mu_o\epsilon(r))\mathcal{E}_y^m(x)e^{j\beta_m z} \\ + & \sum_m \tfrac{1}{2}(\tfrac{\partial^2 A'_m}{\partial z^2} - 2j\beta_m\tfrac{\partial A'_m}{\partial z})\mathcal{E}_y{}^m(x)e^{-j\beta_m z} \\ + & \sum_m \tfrac{1}{2}(\tfrac{\partial^2 B'_m}{\partial z^2} + 2j\beta_m\tfrac{\partial B'_m}{\partial z})\mathcal{E}_y{}^m(x)e^{j\beta_m z}\} \\ & = \mu_o^2\tfrac{\partial^2}{\partial t^2}[\mathbf{P}_{\text{pert}}]_y \end{aligned} \qquad (3.8)$$

The above equation can be simplified considerably by realizing that the first two summations are zero according to (3.7). Thus far no approximations have been made. The above equations are exact provided we assume that the modes of the unperturbed

guide form a complete set. We now make our first approximation. Since the perturbation is small, we assume that A'_m and B'_m are slowly varying functions of z. This is a sensible assumption since in the limit that the perturbation tends to zero, A'_m and B'_m become constants as in (2.19). Using this "slow" varying approximation, we conclude that [15]

$$\left|\frac{\partial^2 A'_m}{\partial z^2}\right| \ll \left|\beta_m \frac{\partial A'_m}{\partial z}\right|$$

and

$$\left|\frac{\partial^2 B'_m}{\partial z^2}\right| \ll \left|\beta_m \frac{\partial B'_m}{\partial z}\right|$$

Taking this into account, we can rewrite (3.8) as

$$e^{j\omega t}\sum_m -j\beta_m\left[\frac{\partial A'_m}{\partial z}e^{-j\beta_m z} - \frac{\partial B'_m}{\partial z}e^{j\beta_m z}\right]\mathcal{E}_y{}^m(x) + \text{c.c} = \mu_o\frac{\partial^2}{\partial t^2}[\mathbf{P}_{\text{pert}}]_y \qquad (3.9)$$

To eliminate the summation and so as to be able to deal with a specific mode, we use the fact that different modes are orthogonal to each other. In this chapter we use a slightly different normalization condition for the fields. Instead of normalizing the power in the mode to be unity we choose the integral of the square of the **E** field to be unity. This choice yields a particularly simple form for the coupling coefficient, as we will see later.

$$\int_\infty^\infty \mathcal{E}_y^m(x)\mathcal{E}_y^l(x)dx = \delta_{lm}$$

as found in chapter 2. (δ_{lm} is the Kronecker delta function.) Multiplying both sides of (3.9) with $\mathcal{E}_y^s(x)$ and integrating over x, we obtain

$$\frac{dA'_s}{dz}e^{j(\omega t-\beta_s z)} - \frac{dB'_s}{dz}e^{j(\omega t-\beta_s z)} + \text{c.c} = j\frac{\mu_o}{\beta_s}\frac{\partial^2}{\partial t^2}\int_\infty^\infty [\mathbf{P}_{\text{pert}}]_y\,\mathcal{E}^s{}_y(x)dx \qquad (3.10)$$

We have not yet discussed how P_{pert} is related to the perturbation. The perturbation along the guide is described by a dielectric perturbation $\Delta\epsilon(r)$. The total dielectric

constant ϵ_{tot} is given by

$$\epsilon_{tot} = \epsilon(r) + \Delta\epsilon(r) \tag{3.11}$$

$\Delta\epsilon$ may be purely real, imaginary or complex depending on whether we have a pure index grating, a gain grating or a grating produced by a combination of index and gain variations. Since $\Delta\epsilon$ is a scalar, we see that this type of structures can only couple TE to TE and TM and TM modes [15]. It is not possible to couple TE to TM with either a gain or a passive grating. In our case $\Delta\epsilon$ is purely imaginary since we have only gain/loss variations and thus $\Delta\epsilon = j\Delta\epsilon_g$. We know that

$$\epsilon_{tot}\mathbf{E} = \epsilon_o\mathbf{E} + \mathbf{P}_{tot}$$

where P_{tot} is the total polarization defined in (3.4). Using (3.4), (3.5) and (3.11) in the above expression, we find that

$$\mathbf{P}_{pert} = \Delta\epsilon(r)\mathbf{E}$$

Use of eq. (3.6) and the above expression yields

$$\begin{aligned}&\frac{dA'_s}{dz}e^{j(\omega t-\beta_s z)} - \frac{dB'_s}{dz}e^{j(\omega t+\beta_s z)} + \text{c.c} = \\ &\frac{\omega^2\mu_o}{2\beta_s}e^{j\omega t}\int_{-\infty}^{\infty}\Delta\epsilon_g\mathcal{E}_y^s(x)\mathcal{E}_y^m(x)\left[\sum_m A'_m(z)e^{-j\beta_m z} + B'_m(z)e^{j\beta_m z}\right]dx\end{aligned} \tag{3.12}$$

$\Delta\epsilon_g$ is a periodic function of z which can expanded in a Fourier series as:

$$\Delta\epsilon_g(x,z) = \Delta\epsilon_g(x)\sum_n a_n e^{j\frac{2\pi n}{\Lambda}}$$

where

$$\Delta\epsilon_g(x) = \begin{cases}\epsilon'' & \text{if } |x| \le d \\ 0 & |x| > d\end{cases}$$

and Λ is the wavelength of the perturbation. Use of the above expression in (3.12)

results in

$$\frac{dA'_s}{dz}e^{-j\beta_s z} - \frac{dB'_s}{dz}e^{j\beta_s z} = \frac{k_o^2}{2\beta_s}\int_{-\infty}^{\infty}\frac{\Delta\epsilon_g(x)}{\epsilon_o}\mathcal{E}_y{}^s(x)\mathcal{E}_y{}^m(x)\times \left[\sum_n a_n \sum_m A'_m(z)e^{-j(\beta_m-\frac{2\pi n}{\Lambda})z}B'_m(z)e^{j(\beta_m+\frac{2\pi n}{\Lambda})z}\right]dx$$

where we have divided out by the common time dependence, $e^{j\omega t}$. The term on the right hand side acts as a driving term for the propagating modes A'_s and B'_s. Only the term which is phase matched to those on the left side will effectively couple to them. Thus, if there is a term on the right hand side of the form $e^{-j\beta z}$ where $\beta \approx \beta_s$, it will strongly couple to the forward travelling mode, $A'_s(z)$ and we can ignore the contribution due to those terms for which β is not approximately equal to β_s. [15] To be specific, let us assume that

$$\beta_o \equiv \beta_s(\omega_o) \approx \frac{\pi}{\Lambda}$$

so that

$$\beta_s(\omega_o) - \frac{2\pi}{\Lambda} \approx -\beta_s(\omega_o)$$

For this case the term on the right hand side which effectively couples power to the forward propagating mode is the $m = s$ and $n = -1$. Similarly the term which effectively drives the backward propagating mode is the $m = s$ and $n = 1$. Writing out the equation for the modes separately, we obtain:

$$\frac{dA'_s}{dz} = \left[\frac{k_o^2}{2\beta_s}\int a_{-1}\frac{\Delta\epsilon_g(x)}{\epsilon_o}[\mathcal{E}_y{}^s(x)]^2dx\right]B'_s e^{2j(\beta_s-\frac{\pi}{\Lambda})z} \tag{3.13}$$

$$\frac{dB'_s}{dz} = \left[-\frac{k_o^2}{2\beta_s}\int a_1\frac{\Delta\epsilon_g(x)}{\epsilon_o}[\mathcal{E}_y{}^s(x)]^2dx\right]A'_s e^{-2j(\beta_s-\frac{\pi}{\Lambda})z} \tag{3.14}$$

We define the following coupling coefficients

$$\kappa_{AB} = \frac{k_o^2}{2\beta_s}\int a_{-1}\frac{\Delta\epsilon_g(x)}{\epsilon_o}[\mathcal{E}_y^s(x)]^2dx \tag{3.15}$$

$$\kappa_{BA} = -\frac{k_o^2}{2\beta_s}\int a_1\frac{\Delta\epsilon_g(x)}{\epsilon_o}[\mathcal{E}_y^s(x)]^2dx \tag{3.16}$$

Using these definitions of coupling coefficients (3.13) and (3.14) can be rewritten as

$$\frac{dA'_s}{dz} = \kappa_{AB} B'_s e^{2j(\beta_s - \frac{\pi}{\Lambda})z} \tag{3.17}$$

$$\frac{dB'_s}{dz} = \kappa_{BA} A'_s e^{-2j(\beta_s - \frac{\pi}{\Lambda})z} \tag{3.18}$$

To express these equations in the conventional coupled-mode form, we define two new quantities $A(z)$ and $B(z)$ which are related to $A_s'(z)$ and $B_s'(z)$ as follows

$$\begin{aligned} A(z)e^{-j\beta_o z} &= A_s'(z)e^{-j\beta_s z} \\ B(z)e^{j\beta_o z} &= B_s'(z)e^{j\beta_s z} \end{aligned}$$

The total z-dependence of the modes is expressed by either side of the above equations. Substituting for A'_s and B'_s into (3.17) and (3.18) we get

$$\begin{aligned} \frac{dA(z)}{dz} &= -j\delta A(z) + \kappa_{AB} B(z) \\ \frac{dB(z)}{dz} &= j\delta B(z) + \kappa_{BA} A(z) \end{aligned}$$

where

$$\delta \equiv \beta_s - \beta_o$$

Expanding $\beta_s(\omega)$ around ω_o we find that

$$\begin{aligned} \beta_s(\omega_o) &= \beta_s(\omega_o) + \left.\frac{d\beta_s}{d\omega}\right|_{\omega=\omega_o} (\omega - \omega_o) \\ &= \beta_o + \frac{(\omega - \omega_o)}{v_g} \end{aligned}$$

where we have used the fact that the group velocity, $v_g = \frac{d\omega}{d\beta_s}$. The above expansion assumes that dispersion effects in the guide are negligible and can be ignored, that is $\left|\frac{d^2\beta}{d\omega^2}\right| \ll \left|\frac{d\beta}{d\omega}\right|$. Consequently,

$$\delta = \frac{\omega - \omega_o}{v_g}$$

and is the "frequency" parameter of the system. Note that the definitions of κ_{AB}

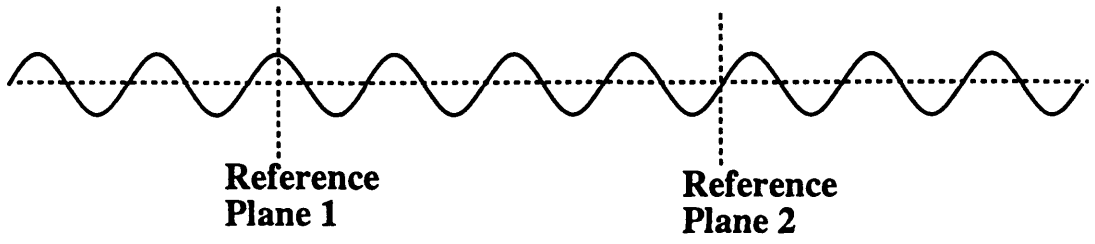

Figure 3-3: Defining Reference Planes for Fourier Series Expansion

and κ_{BA} have Fourier coefficients, $a_{\pm 1}$. These coefficients depend on where we define the reference plane for the series expansion. Consequently the phase of κ_{AB} and κ_{BA} depends on our choice of the reference plane. Two obvious choice of planes are marked in the fig. (3-3). For the choice of plane 1, from the symmetry of the waveform we know that

$$a_1 = a_{-1} \quad \text{and} \quad \Im\{a_{\pm 1}\} = 0$$

For this case, then κ_{AB} and κ_{BA} are real and of opposite sign.

$$\kappa_{AB} = -\kappa_{BA} \equiv \kappa$$

and the coupled mode equations become

$$\frac{dA}{dz} = -j\delta A + \kappa B \tag{3.19}$$

$$\frac{dB}{dz} = j\delta B - \kappa A \tag{3.20}$$

Likewise if plane 2 is chosen, we have

$$a_1 = -a_{-1} \quad \text{and} \quad \Re\{a_{\pm 1}\} = 0$$

In this case κ_{AB} and κ_{BA} are purely imaginary and are related by

$$\kappa_{AB} = \kappa_{BA} \equiv j\kappa$$

To relate κ to the peak to peak material gain oscillation, Δg, in the guide, we make use of the dispersion relation, i.e

$$k^2 = \omega^2 \mu_o \epsilon = \omega^2 \mu_o (\epsilon' + j\epsilon'')$$

where k is the complex propagation constant and is given by

$$k = \beta_s + j\frac{\Delta g}{2}.$$

Assuming that $\epsilon'' \ll \epsilon'$ which is true for most achievable values of material gain, we know that $\Delta g \ll \beta_s$. Thus to lowest order we have that

$$\begin{aligned} \beta_s^2 + j\beta_s \Delta g &= \omega^2 \mu_o (\epsilon' + j\epsilon'') \quad \Rightarrow \\ \frac{\epsilon''}{\epsilon_o} &= \frac{\beta_s}{k_o^2} \Delta g \end{aligned} \tag{3.21}$$

where, $k_o = \omega\sqrt{\mu_o \epsilon_o}$, is the free space propagation constant. For the choice of reference plane 1, substituting the above result in eq. (3.15) we find that

$$\kappa = \frac{1}{2} \int a_1 \Delta g \, [\mathcal{E}_y{}^s(x)]^2 dx \tag{3.22}$$

For a first-order square wave oscillation of the gain, $a_1 = 1/\pi$ and the coupling coefficient κ is given by

$$\kappa = \frac{\Delta g}{2\pi} \Gamma \tag{3.23}$$

where Γ is the overlap integral of the power in the field over the cross section of the grating. Although we have derived the coupled-mode equations for the planar structure with periodic perturbations, the form of the equations is unchanged if we have a guiding structure which confines the mode in both transverse dimensions as in figure (2-4). The only change that occurs is in the definition of κ. Instead of $\mathcal{E}_y^m(x)$, we now have $\mathcal{E}_y^m(x, y)$ and the single integration in x becomes a double integration over the cross section of the guide. [7]

Having derived the coupled mode equations for the distributed feedback struc-

tures, we turn to solve them for the case of a gain distributed feedback resonatoror gain grating. The GDFB resonator is discussed and an equivalent circuit representing the structure is derived.

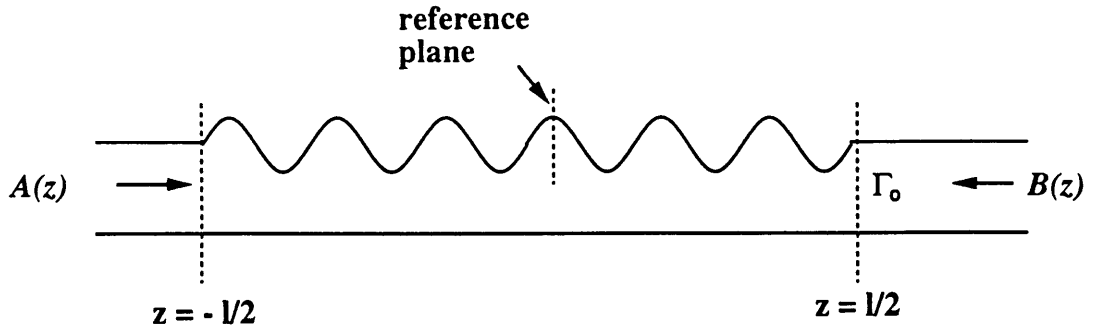

Figure 3-4: GDFB Resonator

3.2 GDFB Resonator [9]

Figure (3.2) shows a GDFB resonator. The equations describing the forward and backward travelling waves $A(z)$ and $B(z)$ of a gain grating are:

$$\frac{dA}{dz} = -j\delta A + \kappa B \tag{3.24}$$

$$\frac{dB}{dz} = j\delta B - \kappa A \tag{3.25}$$

Notice that we have chosen the reference plane at the peak of the gain. As a result κ is real and positive. We will see later that this choice of the reference plane allows us to exploit the symmetry of the problem thus simplifying calculations enormously. The above equations can be cast in matrix form.

$$\frac{d}{dz}\begin{bmatrix} A \\ B \end{bmatrix} = \begin{bmatrix} -j\delta & \kappa \\ -\kappa & j\delta \end{bmatrix}\begin{bmatrix} A \\ B \end{bmatrix}$$

For an assumed dependence of $\exp(j\beta z)$, we find that a non-trivial solution exists if

$$\det\begin{bmatrix} -j(\delta+\beta) & \kappa \\ -\kappa & j(\delta-\beta) \end{bmatrix} = 0$$

The determinantal equation is

$$\delta^2 - \beta^2 + \kappa^2 = 0$$

which leads to

$$\beta = \pm\sqrt{\delta^2 + \kappa^2} \tag{3.26}$$

We see that β is real for all δ unlike for the case of the passive index grating. [7] Even though β is always real, we denote the range $|\delta| \leq |\kappa|$ as the "stop-band" in analogy with the passive index grating. The solution is

$$B(z) = B_+ e^{-j\beta z} + B_- e^{j\beta z} \tag{3.27}$$

Use of equation (3.25) gives

$$A(z) = -\left(\frac{\beta+\delta}{j\kappa}\right) B_+ e^{-j\beta z} + \left(\frac{\beta-\delta}{j\kappa}\right) B_- e^{j\beta z} \tag{3.28}$$

B_+ can be related to B_- by using the fact that the reflection coefficient at $z = l/2$ is Γ_o, that is

$$\frac{B(l/2)}{A(l/2)} = \Gamma_o$$

Using the expressions for $A(z)$ and $B(z)$, we get

$$B_- = -\frac{B_+ e^{-j\beta l}\left[1 + \Gamma_o\left(\frac{\beta+\delta}{j\kappa}\right)\right]}{\left[1 - \Gamma_o\left(\frac{\beta-\delta}{j\kappa}\right)\right]}$$

The above expressions when substituted in (3.27) and (3.28) result in

$$\begin{aligned} B(z) &= \frac{B_+}{1-\Gamma_o\left(\frac{\beta-\delta}{j\kappa}\right)}\left\{\left[1-\Gamma_o\left(\frac{\beta-\delta}{j\kappa}\right)\right]e^{-j\beta z} - e^{-j\beta l}\left[1+\Gamma_o\left(\frac{\beta+\delta}{j\kappa}\right)\right]e^{j\beta z}\right\} \\ A(z) &= \frac{B_+}{1-\Gamma_o\left(\frac{\beta-\delta}{j\kappa}\right)}\left\{\left[-\left(\frac{\beta+\delta}{j\kappa}\right)-\Gamma_o\right]e^{-j\beta z} - e^{-j\beta l}\left[\left(\frac{\beta-\delta}{j\kappa}\right)-\Gamma_o\right]e^{j\beta z}\right\} \end{aligned}$$

It is convenient to define a reflection coefficient $\Gamma(z)$ as function of the distance along

the grating. As we will see $\Gamma(z)$ enables us to find the oscillation condition and the filter characteristics of the GDFB resonator.

$$\Gamma(z) \equiv \frac{B(z)}{A(z)} = \frac{e^{j\beta l}\left[1 - \Gamma_o\left(\frac{\beta-\delta}{j\kappa}\right)\right]e^{-j\beta z} - \left[1 + \Gamma_o\left(\frac{\beta+\delta}{j\kappa}\right)\right]e^{j\beta z}}{e^{j\beta l}\left[-\left(\frac{\beta+\delta}{j\kappa}\right) - \Gamma_o\right]e^{-j\beta z} - \left[\left(\frac{\beta-\delta}{j\kappa}\right) - \Gamma_o\right]e^{j\beta z}} \tag{3.29}$$

For the case that the structure is matched at $z = l/2$, i.e $\Gamma_o = 0$, $\Gamma(z)$ simplifies to

$$\Gamma(z) = \frac{-j\sin\beta(z - l/2)}{j\frac{\beta}{\kappa}\cos\beta(z - l/2) + \frac{\delta}{\kappa}\sin\beta(z - l/2)} \tag{3.30}$$

Notice, $\Gamma(-l/2) = \infty$ when $\delta = 0$ and $|\beta l| = \kappa l = \frac{\pi}{2}$. $\Gamma(-l/2) = B(-l/2)/A(-l/2) = \infty$ means that there is emission from the left end of the structure without an incident wave. The system is, therefore, an oscillator at the threshold of oscillation. Recall that the GDFB resonator alternates gain with loss along the guide and has no DC gain. The fact that the structure lases without DC gain may be puzzling at first. However, a little thought makes it clear why the oscillations occur. The answer lies in the field distribution within the guide. For a matched structure, the amplitudes of the counter-propagating waves at resonance (i.e $\delta = 0$) are given by

$$\begin{aligned} A(z) &= 2je^{j\beta l/2}\cos\beta(z - l/2) \\ B(z) &= -2je^{j\beta l/2}\sin\beta(z - l/2) \end{aligned}$$

Recall that the total z-dependence of the waves is given by

$$a(z) = A(z)e^{-\frac{j\pi z}{\Lambda}}$$

for the forward propagating wave and

$$b(z) = B(z)e^{\frac{j\pi z}{\Lambda}}$$

for the backward travelling wave. We can see from above that at $z = 0$ (and near it) we have two counter propagating waves of equal (and nearly equal) amplitude which

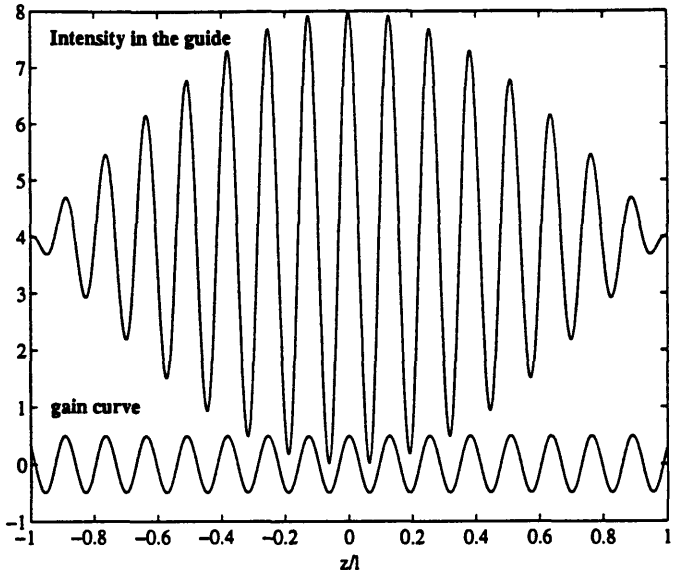

Figure 3-5: Overlay of electric field intensity distribution and gain in the guide

form a standing wave pattern. As we move away from $z = 0$ towards either end, the nature of the waves changes from a pure standing wave to a pure travelling wave. Perfect travelling waves experience no net gain as the GDFB structure alternates gain and loss and a travelling averages the two . On the other hand, a standing wave pattern of appropriate spatial phase whose intensity maxima coincide with regions of gain and whose intensity minima fall under regions of loss experiences net gain. [9] As a result, although the GDFB structure has no DC gain, it does have net gain and this makes it possible for the structure to lase. The intensity in the actual guide at $\delta = 0$ is shown overlayed on the gain curve. In this figure we intentionally chose Λ much larger than its actual value so that the oscillation are easily visible. In a practical device there are hundreds of wavelengths, Λ, across the length of the structure. As expected we see a standing wave near the center where the intensity maxima are aligned with the regions of gain resulting in the optical wave experiencing net gain in the absence of dc gain.

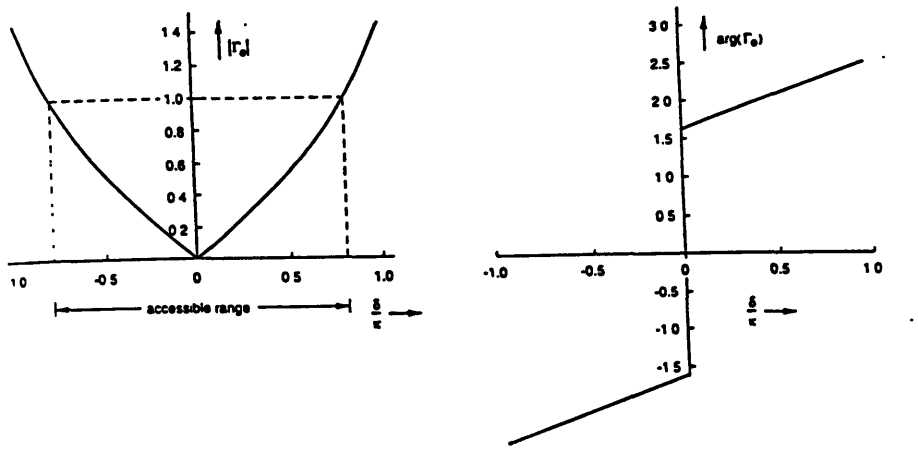

Figure 3-6: Γ_o needed to maintain oscillations

3.3 Tuning the Laser

We know from the previous section that the system is an oscillator if $\Gamma(-l/2) = \infty$ or alternately $\frac{1}{\Gamma(-l/2)} = 0$. Using this condition and (3.29), we see that the system lases at frequency δ_o if

$$e^{j\beta_o l}\left[-\left(\frac{\beta_o + \delta_o}{j\kappa}\right) - \Gamma_o\right] e^{j\beta_o l/2} - \left[\left(\frac{\beta_o - \delta_o}{j\kappa}\right) - \Gamma_o\right] e^{-j\beta_o l/2} = 0$$

where $\beta_o = \sqrt{\delta_o^2 + \kappa^2}$ Solving for Γ_o, we find

$$\Gamma_o = \frac{\beta_o}{\kappa} \cot \beta_o l + j\frac{\delta_o}{\kappa} \tag{3.31}$$

When the above value of Γ_o is presented to the right hand side of the structure by appropriate means, the structure oscillates at the "frequency" δ_o. Thus, we see that by changing Γ_o we may continuously tune the laser . Tuning may be achieved in two ways. In the first scheme the value of κ is kept fixed so that $|\kappa l| = \pi/2$. In this case, the magnitude and phase of Γ_o needed to maintain threshold at δ_o are shown in fig. (3-6) As can be seen from the figure, using this scheme the laser can be tuned over about 80% of the stopband with a passive ($|\Gamma_o| < 1$) external adjustment. Alternately, suppose that $\beta_o l = \pi/2$. In this case, the value of Γ_o needed to make the structure lase at δ_o is given by $\Gamma_o = j\frac{\delta_o}{\kappa}$ using (3.31). As $|\delta_o|$ is increased from zero and $\beta_o l$ is kept fixed at $\pi/2$, smaller and smaller values of κ are needed to maintain

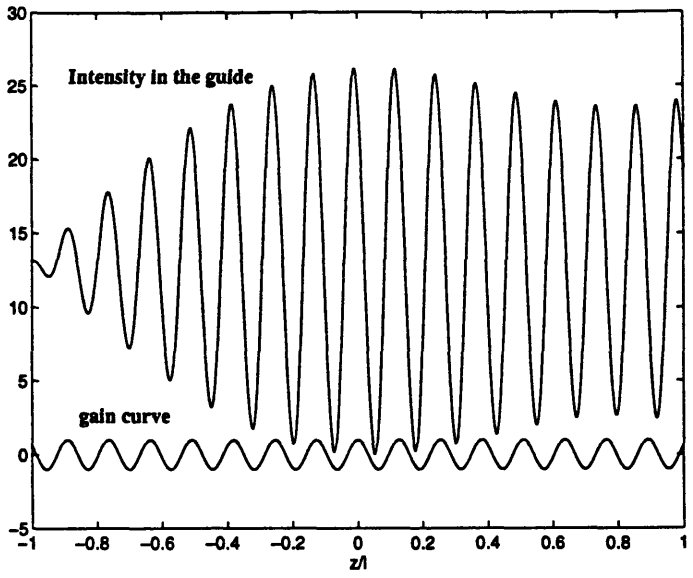

Figure 3-7: Overlay of the electric field intensity distribution and the gain curve for $\frac{\delta_o}{\kappa} = 0.5$

oscillation. If the gain is produced by carrier injection, the current supply to the grating must be decreased. These finding appear to be counter intuitive at first sight. As we move off away from the Bragg frequency, $\delta = 0$ ($\omega = \omega_o$), the effectiveness of the grating is reduced. Why is it then possible to lower the current drive (i.e κ) as the lasing frequency, δ_o, changes and the grating becomes detuned. The answer lies in the nature of the gain of a GDFB structure as explained in the previous section. When a reflection is presented at one end of the structure, the standing wave pattern extends over a larger length of the grating (see fig. (3-7) and compare with fig. (3-5)). As a result, in accordance with the previous discussion, the net gain of the structure increases allowing the frequency to shift inspite of the fact that the effectiveness (phase matching) of the grating is decreased.

3.4 Operation below Threshold

We saw in the previous section that when $\beta_o l = \pi/2$ and a reflection coefficient of $\Gamma_o = j\frac{\delta_o}{\kappa}$ is presented to the right hand side of the grating, the system is a laser

at the threshold of oscillation, with an oscillation "frequency", δ_o. In this case, $|\Gamma(-l/2,\delta_o)| = \infty$ [1] and the bandwidth of $\Gamma(-l/2,\delta_o)$ is zero. Imagine that the current drive (i.e κ) is reduced so that $\beta_o l = \pi/2 - \Delta$ where Δ is positive and $\Delta \ll 1$. The laser is below threshold and the oscillation condition is no longer satisfied exactly. $\Gamma(-l/2,\delta_o)$ becomes finite. Moreover, $\Gamma(-l/2,\delta)$ also acquires a non-zero bandwidth. The reason why the magnitude of $\Gamma(-l/2,\delta_o)$ is reduced is because the field distribution in the guide is altered. The standing waves near the center of the grating are slightly displaced relative to the gain curve so that the intensity maxima no longer coincide with the peak gain. The gain is reduced and Γ becomes finite. The gain grating below threshold acts as a reflection filter with filter characteristics described by $\Gamma(-l/2,\delta)$. Use of (3.29) gives

$$\Gamma(-\frac{l}{2},\delta_o) = \frac{\left[1-\Gamma_o\left(\frac{\beta_o-\delta_o}{j\kappa}\right)\right]e^{j\beta_o l} - \left[1+\Gamma_o\left(\frac{\beta_o+\delta_o}{j\kappa}\right)\right]e^{-j\beta_o l}}{\left[-\left(\frac{\beta_o+\delta_o}{j\kappa}\right)-\Gamma_o\right]e^{j\beta_o l} - \left[\left(\frac{\beta_o-\delta_o}{j\kappa}\right)-\Gamma_o\right]e^{j\beta_o l}}$$

where $\beta_o = \sqrt{\delta_o^2+\kappa^2}$ and $\Gamma_o = j\frac{\delta_o}{\kappa}$. Since $\beta_o l = \frac{\pi}{2} - \Delta$ and $\Delta \ll 1$, a Taylor series expansion reveals that

$$e^{j\beta_o l} \simeq j + \Delta \tag{3.32}$$

$$e^{-j\beta_o l} \simeq -j + \Delta \tag{3.33}$$

Substitution of the above in the expression for Γ, followed by some simplification leads to

$$\Gamma(-\frac{l}{2},\delta_o) = \frac{-\Delta\left(\frac{\beta_o\delta_o}{\kappa^2}\right) + j\left(1+\frac{\delta_o^2}{\kappa^2}\right)}{j\frac{\beta_o}{\kappa}\Delta} \tag{3.34}$$

Thus, the gain of the filter is given by

$$\left|\Gamma(-\frac{l}{2},\delta_o)\right| = \left[\frac{\delta_o^2}{\kappa^2} + \frac{1}{\Delta^2}\left(1+\frac{\delta_o^2}{\kappa^2}\right)\right]^{\frac{1}{2}}$$

[1] Note that we have added δ as an argument of Γ so as to emphasize that Γ varies with δ.

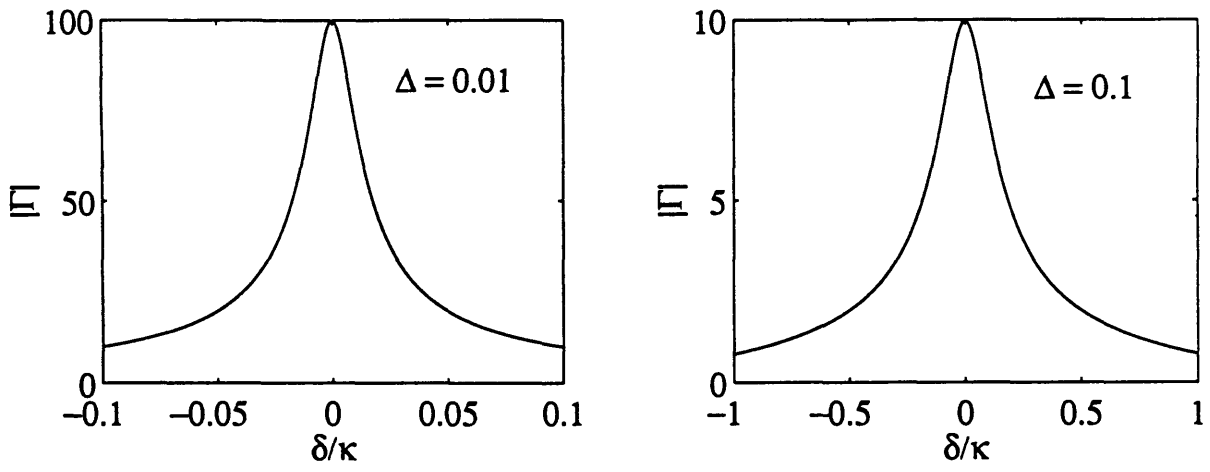

Figure 3-8: Filter characteristics for (a) $\Delta = 0.01$, (b) $\Delta = 0.1$

Since $\Delta \ll 1$, the second term dominates and we can ignore the contribution due to the first term. This leads to

$$\left|\Gamma_o\left(-\frac{l}{2}, \delta_o\right)\right| = \frac{\sqrt{1+\frac{\delta_o^2}{\kappa^2}}}{\Delta} \tag{3.35}$$

The gain is, thus, inversely proportional to Δ and approaches infinity in the limit that $\Delta \to 0$, as expected.

The bandwidth of the filter, $(\Delta\delta)$, is defined as

$$(\Delta\delta) = 2(\delta_{hp} - \delta_o)$$

where δ_{hp} is the half power "frequency" and obeys the following equation

$$\left|\Gamma\left(-\frac{l}{2}, \delta_{hp}\right)\right|^2 = \frac{1}{2}\left|\Gamma\left(-\frac{l}{2}, \delta_o\right)\right|^2 \tag{3.36}$$

To calculate the bandwidth, we thus evaluate δ_{hp} using the above equation. In the following analysis, we assume a sufficiently narrow-band filter such that $\beta_{hp} = \sqrt{\delta_{hp}^2 + \kappa^2}$

is approximately equal to β_o so that

$$\beta_{hp} l \approx \frac{\pi}{2} - \Delta$$

Use of eqs.(3.29), (3.32) and (3.33) leads to

$$\Gamma\left(-\frac{l}{2}, \delta_{hp}\right) = \frac{-\Delta\left(\frac{\beta_{hp}\delta_o}{\kappa^2}\right) + j\left(1 + \frac{\delta_{hp}\delta_o}{\kappa^2}\right)}{-\left(\frac{\delta_{hp}-\delta_o}{\kappa}\right) + j\Delta\frac{\beta_{hp}}{\kappa}}$$

Substituting for δ_{hp} in the above equation and retaining terms to first order , we find that

$$(\Delta\delta) = 2\kappa\Delta\sqrt{1 + \frac{\delta_o^2}{\kappa^2}}. \tag{3.37}$$

This expression yields the correct answer in the limit that Δ approaches zero. The gain and the bandwidth of a matched resonator ($\delta_o = 0$) tuned slightly below threshold such that $\kappa l = \frac{\pi}{2} - \Delta$ is given by

$$|\Gamma(-\frac{l}{2})| = \frac{1}{\Delta} \tag{3.38}$$

$$\frac{(\Delta\delta)}{\kappa} = 2\Delta \tag{3.39}$$

$$\tag{3.40}$$

3.5 Equivalent Circuit for a GDFB Resonator

[9] Equivalent circuits are a convenient and useful way to model optical structures. Not only do they allow circuit synthesis methods to be applied to optical networks, but familiarity with circuits enables greater insight into the workings of the optically devices they model. In this section we develop equivalent circuits for the symmetric gain grating structure shown in fig. (3-9). Unlike the structure of the previous section, this gain grating has reflection coefficients on either ends. Notice that the reflection coefficient of the left-hand side is defined differently from that on the right-hand side. These definitions are, however, consistent with reflection coefficients seen looking into the ports as defined by the arrows in the figure. In order to develop equivalent

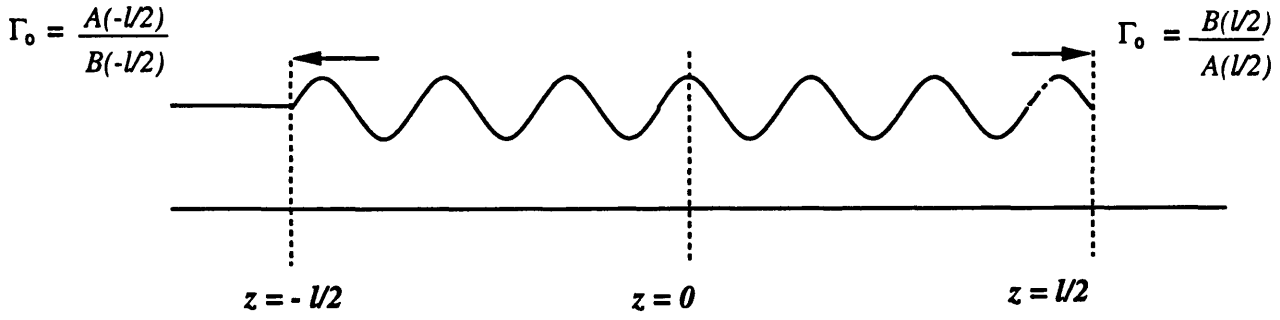

Figure 3-9: Symmetrically loaded GDFB Resonator

circuits, it is necessary to define equivalent voltages and currents. This is done in analogy Transmission Line Theory by defining the "voltage" [9]

$$V(z) = A(z) + B(z)$$

and the "current"

$$I(z) = A(z) - B(z)$$

Voltage and current are written under quotes since V and I actually represent the normalized electric fields and magnetic fields respectively. However, we will drop the quotation marks bearing in mind that they correspond to the total E and H fields in the structure. By appropriately adding and substracting the coupled mode equations we obtain

$$\frac{dV}{dz} = -(\kappa + j\delta)I \tag{3.41}$$

$$\frac{dI}{dz} = (\kappa - j\delta)V \tag{3.42}$$

The symmetric gain grating structure can be modelled using a pi-circuit representation of the form shown in fig. (3-10) where $y_a^{(1)}$ and $y_b^{(1)}$ are susceptances to be determined. This is a completely general representation for a symmetric two-port structure [26]. The two parallel susceptances, $y_a^{(1)}$ are of equal value because the grating looks identical when viewed from either port. $y_a^{(1)}$ and $y_b^{(1)}$ can be evaluated by

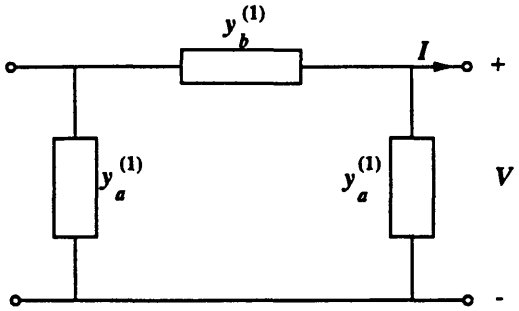

Figure 3-10: Pi-circuit representation of a symmetric structure

considering the symmetric and antisymmetric excitations of the grating. Equations (3.41) and (3.42) can be decoupled by differentiating (3.41) and using (3.42) to obtain

$$\frac{d^2V}{dz} = -\beta^2 V$$

where $\beta^2 = \delta^2 + \kappa^2$. Therefore,

$$V(z) = V_s \cos \beta z + V_a \sin \beta z$$

For a symmetric excitation, $V_a = 0$ (we choose $V_s = V_o$) and we have

$$V(z) = V_o \cos \beta z$$

Use of (3.41) results in

$$I(z) = \frac{\kappa - j\delta}{\beta} = V_o \sin \beta z$$

It is clear from fig. 3-11(a) that for a symmetric excitation, the admittance seen from the right hand side is

$$-\frac{I}{V}\Big|_{z=\frac{l}{2}} = y_a^{(1)} = -\frac{\kappa - j\delta}{\beta} \tan \frac{\beta l}{2} \tag{3.43}$$

The minus sign arises as a result of the way I has been defined (see fig. (3-10)).

To evaluate $y_b^{(1)}$, one must consider the antisymmetric excitation of the grating.

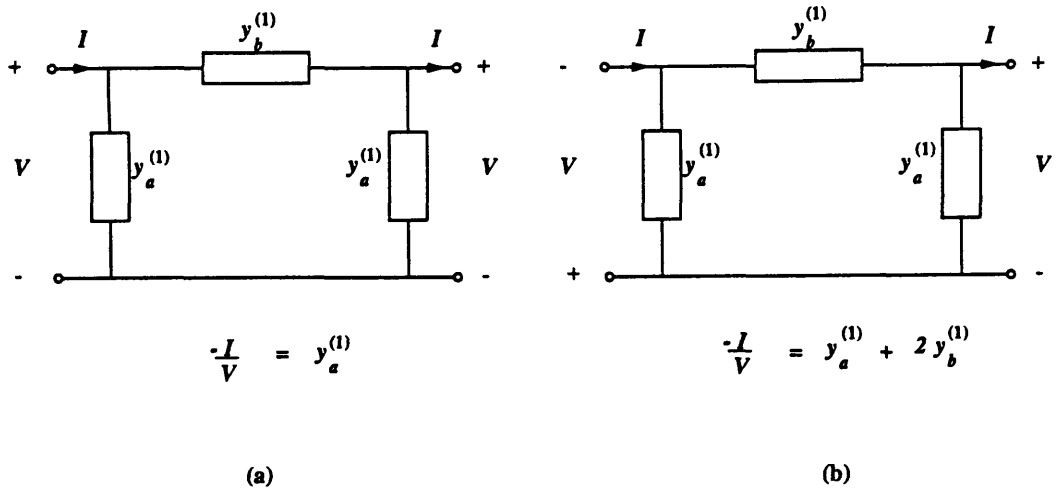

Figure 3-11: (a) Symmetric excitation, (b) Antisymmetric excitation.

In this case

$$V(z) = V_o \sin \beta z$$

$$I(z) = -\frac{\kappa - j\delta}{\beta} V_o \cos \beta z$$

Use of fig. 3-10(b) shows that

$$-I = V(y_a^{(1)} + 2y_b^{(1)})$$

Thus,

$$-\frac{I}{V}\Big|_{z=\frac{l}{2}} = y_a^{(1)} + 2y_b^{(1)} = \frac{\kappa - j\delta}{\beta} \cot \frac{\beta l}{2}$$

which can be solved for $y_b^{(1)}$ to obtain

$$y_b^{(1)} = \frac{\kappa - j\delta}{2\beta} \left[\cot \frac{\beta l}{2} + \tan \frac{\beta l}{2} \right] \tag{3.44}$$

We consider the case of a matched laser, ($\Gamma_o = 0$), that is tuned slightly below threshold i.e $\kappa l = \frac{\pi}{2} - \Delta$. Moreover, we are only concerned with the behavior of the laser near resonance, $\delta = 0$. In this limit of small frequency deviations such that

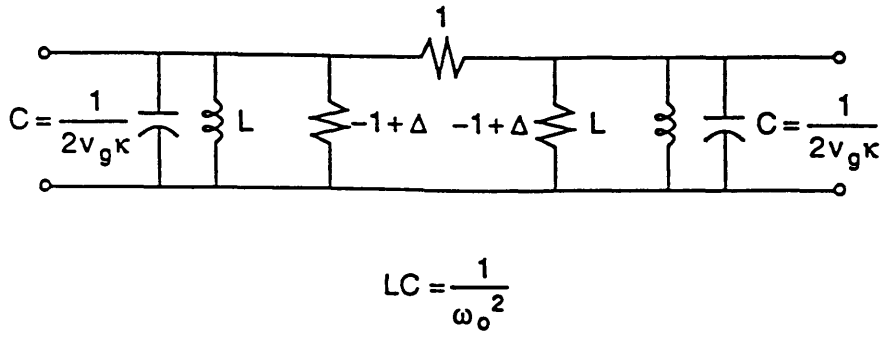

Figure 3-12: Equivalent circuit of a symmetrically matched GDFB resonator

$\delta/\kappa \ll 1$, $\beta \approx \kappa$ and

$$\begin{aligned} \tan\frac{\beta l}{2} &\approx 1-\Delta \\ \cot\frac{\beta l}{2} &\approx 1+\Delta \end{aligned}$$

The above approximation when used in (3.43) and (3.44) results in

$$y_a^{(1)} \approx \Delta - 1 + j\frac{\delta}{\kappa} \tag{3.45}$$

$$y_b^{(1)} \approx (1 - j\frac{\delta}{\kappa}) \tag{3.46}$$

As can be seen from above, $y_a^{(1)}$ is a negative conductance corresponding to the gain in the structure whereas $y_b^{(1)}$ is a positive conductance and corresponds to the loss in the system. A symmetric excitation excites only $y_a^{(1)}$. Hence, a symmetric excitation experiences net gain by placing the electric field maxima at the position of gain. On the other hand, an antisymmetric excitation displaces the field distribution relative to the gain/loss curve so that the intensity maxima fall on loss segments. As a result the conductance accessed by it is positive. The imaginary parts of the admittances correspond to energy storage elements and are responsible for bandwidth limiting. Recall that the admittance of a parallel GLC circuit near resonance, i.e $\omega = \omega_o + \Delta\omega$, is given by

$$y = G + 2j\Delta\omega C$$

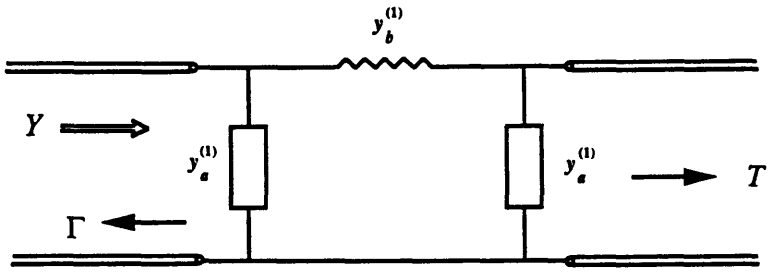

Figure 3-13: Equivalent circuit of a matched GDFB resonator

Comparing the imaginary parts, we get

$$C = \frac{1}{2\kappa v_g}$$

where the imaginary contribution of $y_b^{(1)}$ has been ignored and we have made use of the fact that $\delta = \frac{\Delta\omega}{v_g}$. The complete circuit for a symmetric GDFB resonator is shown in the fig. (3-12).

3.5.1 Comparison of equivalent circuit and exact analysis

Figure (3-13) shows the equivalent circuit a matched GDFB resonator. The response of the grating can easily be derived using standard transmission line theory. The impedance seen looking into the transmission line is Y, as indicated in the figure and is given by

$$\begin{aligned} Y &= y_a^{(1)} + \frac{y_b^{(1)}(1+y_a^{(1)})}{y_b^{(1)} + y_a^{(1)} + 1} \\ &\simeq 2y_a^{(1)} + 1 = 2\left(\Delta + j\frac{\delta}{\kappa}\right) - 1 \end{aligned} \tag{3.47}$$

The reflectivity, Γ of the grating is given by

$$\begin{aligned} \Gamma &= \frac{1-Y}{1+Y} = \frac{1-\left(\Delta + j\frac{\delta}{\kappa}\right)}{\Delta + \frac{\delta}{\kappa}} \\ &\simeq \frac{1}{\Delta + j\frac{\delta}{\kappa}} \end{aligned} \tag{3.48}$$

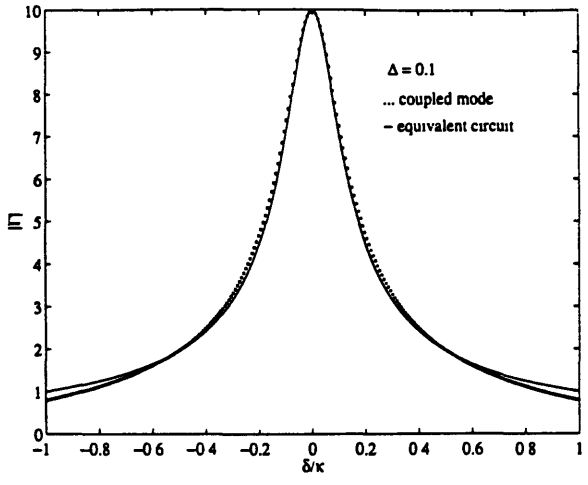

Figure 3-14: Comparison of equivalent circuit (solid line) and exact response (dotted line) for $\Delta = 0.1$

As is obvious from eq. (3.48) the peak gain occurs at $\delta = 0$ and is

$$\Gamma(\delta = 0) = \frac{1}{\Delta}$$

The half frequency points δ_{hp} occur at

$$\frac{\delta_{hp}}{\kappa} = \Delta$$

$$(\Delta\delta) = 2\kappa\Delta$$

as found before, eqs. (3.38) and (3.39). Moreover the transmitivity, T, of the grating is given by

$$\begin{aligned} T &= 1 + \Gamma = 1 + \frac{1}{\Delta + j\frac{\delta}{\kappa}} \\ &\simeq \frac{1}{\Delta + j\frac{\delta}{\kappa}} = \Gamma \end{aligned} \tag{3.49}$$

We see that to lowest order the transmittivity is equal to the reflectivity Γ. Figure (3-14) compares the response of the grating computed using the exact analysis and the equivalent circuit. The fit is very good. For the case of the single GDFB resonator

the advantage gained from using an equivalent circuit is not obvious. However, as we will see in the following chapters, equivalent circuits are very powerful and useful in analyzing more complicated structures where the mathematics becomes complicated. For these cases equivalent circuits provide a very simple and intuitive approach to solving these problems.

Chapter 4

Two Coupled Resonators

In the previous chapter we reviewed, in detail, the behavior of a single GDFB resonator. We saw that a GDFB resonator below threshold acts as a reflection filter. This filter is a single-pole filter with a Lorentzian response. Frequencies near the resonant frequency of the resonator are strongly reflected while those further away fall off inversely with frequency, characteristic of a first-order system. In many application it is advantageous to use higher-order systems. Two coupled resonator constitute the simplest higher-order system and this chapter will be devoted to their study. From the previous chapter, we saw that equivalent circuits are a convenient way of gaining insight into GDFB structures and we will focus on deriving an equivalent circuit for two coupled resonators. Coupled resonators are interesting because their frequency responses may be shaped by pole manipulation and also because they form the basic component of higher-order channel dropping filters. Moreover, the study of two coupled resonator also serves to increase our intuition about how adjacent resonators interact. Gaining an understanding of this will prove to be essential in the study of channel-dropping filters which are the topic of the subsequent chapters.

4.1 Two Evanescently Coupled Resonators

Figure (4-1) shows a schematic representation of two coupled resonators where μ is the parameter characterising the coupling strength. In the limit that the resonators

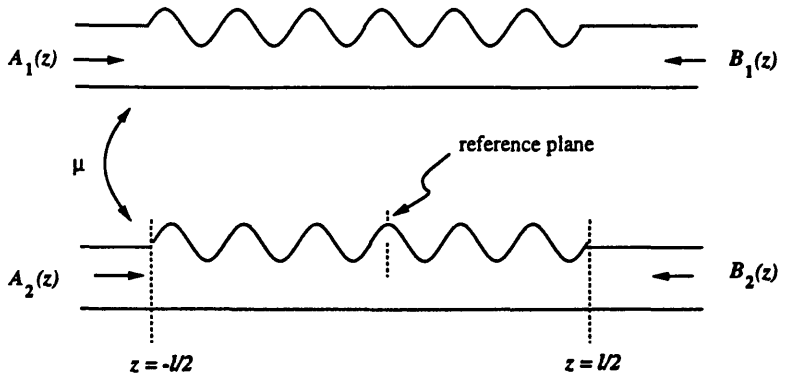

Figure 4-1: Two evanescently coupled GDFB resonators.

are very far apart and do not interact with each other (i.e $\mu \rightarrow 0$) the equations describing A_i, B_i $(i = 1, 2)$ were derived in chapter 2. However, when the resonators are close to one another the forward travelling wave A_1, in resonator 1 can couple to and excite the forward travelling wave A_2 in resonator 2 and vice-versa. Likewise, B_1 can couple to B_2 and vice-versa. This is similar to what was observed in chapter 2 when two guides were fabricated close to one another. As in that case, the equations of the isolated systems are modified through the introduction of the coupling term. The equations of the two coupled resonators, therefore, are:

$$\frac{dA_1}{dz} = -j\delta A_1 + \kappa B_1 - j\mu A_2 \tag{4.1}$$

$$\frac{dA_2}{dz} = -j\delta A_2 + \kappa B_2 - j\mu A_1 \tag{4.2}$$

$$\frac{dB_1}{dz} = j\delta B_1 - \kappa A_1 + j\mu B_2 \tag{4.3}$$

$$\frac{dB_2}{dz} = j\delta B_2 - \kappa A_2 + j\mu B_1 \tag{4.4}$$

The fact that $-j\mu \rightarrow j\mu$ for the backward travelling wave follows from arguments of time reversibility [7].

We digress slightly at this point to make a few observations. First of all, notice that there are two coupling coefficients, namely κ and μ, in eqs. (4.1), (4.2), (4.3) and (4.4). These coupling coefficients are produced by and correspond to two very different

physical mechanisms. κ represents the coupling between the counter propagating waves of the same mode in the GDFB resonator. This coupling occurs due to the presence of the periodic gain/loss variations along the resonator and is given by eq. (3.15). On the other hand, μ represents the coupling between co-directional modes of adjacent waveguides which are sufficiently close to one another. The forward travelling mode of resonator 1 couples only to the forward propagating wave in resonator 2 and vice-versa. It cannot directly couple to a backward mode of the adjacent resonator except via the coupling between A_2 and B_2. The fact that we have the same δ parameters in (4.1)...(4.4) means that the isolated structures are assumed to have identical propagation constants and are, therefore, synchronous. Finally, it must be stressed that the above equations are valid in the weak coupling limit in which perturbation theory allows "adding on" coupling terms to the equations of the isolated resonators.

4.1.1 Equivalent Circuit for Two Coupled Resonators

In this section, we will derive the equivalent circuit for the two coupled resonators of fig. (4-1). The approach followed is very similar to that of the previous chapter. As before, we begin by defining the "voltages" and "currents".

$$V_i = A_i + B_i \tag{4.5}$$

$$I_i = A_i - B_i, \tag{4.6}$$

where V_i and I_i are the normalized electric and magnetic fields respectively in resonator i. It is obvious from fig. (4-1) that the system of two coupled resonators is symmetric about $z = 0$. The reference plane defining κ was deliberately chosen at the peak of the gain so as to preserve this symmetry. A symmetric two port, as we saw earlier, may be represented by a symmetric pi-circuit. The coupled resonator system is a four port device. However, by forcing that the system is only excited through resonator 2, i.e $A_1(-l/2) = B_1(l/2) = 0$, it is a two port device. Therefore, the equivalent circuit representing the coupled resonator system, as viewed from resonator 2

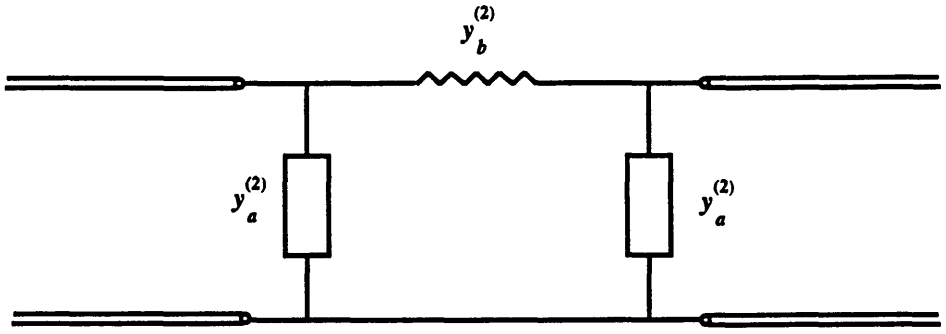

Figure 4-2: Pi-circuit representation of 2 coupled GDFB resonators.

ports, is the pi-circuit of fig. (4-2). $y_a^{(2)}$ and $y_b^{(2)}$ are the admittance seen looking into the input ports of resonator 2 at $z = \pm l/2$. The superscript (2) differentiates the admittances of the two resonator case from those of the single resonator $y_a^{(1)}$ etc, found in chapter 2. The main simplification that a symmetric structure offers is that it allows $y_a^{(2)}$ and $y_b^{(2)}$ to be found by considering only the symmetric and antisymmetric excitations of the system. Once these admittances are known the response of the system to an arbitrary excitation may be computed quite readily.

In what follows, the equations describing V_i and I_i will be written down. Using these equations explicit expressions for I_1, I_2 and V_2 will be found in terms of V_1 such that if V_1 were known, the other three quantities can be calculated. For the case of symmetric and antisymmetric excitations, the expression for V_1 is trivial and the admittances $y_a^{(2)}$ and $y_b^{(2)}$ can be readily computed. The equation governing V_i and I_i are obtained by adding and subtracting eqs. (4.1)...(4.4).

$$\frac{dV_1}{dz} = -(j\delta + \kappa)I_1 - j\mu I_2 \tag{4.7}$$

$$\frac{dV_2}{dz} = -j\mu I_1 - (j\delta + \kappa)I_2 \tag{4.8}$$

$$\frac{dI_1}{dz} = (\kappa - j\delta)V_1 - j\mu V_2 \tag{4.9}$$

$$\frac{dI_2}{dz} = -j\mu V_1 + (\kappa - j\mu)V_2 \tag{4.10}$$

For an assumed solution of the form $\vec{V} = \vec{V}_o e^{j\beta z}$, the

$$\det \begin{bmatrix} -j\beta & 0 & -(j\delta+\kappa) & -j\mu \\ 0 & -j\beta & -j\mu & -(j\delta+\kappa) \\ (\kappa - j\delta) & -j\mu & -j\beta & 0 \\ -j\mu & (\kappa - j\delta) & 0 & -j\beta \end{bmatrix} = 0 \tag{4.11}$$

for a non-trivial solution. The determinantal equation is

$$\beta^4 - 2(\kappa^2 + \delta^2 + \mu^2)\beta^2 + \delta^4 - 2\mu^2\delta^2 + 2\kappa^2\delta^2 + (\mu^2 + \kappa^2)^2 = 0 \tag{4.12}$$

which is quadratic in β^2 and can be solved to yield

$$\beta = \pm\{\kappa^2 + (\delta \pm \mu)^2\}^{1/2}. \tag{4.13}$$

Let us make the following definitions

$$\pm\beta_a \equiv \pm\{\kappa^2 + (\delta + \mu)^2\}^{1/2}, \tag{4.14}$$

$$\pm\beta_b \equiv \pm\{\kappa^2 + (\delta - \mu)^2\}^{1/2}. \tag{4.15}$$

In the following analysis, we will be interested in the response of the system near the lasing frequency of the individual resonator (i.e $\delta = 0$). Moreover, we will assume that coupling between the resonators is weak which is consistent with equations (4.1...4.4). Stated explicitly, it will be assumed that

$$\frac{\delta^2}{\kappa^2} \ll 1, \quad \frac{\mu^2}{\kappa^2} \ll 1, \quad \frac{2\mu\delta}{\kappa^2} \ll 1$$

Using the above, β_a and β_b can be approximated as

$$\beta_a \simeq \kappa\left(1 + \frac{(\delta+\mu)^2}{2\kappa^2}\right) \tag{4.16}$$

$$\beta_b \simeq \kappa\left(1 + \frac{(\delta-\mu)^2}{2\kappa^2}\right) \tag{4.17}$$

$$\tag{4.18}$$

We proceed to write down explicit equations for I_1, I_2 and V_2 in terms of V_1. Substituting for $-j\mu V_2$ from equation (4.9) into equation (4.10), we find that

$$-j\mu\frac{dI_2}{dz} = (\kappa - j\delta)\left[\frac{dI_1}{dz} - (\kappa - j\delta)V_1\right] - \mu^2 V_1. \tag{4.19}$$

Differentiating equation (4.7) with respect to z and substituting for $\frac{dI_2}{dz}$ in the above equations, we get

$$\frac{d^2V_1}{dz^2} + (j\delta + \kappa)\frac{dI_1}{dz} = (\kappa - j\delta)\frac{dI_1}{dz} - \left[(\kappa - j\delta)^2 + \mu^2\right] V_1$$

$\Rightarrow$

$$\frac{dI_1}{dz} = \frac{j}{2\delta}\left\{\left[(\kappa - j\delta)^2 + \mu^2\right] V_1 + \frac{d^2V_1}{dz^2}\right\} \tag{4.20}$$

From equation (4.7), we have

$$I_2 = \frac{j}{\mu}\left[\frac{dV_1}{dz} + (\kappa + j\delta)I_1\right] \tag{4.21}$$

and finally from equation (4.9), we have

$$V_2 = \frac{j}{\mu}\left[\frac{dI_1}{dz} - (\kappa - j\delta)V_1\right] \tag{4.22}$$

Next we turn our attention to finding V_1. In general, for an arbitrary excitation of the two resonator system, V_1 is given by

$$V_1 = V_a^+ e^{j\beta_a z} + V_a^- e^{-j\beta_a z} + V_b^+ e^{j\beta_b z} + V_b^- e^{-j\beta_b z},$$

where the constants $V_a^{\pm}$ and $V_b^{\pm}$ are determined from the boundary conditions. Such a calculation can be quite mathematically involved even for the simplest boundary conditions. Instead we exploit the symmetry of the problem.

4.1.2 Symmetric Excitation

For a symmetric excitation (symmetry is defined with respect to the **E** fields), the response V_1 must be symmetric and we immediately recognize that $V_a^+ = V_a^- \equiv V_a/2$ and $V_b^+ = V_b^- \equiv V_b/2$. Thus,

$$V_1 = V_a \cos \beta_a z + V_b \cos \beta_b z. \tag{4.23}$$

Substituting for V_1 in equation (4.20) we get

$$\frac{dI_1}{dz} = \frac{j}{2\delta} \left\{ \left[(\kappa - j\delta)^2 + \mu^2 - \beta_a^2 \right] V_a \cos \beta_a z + \left[(\kappa - j\delta)^2 + \mu^2 - \beta_b^2 \right] V_b \cos \beta_b z \right\} \tag{4.24}$$

but

$$(\kappa - j\delta)^2 + \mu^2 - \beta_a^2 = -2\delta(\delta + j\kappa + \mu)$$

and

$$(\kappa - j\delta)^2 + \mu^2 - \beta_b^2 = -2\delta(\delta + j\kappa - \mu)$$

which follows simply by substituting for β_a^2 and β_b^2 from eq. (4.14) and (4.15) in the above expressions. Eq. (4.24) can be integrated to yield

$$I_1 = -j \left[\frac{(\delta + \mu + j\kappa)}{\beta_a} V_a \sin \beta_a z + \frac{(\delta - \mu + j\kappa)}{\beta_b} V_b \sin \beta_b z \right] \tag{4.25}$$

Use of eq. (4.22) and the above expression gives

$$V_2 = V_a \cos \beta_a z - V_b \cos \beta_b z \tag{4.26}$$

Moreover,

$$I_2 = \frac{j}{\mu} \left[\frac{dV_1}{dz} + (\kappa + j\delta) I_1 \right]$$

Consider first the term

$$(\kappa + j\delta) I_1 \;=\; -j(\kappa + j\delta) \left[\frac{(\delta + \mu + j\kappa)}{\beta_a} V_a \sin \beta_a z + \frac{(\delta - \mu + j\kappa)}{\beta_b} V_b \sin \beta_b z \right]$$

$$= \frac{\kappa}{\beta_a}\kappa\left(1+j\frac{\delta}{\kappa}\right)\left\{\left[1-j\frac{(\delta+\mu)}{\kappa}\right]V_a\sin\beta_a z+\left[1-j\frac{(\delta-\mu)}{\kappa}\right]\left(\frac{\beta_a}{\beta_b}\right)V_b\sin\beta_b z\right\}$$
$$= \frac{\kappa}{\beta_a}\left\{\kappa\left[1-j\frac{\mu}{\kappa}+\frac{\delta}{\kappa}\left(\frac{\delta+\mu}{\kappa}\right)\right]V_a\sin\beta_a z+\kappa\left[1+j\frac{\mu}{\kappa}+\frac{\delta}{\kappa}\left(\frac{\delta-\mu}{\kappa}\right)\right]\left(\frac{\beta_a}{\beta_b}\right)V_b\sin\beta_b z\right\}$$

In the above expression, both first and second order terms have been retained. It is necessary to keep the second order terms at this stage to ensure the correct answer as we will see later. Use of eqs. (4.16) and (4.17) gives

$$\frac{\beta_a}{\beta_b}=\frac{\left[1+\frac{(\delta+\mu)^2}{2\kappa^2}\right]}{\left[1+\frac{(\delta-\mu)^2}{2\kappa^2}\right]}\simeq 1+\frac{2\mu\delta}{\kappa^2} \tag{4.27}$$

Substituting the above results in eq. (4.21) and simplifying we get

$$I_2 = j\frac{1}{(\mu/\kappa)}\frac{\kappa}{\beta_a}\left\{\left[1-j\frac{\mu}{\kappa}+\frac{\delta}{\kappa}\left(\frac{\delta+\mu}{\kappa}\right)-\frac{\beta_a^2}{\kappa^2}\right]V_a\sin\beta_a z + \left(\left[1+j\frac{\mu}{\kappa}+\frac{\delta}{\kappa}\left(\frac{\delta-\mu}{\kappa}\right)\right]\left(1+\frac{2\mu\delta}{\kappa^2}\right)-\frac{\beta_a\beta_b}{\kappa^2}\right)V_b\sin\beta_b z\right\}$$

The terms in the parenthesis are correct to second order. However, there is division by (μ/κ) so that the overall expression for I_2 is correct only to first order.

$$\frac{\beta_a\beta_b}{\kappa^2} \simeq \left[1+\frac{(\delta+\mu)^2}{2\kappa^2}\right]\left[1+\frac{(\delta-\mu)^2}{2\kappa^2}\right] \simeq 1+\frac{\delta^2+\mu^2}{\kappa^2} \tag{4.28}$$

Using this we find that

$$I_2 = \frac{j\kappa}{\mu\beta_a}\left\{\kappa\left[1-j\frac{\mu}{\kappa}+\frac{\delta}{\kappa}\left(\frac{\delta+\mu}{\kappa}\right)-\left(\frac{\delta+\mu}{\kappa}\right)^2-1\right]V_a\sin\beta_a z + \kappa\left[1+j\frac{\mu}{\kappa}+\frac{\delta}{\kappa}\left(\frac{\delta-\mu}{\kappa}\right)+\frac{2\mu\delta}{\kappa^2}-1-\frac{(\delta^2+\mu^2)}{\kappa^2}\right]V_b\sin\beta_b z\right\}$$
$$= \frac{j\kappa}{\mu\beta_a}\left\{\left[-j\mu-\mu\left(\frac{\delta+\mu}{\kappa}\right)\right]V_a\sin\beta_a z+\left[j\mu+\mu\left(\frac{\delta-\mu}{\kappa}\right)\right]V_b\sin\beta_b z\right\},$$

where terms higher than second-order have been ignored. This simplifies to

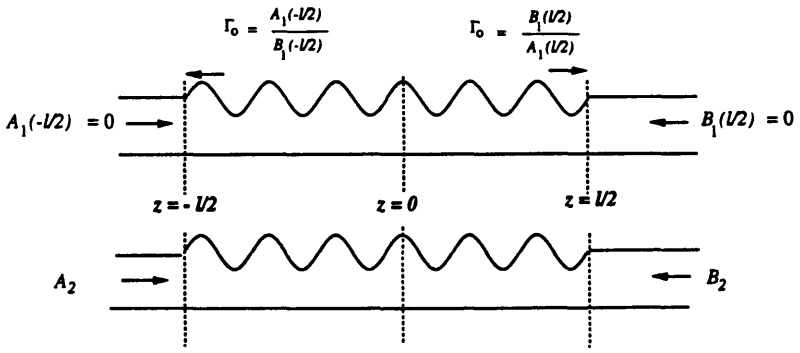

Figure 4-3: Boundary conditions of resonator 1

$$I_2 = \frac{\kappa}{\beta_a}\left\{\left[1 - j\left(\frac{\delta+\mu}{\kappa}\right)\right] V_a \sin\beta_a z - \left[1 - j\left(\frac{\delta-\mu}{\kappa}\right)\right] V_b \sin\beta_b z\right\} \tag{4.29}$$

To relate V_b to V_a, the boundary conditions of the problem have to be considered. As was mentioned earlier and as shown in fig. (4-3), $A_1(-l/2) = B_1(l/2) = 0$. Alternately, resonator 1 is matched at both ends, i.e $\Gamma_o = \frac{B_1(l/2)}{A_1(l/2)} = 0$. We know from standard Transmission Line Theory that the reflection coefficient seen looking into $z = l/2$, Γ_o, is given by

$$\Gamma_o = \frac{Z_n - 1}{Z_n + 1}$$

where Z_n is the normalized impedance of the line. A match at $z = l/2$ implies that

$$Z_n = \frac{V_1(l/2)}{I_1(l/2)} = 1.$$

The matched condition is automatically met at $z = -l/2$ if the above equation is satisfied. Thus, V_a and V_b are related by the equation

$$Z_n = \frac{V_1(l/2)}{I_1(l/2)} = \frac{\cos\beta_a\frac{l}{2} + \left(\frac{V_b}{V_a}\right)\cos\beta_b\frac{l}{2}}{-j\left[\left(\frac{\delta+\mu+j\kappa}{\beta_a}\right)\sin\beta_a\frac{l}{2} + \left(\frac{\delta-\mu+j\kappa}{\beta_b}\right)\left(\frac{V_b}{V_a}\right)\sin\beta_b\frac{l}{2}\right]} = 1$$

To lowest order $\beta_a \simeq \beta_b \simeq \kappa$ and the above expression simplifies to

$$Z_n \simeq \frac{\cot \kappa \frac{l}{2} \left[1 + \frac{V_b}{V_a}\right]}{\left[1 - j\left(\frac{\delta+\mu}{\kappa}\right)\right] + \left[1 - j\left(\frac{\delta-\mu}{\kappa}\right)\right]\left(\frac{V_b}{V_a}\right)} = 1. \tag{4.30}$$

As in chapter 2, we are interested in the case when the two resonators are below threshold and $\kappa l = \pi/2 - \Delta$, where $\Delta \ll 1$. A simple Taylor series expansion shows that $\cot \kappa l/2 \simeq 1 + \Delta$. Using this and eq. (4.30), we find that

$$\frac{V_b}{V_a} = -\frac{\left[\Delta + j\left(\frac{\delta+\mu}{\kappa}\right)\right]}{\left[\Delta + j\left(\frac{\delta-\mu}{\kappa}\right)\right]}. \tag{4.31}$$

With V_b/V_a known, $y_a^{(2)}$ may be computed. For a symmetric excitation, $y_a^{(2)}$ is given by

$$y_a^{(2)} = \frac{-I_2(l/2)}{V_2(l/2)} = \frac{-\frac{\kappa}{\beta_a}\left(\left[1 - j\left(\frac{\delta+\mu}{\kappa}\right)\right]\sin\beta_a\frac{l}{2} - \left[1 - j\left(\frac{\delta-\mu}{\kappa}\right)\right]\left(\frac{V_b}{V_a}\right)\sin\beta_b\frac{l}{2}\right)}{\left(\cos\beta_a\frac{l}{2} - \left(\frac{V_b}{V_a}\right)\cos\beta_b\frac{l}{2}\right)}.$$

Again assuming that $\beta_a \simeq \beta_b \simeq \kappa$, we have

$$\begin{aligned} y_a^{(2)} &= \frac{-(1-\Delta)\left\{\left(1 - j\frac{\delta}{\kappa}\right)\left(1 - \frac{V_b}{V_a}\right) - j\frac{\mu}{\kappa}\left(1 + \frac{V_b}{V_a}\right)\right\}}{\left(1 - \frac{V_b}{V_a}\right)} \\ &= (\Delta - 1)\left\{1 - j\frac{\delta}{\kappa} - j\frac{\mu}{\kappa}\frac{(1 + V_b/V_a)}{(1 - V_b/V_a)}\right\} \end{aligned}$$

where we have used the fact that $\tan \kappa l/2 = 1 - \Delta$. Use of eq. (4.31) gives

$$\begin{aligned} \frac{1 + V_b/V_a}{1 - V_b/V_a} &= \frac{-j(\mu/\kappa)}{\Delta + j(\delta/\kappa)} \qquad \Rightarrow \\ y_a^{(2)} &= (\Delta - 1)\left\{1 - j\frac{\delta}{\kappa} - \frac{\mu^2/\kappa^2}{\Delta + j\frac{\delta}{\kappa}}\right\} \\ y_a^{(2)} &\simeq (\Delta - 1) + j\frac{\delta}{\kappa} + \frac{\mu^2/\kappa^2}{\Delta + j\frac{\delta}{\kappa}}. \end{aligned} \tag{4.32}$$

The above expression can be written in a form that is more revealing:

$$y_a^{(2)} = y_a^{(1)} + \frac{\mu^2/\kappa^2}{y_a^{(1)} + 1}, \tag{4.33}$$

where $y_a^{(1)}$ are the admittances of the isolated GDFB resonators found in chapter 2. We shall interpret this result later.

4.1.3 Antisymmetric Excitation

To calculate $y_b^{(2)}$ an analysis similar to the one presented must be performed for an antisymmetric excitation of the system. For an antisymmetric excitation, the response V_1 must be also be antisymmetric $\Rightarrow$

$$V_1 = V_a \sin \beta_a z + V_b \sin \beta_b z \tag{4.34}$$

Use of eqs. (4.20), (4.14) and (4.15) gives

$$I_1 = j \left\{ \frac{(\delta + \mu + j\kappa)}{\beta_a} V_a \cos \beta_a z + \frac{(\delta - \mu + j\kappa)}{\beta_b} V_b \cos \beta_b z \right\}. \tag{4.35}$$

Substituting into eq. (4.22), we get that

$$V_2 = V_a \sin \beta_a z - V_b \sin \beta_b z. \tag{4.36}$$

Finally,

$$I_2 = \frac{j}{\mu} \left[\frac{dV_1}{dz} + (j\delta + \kappa) I_1 \right]$$

but

$$\begin{aligned} (j\delta + \kappa) I_1 \;=\; & j \frac{j\kappa}{\beta_a} \kappa \left(1 + j \frac{\delta}{\kappa} \right) \left\{ \left[1 - j \left(\frac{\delta + \mu}{\kappa} \right) \right] V_a \cos \beta_a z \right. \\ & \left. + \left[1 - j \left(\frac{\delta - \mu}{\kappa} \right) \right] \left(\frac{\beta_a}{\beta_b} \right) V_b \cos \beta_a z \right\}. \end{aligned}$$

Retaining both the first and second order terms and using eq. (4.27) the above expression can be simplified to yield

$$\begin{aligned}(\kappa + j\delta)I_1 &= \frac{-\kappa}{\beta_a}\left\{\kappa\left[1 - j\frac{\mu}{\kappa} + \frac{\delta}{\kappa}\left(\frac{\delta+\mu}{\kappa}\right)\right]V_a\cos\beta_a z \right. \\ &\qquad \left. + \kappa\left[1 + j\frac{\mu}{\kappa} + \frac{\delta}{\kappa}\left(\frac{\delta+\kappa}{\kappa}\right)\right]V_b\cos\beta_b z\right\}\end{aligned}$$

The above result when substituted into eq. (4.21), gives

$$I_2 = \frac{\kappa}{\beta_a}\left\{\left[-1 + j\left(\frac{\delta+\mu}{\kappa}\right)\right]V_a\cos\beta_a z + \left[1 - j\left(\frac{\delta-\mu}{\kappa}\right)\right]V_b\cos\beta_b z\right\} \qquad (4.37)$$

where use of eqs. (4.28) and (4.34) was made. From the matched boundary relation we have that

$$Z_n = \frac{V_1(l/2)}{I_1(l/2)} = 1 \qquad \Rightarrow$$

$$\frac{\sin\beta_a\frac{l}{2} + \frac{V_b}{V_a}\sin\beta_b\frac{l}{2}}{j\left\{\left(\frac{\delta+\mu+j\kappa}{\beta_a}\right)\cos\beta_a\frac{l}{2} + \left(\frac{\delta-\mu+j\kappa}{\beta_b}\right)\cos\beta_b\frac{l}{2}\right\}} = 1.$$

To lowest order $\beta_a \simeq \beta_b \simeq \kappa$. Moreover, $\kappa l = \pi/2 - \Delta \Rightarrow \tan\kappa l/2 \simeq 1 - \Delta$. Incorporating these approximations, into the above equation we find that

$$\frac{V_b}{V_a} = \frac{-\left[2 - \Delta - j\left(\frac{\delta+\mu}{\kappa}\right)\right]}{\left[2 - \Delta - j\left(\frac{\delta-\mu}{\kappa}\right)\right]} \qquad (4.38)$$

For an antisymmetric excitation, we know that

$$\begin{aligned}y_a^{(2)} + 2y_b^{(2)} &= \frac{-I_2(l/2)}{V_2(l/2)} \\ &= \frac{\kappa/\beta_a\left\{\left[1 - j\left(\frac{\delta+\mu}{\kappa}\right)\right]\cos\beta_a l/2 - \left[1 - j\left(\frac{\delta-\mu}{\kappa}\right)\right]\frac{V_b}{V_a}\cos\beta_b l/2\right\}}{\sin\beta_a l/2 - \frac{V_b}{V_a}\sin\beta_b l/2} \\ &\simeq \cot\frac{\kappa l}{2}\left[1 - j\frac{\delta}{\kappa} - j\frac{\mu}{\kappa}\left(\frac{1 + V_b/V_a}{1 - V_b/V_a}\right)\right]\end{aligned}$$

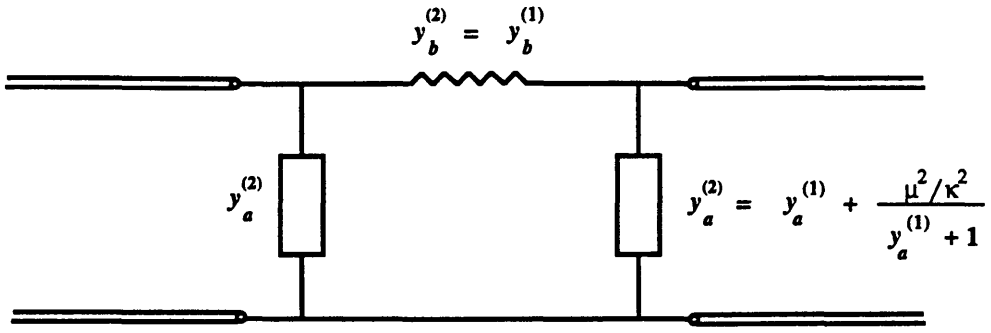

Figure 4-4: Equivalent circuit of two evanescently coupled resonators

Substituting for $y_a^{(2)}$ and solving for $y_b^{(2)}$, we get

$$y_b^{(2)} \simeq \left(1 - j\frac{\delta}{\kappa}\right) - \frac{\mu^2/\kappa^2}{2\left(\Delta + j\frac{\delta}{\kappa}\right)} \approx 1 \tag{4.39}$$

to lowest order.

Recapitulating,

$$y_a^{(2)} = (\Delta - 1) + j\frac{\delta}{\kappa} + \frac{\mu^2/\kappa^2}{\Delta + j\frac{\delta}{\kappa}} = y_a^{(1)} + \frac{\mu^2/\kappa^2}{y_a^{(1)}+1}, \tag{4.40}$$

$$y_b^{(2)} \simeq 1 = y_b^{(1)}. \tag{4.41}$$

We see that the equivalent circuit for the coupled resonators, (fig. (4-4)), looks very similar to that of the isolated resonator except for the additional admittance $\left(\frac{\mu^2/\kappa^2}{y_a^{(1)}+1}\right)$ in parallel with $y_a^{(1)}$. The circuit of fig. (4-4) can be redrawn to explicitly show the coupling between the equivalent circuits of the individual resonators (see fig. (4-5)). The coupling between the resonators is represented by the transformer coils with the turns ratio of $n1/n2$. The coupling is mediated by a quarter-wave section which is necessary to invert the admittance of resonator 1 appearing across the paralled branches of resonator 2. Note that $y_b^{(2)} = y_b^{(1)}$, implying that the series admittance, $y_b^{(1)}$ of resonator 1 is not "sensed" at resonator 2. Recall that only a antisymmetric excitation accesses series admittances. The fact that $y_b^{(1)}$ is not "felt" across resonator 2 suggests that an antisymmetric excitation does not couple

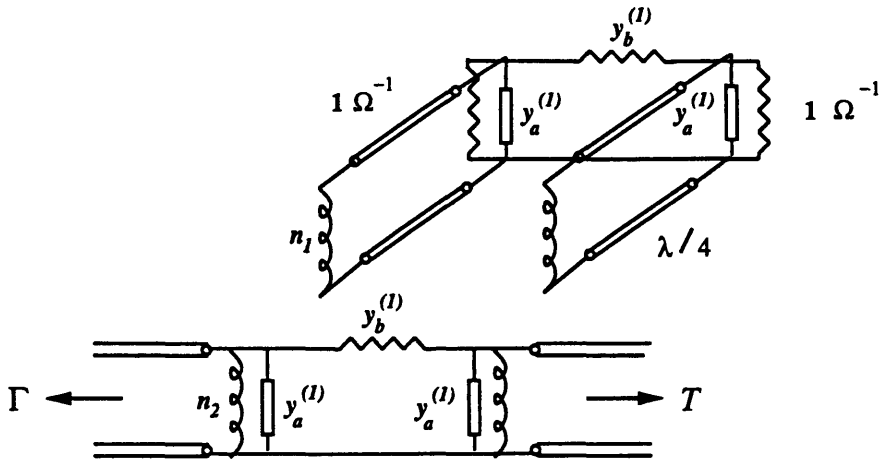

Figure 4-5: Equivalent circuit of the 2 coupled GDFB resonators drawn to explicitly show the equivalent circuit of the individual resonators and the coupling between them.

to resonator 1. This is indeed the case and is clearly seen if we look at eq. (4.38). For an antisymmetric excitation, to lowest order

$$\frac{V_b}{V_a} \simeq -1$$

Substituting this into the expression for V_1, eq. (4.34) and realizing that $\beta_a \simeq \beta_b \simeq \kappa$, we see that

$$V_1 = V_a \sin \kappa z + V_b \sin \kappa z = 0$$

for a non-zero V_2. Thus, to lowest order the antisymmetric excitation does not couple from resonator 2 to resonator 1. To determine the turns ratio, we calculate the total admittance seen across the parallel branches of resonator 2 and equate it to $y_a^{(2)}$. Transforming the total parallel admittance of resonator 1 across the quarter-wave section and using the transformer relation, we find that

$$\begin{aligned} y_a^{(2)} &= y_a^{(1)} + \left(\frac{n_1}{n_2}\right)^2 \frac{1}{\left(y_a^{(1)}+1\right)} \qquad \Rightarrow \\ \frac{n_1}{n_2} &= \frac{\mu}{\kappa}. \end{aligned}$$

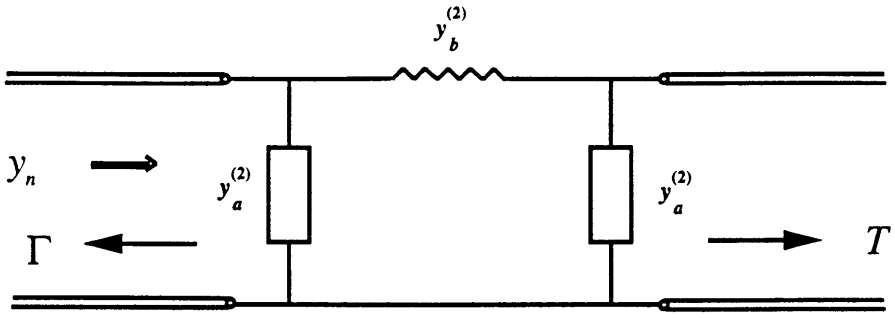

Figure 4-6: Equivalent circuit of the 2 coupled GDFB resonators viewed from resonator 2 ports.

With the coupling ratio determined, the equivalent circuit is complete. Moreover, it makes good physical sense. The two conductances of unity value model the matched ends of resonator 1. As expected from physical reasoning the coupling between the two resonators (modelled by the transformer coils) is related to the strength of the coupling parameter, μ. However, the equivalent circuit analysis reveals that μ/κ and not μ is the relevant parameter. The quarter-wave section leading up to the transformer coils represents the inherent time delay involved in the coupling of the excitation from resonator 2 to resonator 1. Finally, the fact that the antisymmetric excitation does not couple to resonator 1 explains why $y_b^{(2)} \simeq y_b^{(1)}$.

4.2 Comparison of the equivalent circuit with the exact analysis

The equivalent circuit allows us to calculate analytical expressions for the transmitted signal ($A_2(l/2)$), the reflected signal ($B_2(-l/2)$) and the cross-coupled signal ($A_1(l/2)$) using standard Transmission Line Theory. These can then be compared with the exact solutions obtained by numerically solving the full-blown coupled mode equations. In this section we assume that $A_2(l/2) = 1$. Consider fig. (4-6) which shows the equivalent circuit viewed from the ports of resonator 2. y_n is the admittance seen looking into the input port of resonator 2 and is given by

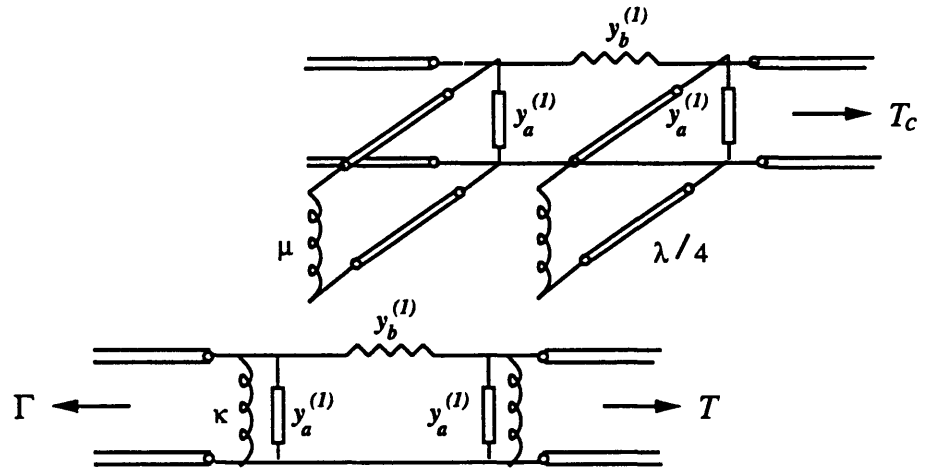

Figure 4-7: T_c represents the signal coupled from resonator 2 to resonator 1.

$$\begin{aligned} y_n &= y_a^{(2)} + \frac{y_b^{(2)}(1+y_a^{(2)})}{1+y_a^{(2)}+y_b^{(2)}} \\ &\simeq y_a^{(2)} + \frac{1+y_a^{(2)}}{2+y_a^{(2)}}. \end{aligned}$$

Γ, the reflection coefficient of resonator 2 as indicated in the figure is given by

$$\begin{aligned} \Gamma &= \frac{B_2(-l/2)}{A_2(-l/2)} = \frac{1-y_n}{1+y_n} \\ &= \frac{1-2y_a^{(2)}-\left(y_a^{(2)}\right)^2}{3+4y_a^{(2)}+\left(y_a^{(2)}\right)^2} \end{aligned} \tag{4.42}$$

The transmission coefficient T is given by

$$T = \frac{y_b^{(2)}}{1+y_a^{(2)}+y_b^{(2)}}(1+\Gamma)A_2 \simeq \frac{1}{2+y_a^{(2)}}(1+\Gamma)$$

Now

$$\begin{aligned} y_a^{(2)} &= y_a^{(1)} + \frac{\mu^2/\kappa^2}{1+y_a^{(1)}}, \\ \left(y_a^{(2)}\right)^2 &\simeq \left(y_a^{(1)}\right)^2 + 2\frac{\mu^2}{\kappa^2}\frac{y_a^{(1)}}{1+y_a^{(1)}}, \end{aligned}$$

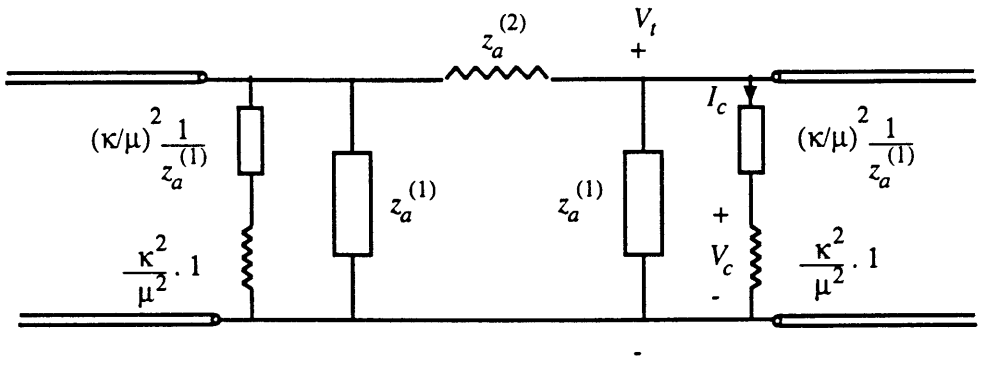

Figure 4-8: Calculating the power coupled to resonator 1.

$$\simeq 1 - 2\Delta - 2j\frac{\delta}{\kappa} - 2\frac{\mu^2/\kappa^2}{\Delta + j\frac{\delta}{\kappa}},$$

where terms higher than first order have been neglected. Substituting the above expressions into eq. (4.42), we get

$$\Gamma = \frac{(\Delta + j\frac{\delta}{\kappa})}{(\Delta + j\frac{\delta}{\kappa})^2 + \frac{\mu^2}{\kappa^2}} \tag{4.43}$$

Moreover,

$$T = \frac{1}{2 + y_a^{(2)}}(1 + \Gamma) = \frac{(\Delta + j\frac{\delta}{\kappa})}{(\Delta + j\frac{\delta}{\kappa})^2 + \frac{\mu^2}{\kappa^2}} = \Gamma. \tag{4.44}$$

Notice that to this order $T = \Gamma$ and the response of the resonator is symmetric.

To find the power coupled to resonator 1, we need to compute the power leaking into the waveguide connected to the resonator 1. In the equivalent circuit, this is indicated by the arrow labelled T_c (fig. (4-7)). Alternately it is the power dissipated in the $1\Omega^{-1}$ hanging off of resonator 1 in fig. (4-5). In the collapsed equivalent circuit as viewed from resonator 2, this power also corresponds to that dissipated in the κ^2/μ^2 resistor shown in fig. (4-8). The circuit of fig. (4-8) is the same as that shown in fig. (4-6) but is drawn in terms of the impedances ($z_a^{(1)} = 1/y_a^{(1)}$) with each component of $z_a^{(2)} = 1/y_a^{(2)}$ drawn explicitly.

$$P_c = \Re\{V_c I_c^*\}$$

but

$$
\begin{aligned}
V_t &= \frac{y_b^{(2)}}{y_b^{(2)} + y_a^{(2)} + 1} V \simeq \frac{1}{2 + y_a^{(2)}} (1 + \Gamma) = T \\
V_c &= \frac{V_t}{(1 + y_a^{(1)})} = \frac{T}{1 + y_a^{(1)}} \\
I_c &= \frac{\mu^2}{\kappa^2} V_c \qquad \Rightarrow
\end{aligned}
$$

$$
P_c = \Re\left\{ \frac{\mu^2}{\kappa^2} |V_c|^2 \right\} = \frac{\mu^2}{\kappa^2} \frac{|T|^2}{|1 + y_a^{(1)}|^2} \tag{4.45}
$$

where T is given by eq. (4.44). Let us define a new quantity T_c denoting the magnitude of the signal coupled to resonator 1.

$$
T_c \equiv \sqrt{P_c} = \frac{\frac{\mu}{\kappa}}{\left| \left(\Delta + j \frac{\delta}{\kappa} \right)^2 + \frac{\mu^2}{\kappa^2} \right|} \tag{4.46}
$$

The expressions derived above are used to compare the response of the two resonator system with the exact solutions of the coupled mode equations calculated using a computer. The responses are shown in figures (4-9) and (4-10). Figure (4-9) makes a comparison between the two analyses using parameters for which the approximations made in deriving the equivalent circuit are strictly met. Notice that the equivalent circuit (solid line) provides an excellent fit to the exact analysis (dotted line). Fig. (4-10) uses $\Delta = 0.1$ and $\mu/\kappa = 0.1$ which are not strictly much less than 1. Even for this case the agreement between the equivalent circuit analysis and the exact analysis is very good.

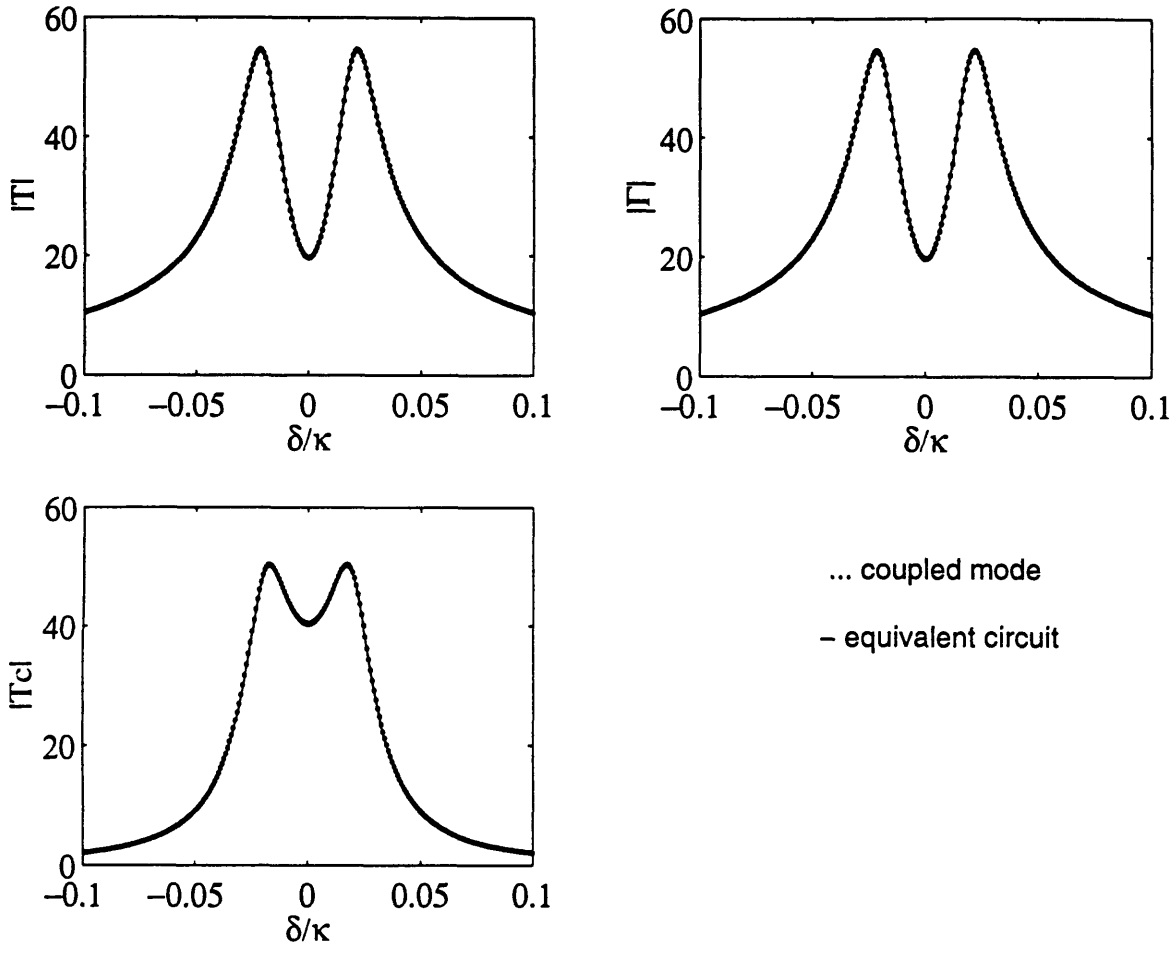

Figure 4-9: Responses computed from equivalent circuit (solid line) and coupled mode analysis (dotted line): (a)Transmitted signal amplitude, T, in resonator 2; (b) Reflected signal amplitude, Γ, in resonator 2; (c) Signal coupled to resonator 1, T_c; $\mu/\kappa = 0.02$, $\Delta = 0.01$

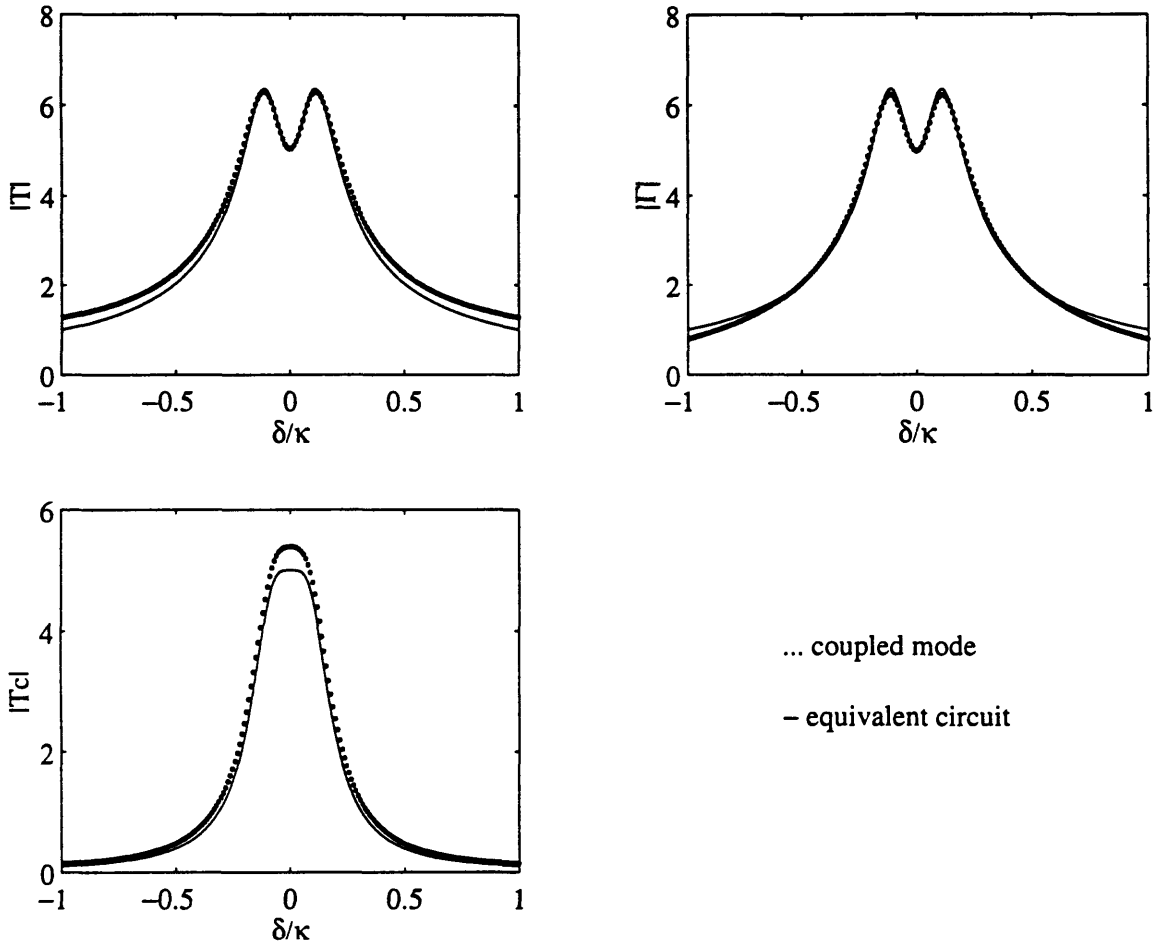

Figure 4-10: Responses computed from equivalent circuit (solid line) and coupled mode analysis (dotted line): (a)Transmitted signal amplitude, T, in resonator 2; (b) Reflected signal amplitude, Γ, in resonator 2; (c) Signal coupled to resonator 1, T_c; $\mu/\kappa = 0.1$, $\Delta = 0.1$.

Chapter 5

First-order Channel Dropping Filter

When a GDFB resonator is evanescently coupled to another waveguide, (signal bus), the combined system forms a channel dropping filter [9]. Signal frequencies that are near the lasing frequency of the GDFB resonator couple more strongly to it and are transferred from the bus to the resonator, allowing a channel to be detected. Since the GDFB resonator is active and can couple waves back onto the bus, the spectrum of the signal transmitted on the bus may be only slightly disturbed. This is a desirable feature as it allows multiple detections of the same channel.

In this chapter, we will study a single GDFB resonator evanescently coupled to a signal guide (fig. (5-1)). This systems as we will see is a first-order channel dropping filter with a characteristic Lorentzian response. Although the system of equations describing the first-order CDF will be given for the sake of completeness it will not be solved explicitly. Instead, the intuition gained from the previous chapter will allow the equivalent circuit of the CDF to be assembled without a mathematical derivation and this will be used to solve the structure.

The equations describing the first-order CDF are:

$$\frac{dA_1}{dz} = -j\delta A_1 + \kappa B_1 - j\mu A_2 \tag{5.1}$$

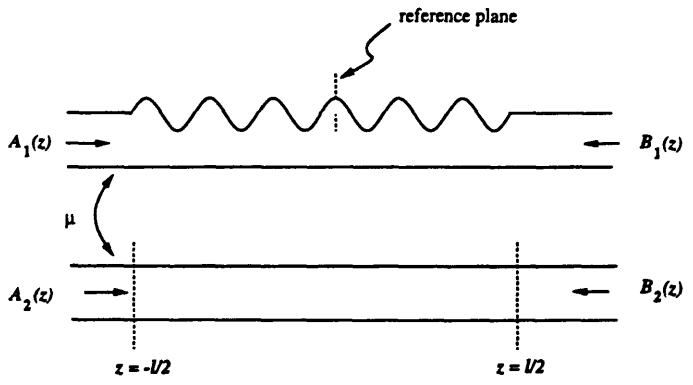

Figure 5-1: GDFB Resonator side-coupled to a Signal Bus – 1^{st}-order CDF

$$\frac{dB_1}{dz} = -\kappa A_1 + j\delta B_1 + j\mu B_2 \tag{5.2}$$

$$\frac{dA_2}{dz} = -j\delta A_2 - j\mu A_1 \tag{5.3}$$

$$\frac{dB_2}{dz} = j\delta B_2 + j\mu B_1 \tag{5.4}$$

Before we proceed with assembling the equivalent circuit, let us see if the response of the CDF can be physically reasoned based on our knowledge of the behavior of the isolated GDFB resonator and the coupling between synchronous guides (chap. 2). In chapter 2 it was seen that a single matched resonator tuned slightly below threshold (i.e $\kappa l = \pi/2 - \Delta$) when excited from one port had an approximately Lorentzian lineshape with a bandwidth of $2\kappa\Delta$ and a gain of $1/\Delta$. Moreover, it is possible to couple power between guides that are fabricated close to one another. This means that in the structure shown in fig. (5-1), it should be possible to excite the resonator via the evanescent fields of the mode in the bus. In the absence of the periodic gain variations in the resonator guide, the broad-band coupling between the synchronous waveguides (i.e the bus and the resonator guide) is frequency insensitive and all frequencies couple equally strongly. However, the periodic gain variations give rise to a frequency dependent mode in the resonator (Lorentzian in shape) and only those frequencies supported in the resonator can couple from the bus to it. Thus, frequencies near the lasing frequency ($\delta = 0$) couple strongly and those further away are suppressed. Based on this we expect the received signal, $B_1(-l/2)$, of the coupled

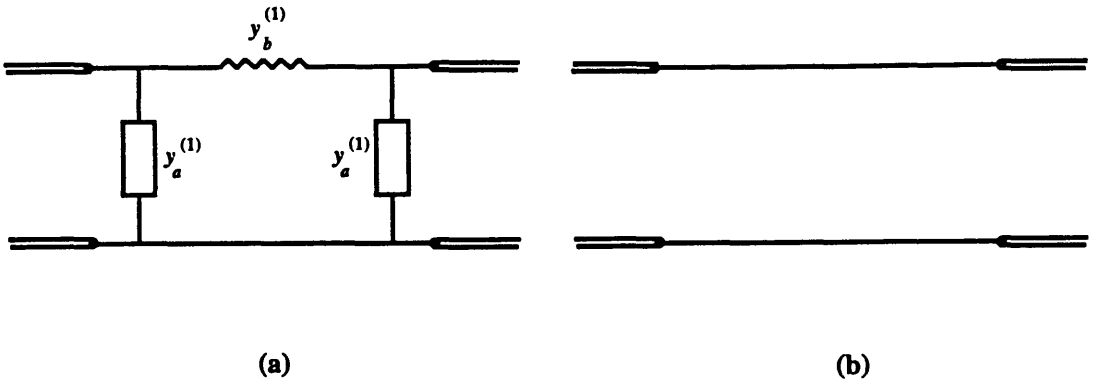

Figure 5-2: (a) Equivalent circuit of a GDFB resonator. (b) Equivalent circuit of the signal waveguide.

structure to be a scaled version of the response of the isolated GDFB resonator where the scaling is related to the coupling strength, μ. We expect a "notch" to be present in the transmitted spectrum near $\delta = 0$ where frequencies have coupled to the GDFB resonator. However, since the waves in the resonator also couple back into the bus and the resonator is active, there is no obvious relationship between the received and transmitted spectrum. In fact as we will see, the transmitted spectrum may be completely restored allowing "transparent" detection of a channel. As a consequence of coupling between the resonator and the bus there is also a backward propagating signal (i.e reflected signal) on the bus. Since this coupling is the only source of the backward propagating signal in the bus, we expect the reflected signal on the bus to be a scaled version of the received signal. The entire physical picture here assumes that the coupling between the bus and the resonator is sufficiently weak so that the resonator modes are unaffected due to the presence of the bus. In this limit, it is clear that the coupled structure does indeed behave like a channel-dropping filter, allowing detection of a channel near the lasing frequency of the resonator.

5.1 Equivalent Circuit for First-Order CDF

To derive an equivalent circuit of the structure shown in fig. (5-1) an approach similar to that of the previous chapter may be followed by considering the symmetric

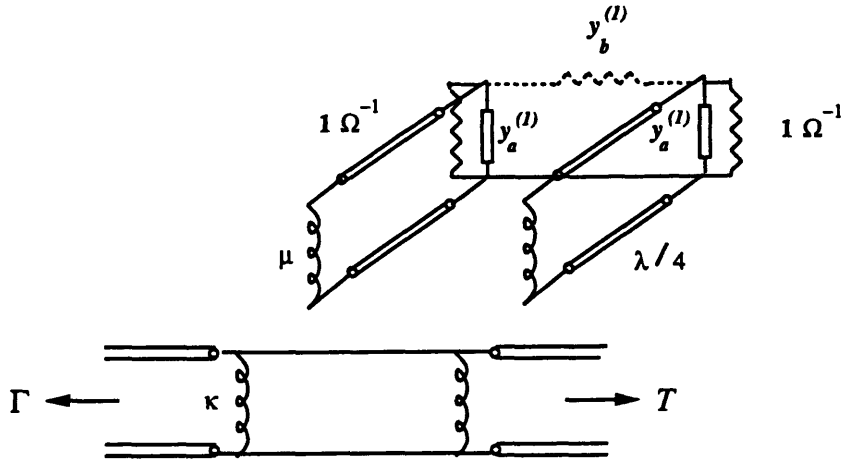

Figure 5-3: Equivalent Circuit of a first-order Channel-Dropping Filter.

and antisymmetric excitations to give the relevant admittances [11]. However, based on our knowledge of the equivalent circuit of an isolated GDFB resonator and an understanding, gathered from the previous chapter, of how excitations couple to resonators, the equivalent circuit for the first-order CDF may be inferred without any calculations. The equivalent circuit of a single matched resonator is shown in fig. (5-2 (a)). The equivalent circuit of the signal bus is a simple transmission line shown in fig. (5-2 (b)). Since the coupling of waves between the bus and the resonator is associated with an time delay, we expect a quarter-waved section to mediate the coupling. The coupling itself is represented by transformer coils with a turns ratio of μ/κ. In the previous chapter we saw that an antisymmetric excitation does not couple to resonator 1 so that $y_b^{(1)}$ is not sensed across the other structure. This has been emphasized by drawing the series admittance $y_b^{(1)}$ in dotted lines to indicate the fact that only symmetric excitations couple from the bus to the resonator so that $y_b^{(1)}$ cannot be accessed from the bus. The equivalent circuit of the first-order CDF is shown in fig. (5-3). This circuit can be collapsed into that shown in fig. (5-4) by transforming the admittances across to the bus. Fig. (5-4) represents the equivalent circuit of the CDF as viewed from the ports of the bus. y is the total admittance

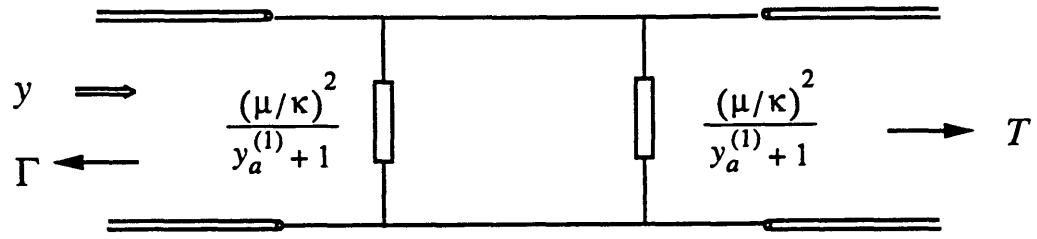

Figure 5-4: Equivalent circuit of a first-order CDF as viewed from the bus ports

seen at the input ports of the bus and is given by

$$y = 1 + \frac{2(\mu^2/\kappa^2)}{1 + y_a^{(1)}}.$$

From transmission line theory, the reflection coefficient, Γ and the transmission coefficient, T, of the bus are given by

$$\Gamma = \frac{1-y}{1+y} = \frac{-\mu^2/\kappa^2}{\left(\Delta + \frac{\mu^2}{\kappa^2}\right) + j\frac{\delta}{\kappa}} \tag{5.5}$$

$$T = 1 + \Gamma = \frac{\Delta + j\frac{\delta}{\kappa}}{\left(\Delta + \frac{\mu^2}{\kappa^2}\right) + j\frac{\delta}{\kappa}} \tag{5.6}$$

Note that for $(\mu^2/\kappa^2) \ll \Delta$, the transmission is approximately unity, i.e $T \simeq 1$. This means that it is possible to completely restore the transmitted spectrum as was suggested in the beginning of the chapter.

Finally, the power coupled to the GDFB resonator, P_c, is found by calculating the dissipation in the $1\Omega^{-1}$ admittance of fig. (5-3). Alternately this is also the power dissipated in the $\frac{\kappa^2}{\mu^2}.1$ resistance of fig. (5-5).

$$P_c = \Re\{V_c I_c^*\}$$

where

$$V_c = \frac{V}{1 + y_a^{(1)}},$$

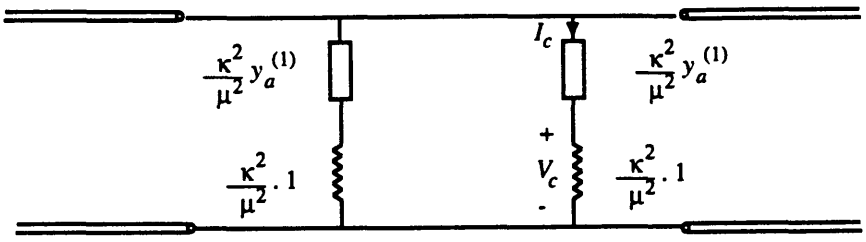

Figure 5-5: Calculating the power coupled to the GDFB resonator

$$I_c = \frac{\mu^2}{\kappa^2} V_c. \qquad \Rightarrow$$

$$\begin{aligned} P_c &= \frac{\mu^2}{\kappa^2} \left| \frac{(1+\Gamma)A_2}{1+y_a^{(1)}} \right|^2 \\ &= \frac{\mu^2/\kappa^2}{\left| \Delta + \frac{\mu^2}{\kappa^2} + j\frac{\delta}{\kappa} \right|^2} \end{aligned} \tag{5.7}$$

where we have used the fact that $(1+\Gamma) = T \approx 1$. The power coupled to the GDFB resonator on resonance is

$$P_c(\delta = 0) = \frac{\mu^2/\kappa^2}{\Delta^2 + \frac{\mu^4}{\kappa^4}} \simeq \frac{\mu^2}{\kappa^2 \Delta^2} \equiv P_{max}$$

The half power points in terms of the normalized frequency are

$$\frac{\delta_{hp}}{\kappa} = \pm \left(\Delta + \frac{\mu^2}{\kappa^2} \right).$$

Thus, the bandwidth, $2(\Delta\delta)$ of the signal coupled to the resonator is given by

$$2(\Delta\delta) \equiv 2\delta_{hp} = 2\kappa \left(\Delta + \frac{\mu^2}{\kappa^2} \right). \tag{5.8}$$

We see that the prediction of the response of the first-order CDF based on physical reasoning was very accurate. The bandwidth of the response of a isolated GDFB resonator as found in chap. 2 was $2\kappa\Delta$. The additional term in the bandwidth of the signal coupled to the resonator represents the increased loss in system due to coupling

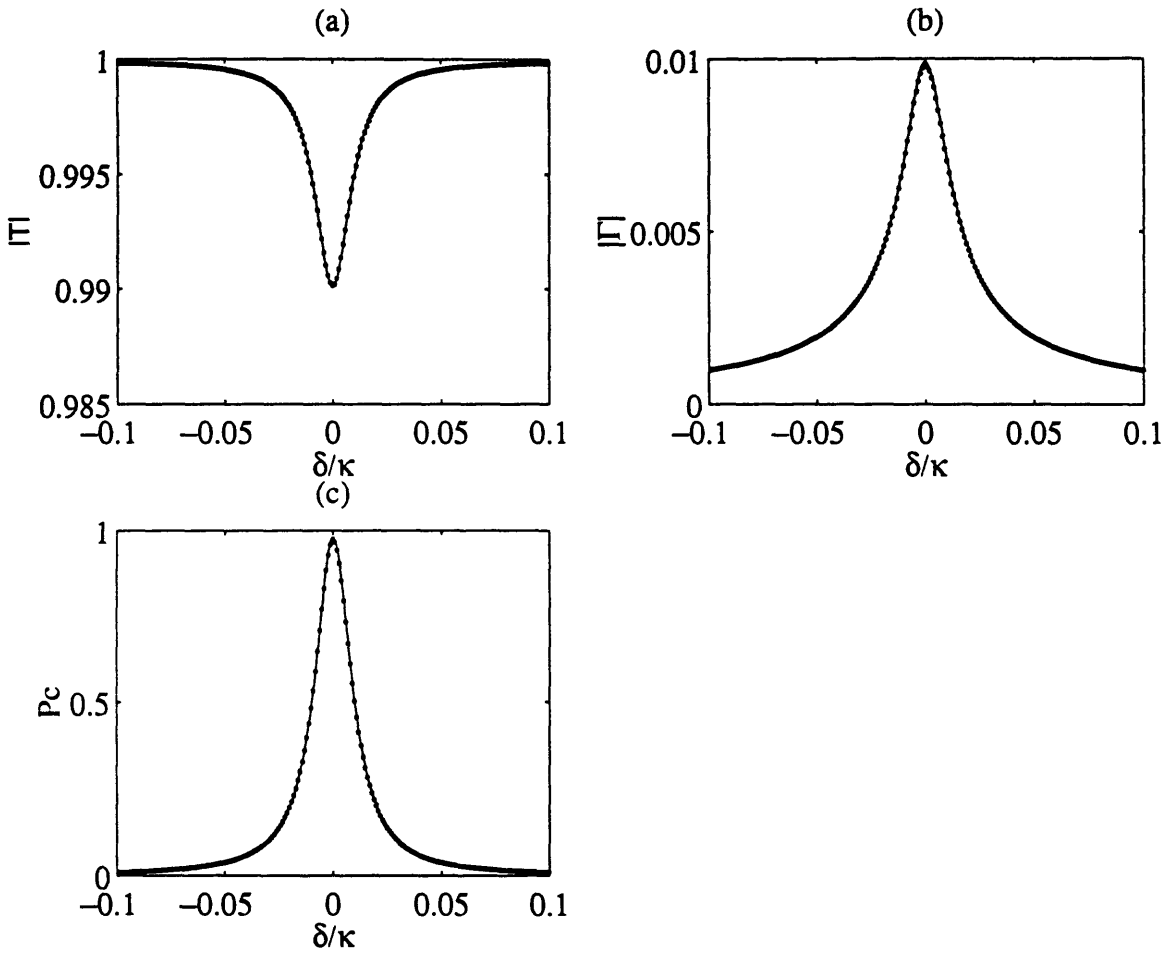

Figure 5-6: Responses computed from equivalent circuit (solid line) and coupled mode analysis (dotted line): (a)Transmitted signal amplitude, T, in the bus; (b) Reflected signal amplitude, Γ, in the bus; (c) Received power, P_c, in resonator 1, P_c; $\mu/\kappa = 0.01$, $\Delta = 0.01$

to the bus in addition to the "losses" from the matched ends of the resonator. Also, we see that $P_{max} = \frac{\mu^2}{\kappa^2\Delta^2}$ as compared to the maximum power in the single isolated resonator tuned below threshold of $\frac{1}{\Delta^2}$. The scaling of μ^2/κ^2 is due to the fact that the resonator is not excited directly but rather via the coupling of the signal from the bus to the resonator. Moreover, notice also that

$$\frac{|\Gamma|}{\sqrt{P_c}} = \frac{\mu}{\kappa},$$

i.e, the reflected signal, as argued earlier, is indeed a scaled version of the received signal, with the scaling given by μ/κ. This confirms that a GDFB resonator evanescently coupled to a signal bus can be used to form a first order channel-dropping filter. The signal picked up by the resonator is Lorentzian in shape as is clear from eq. (5.7). Moreover, if the system is properly designed it is possible to have transparent and consequently multiple detection of the same data channel, properties which offer increased flexibility to a communication system designer. Figure (5-6) shows an overlay of the exact analysis and the equivalent circuit response for filter with bandwith 1 GHz assuming a κ value of $35cm^{-1}$, smaller than that reported in the literature [27]. The equivalent circuit provides an excellent estimate of the exact response.

Chapter 6

Higher-order Channel Dropping Filters

We saw in the previous chapter that a first-order filter has Lorentzian frequency response. The power of the detected channel falls off approximately as the inverse square of the normalized frequency $\frac{1}{(\delta/\kappa)^2}$. In some applications this roll off with frequency may not be sufficient to meet system specifications like acceptable cross-talk levels between adjacent WDM channels. In such an event, it is necessary to use higher-order (or multi-pole) filters. Wheras first-order filters are necessarily Lorentzian in shape near the resonance, higher order filters offer the flexibility of allowing the filter characteristics to be shaped by manipulating the poles of the system. This flexibility is the key to filter design and for many applications the advantages gained by using the multi-pole filters may be sufficient to offset the increased complexity encountered in higher-order systems.

This chapter will be devoted to the study of higher-order channel dropping filters. We will begin by considering the two resonator system of chapter 3, evanescently coupled to a signal waveguide as shown in fig. (6-1). From the intuition gained from the previous chapter, we suspect that this system forms a second-order CDF. It should be possible to excite the modes of the two resonator system by the evanescent tails of the field in the bus thereby transferring power from it to the resonators. We will see that this is indeed the case. The approach adopted to study the second-order

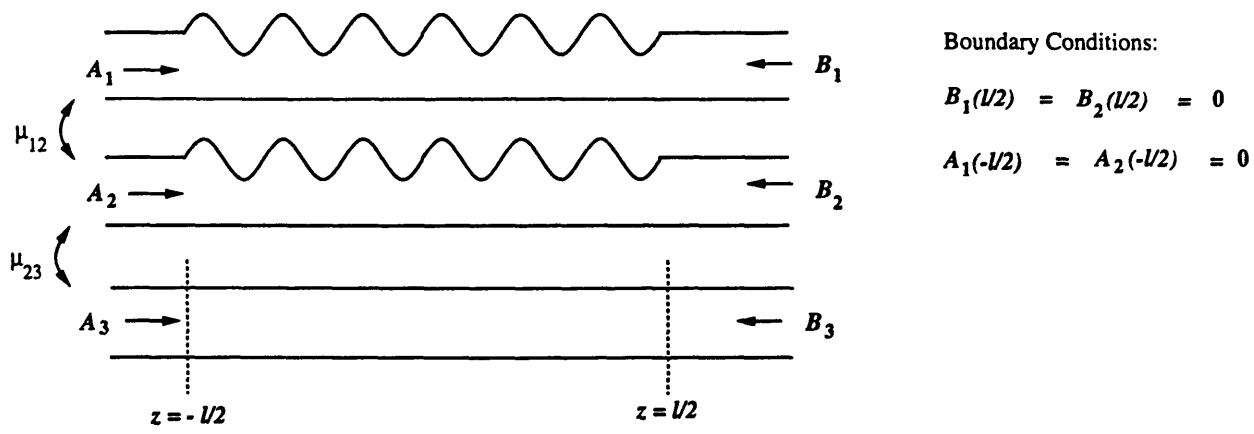

Figure 6-1: Second-order Channel Dropping Filter

CDF will be to draw the equivalent circuit for the system without a mathematical derivation. The equivalent circuit will be used to derive analytical expressions for the responses at the various output ports. Comparisons with the exact analysis and with the first-order channel dropping filter will be made wherever appropriate. We will end the chapter by generalizing the scheme of assembling equivalent circuits for an n^{th}-order filter. Comparisons with the exact analysis will be made.

6.1 Second-order Channel Dropping Filter

The second-order channel dropping filter is shown in fig. (6-1). Instead of solving the coupled mode equations describing this structure, we draw the equivalent circuit for the above structure. This approach is considerably simpler and allows an analytic handle on the higher-order filters which is essential for filter design. The equivalent circuit of a second-order CDF is obtained by coupling the equivalent circuits of the individual matched resonators (chap. 2) via quarter-wave segments. Recalling that antisymmetric excitations do not couple to the resonators and that the transformer ratio corresponding to the coupling between structure i and structure j is given by $\frac{\mu_{ij}}{\kappa}$, the equivalent circuit for the second-order CDF is as shown in fig. (6-2). In fig. (6-2), $y_{ai}^{(1)}$ represents the parallel admittance of the single isolated GDFB resonator i

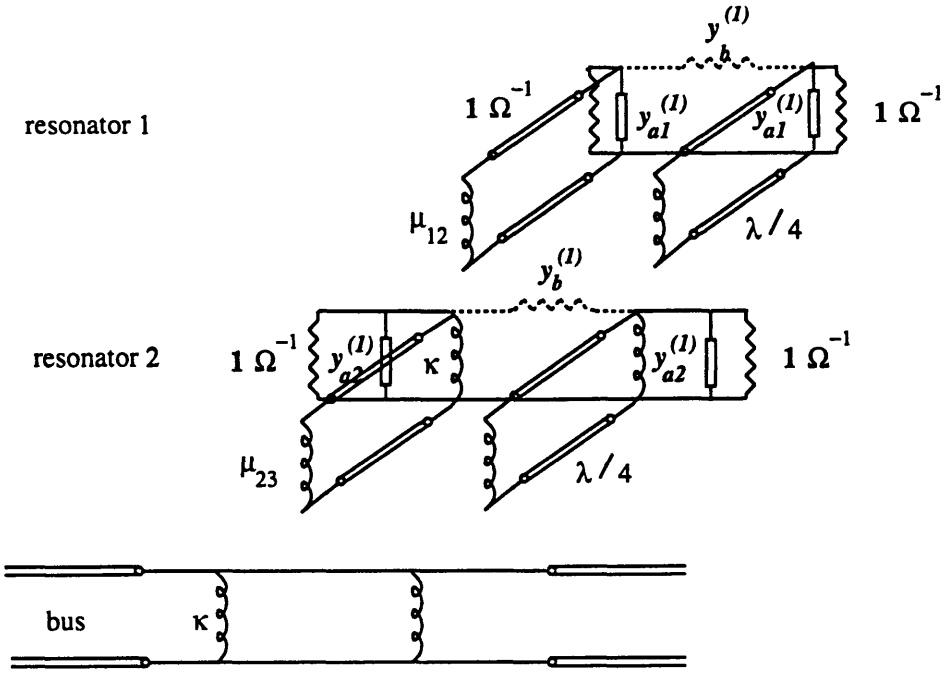

Figure 6-2: Equivalent Circuit for a Second-Order CDF

tuned below threshold, i.e

$$y_{ai}^{(1)} = \Delta_i - 1 + j\frac{\delta}{\kappa}$$

The parallel $1\Omega^{-1}$ conductances represent the matched ends of the resonator or equivalently the fact that resonators are not excited directly, but only via the coupling to the bus. Transforming the admittance of resonator 1 across on to resonator 2, the above circuit can be collapsed to give the circuit shown in fig. (6-3). This looks similar to the equivalent circuit of the first-order CDF except that the parallel admittance, $y_a^{(2)}$ is that of the two resonator of chap. 3, i.e

$$y_a^{(2)} = y_{a2}^{(1)} + \frac{\left(\frac{\mu_{12}}{\kappa}\right)^2}{1 + y_{a1}^{(1)}} \equiv y_{a2}^{(1)} + \frac{\alpha_1^2}{1 + y_{a1}^{(1)}},$$

where

$$\alpha_i \equiv \frac{\mu_{ij}}{\kappa}$$

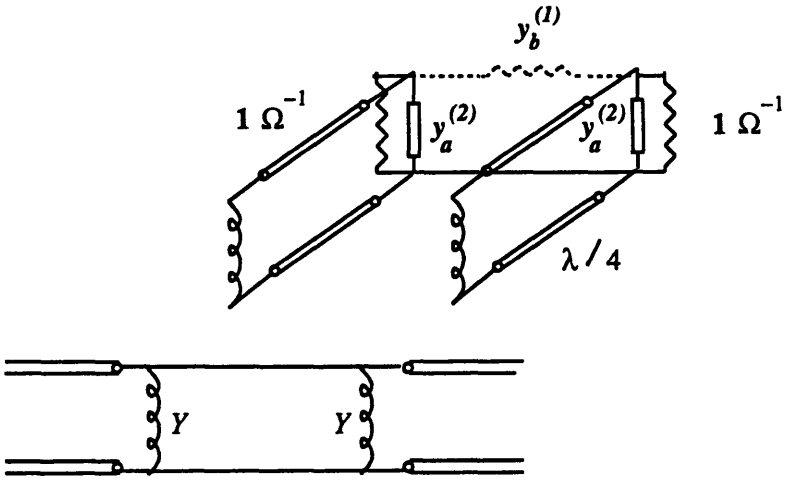

Figure 6-3: Equivalent circuit of 2^{nd}-order CDF

The admittance, Y seen across the transformer coils of the bus is given by

$$Y = \frac{(\mu_{23}/\kappa)^2}{1 + y_a^{(2)}} = \frac{\alpha_2^2}{y_{a2}^{(1)} + 1 + \frac{\alpha_1^2}{y_{a1}^{(1)}+1}} \tag{6.1}$$

Since the factor $\left(y_{ai}^{(1)} + 1\right)$ will be encountered repeatedly, we simplify the notation by defining the new quantity, y_{ai} where

$$y_{ai} \equiv y_{ai}^{(1)} + 1 = \Delta_i + j\frac{\delta}{\kappa} \tag{6.2}$$

In the new notation, thus, Y is given by

$$Y = \frac{\alpha_2^2}{y_{a2} + \frac{\alpha_1^2}{y_{a1}}}$$

The reflection coefficient, Γ, of the bus is given by

$$\begin{aligned} \Gamma &= \frac{1-(2Y+1)}{1+(2Y+1)} = \frac{-Y}{1+Y} \\ &= \frac{-\alpha_2^2 y_{a1}}{\alpha_1^2 + \alpha_2^2 y_{a1} + y_{a1} y_{a2}} \end{aligned} \tag{6.3}$$

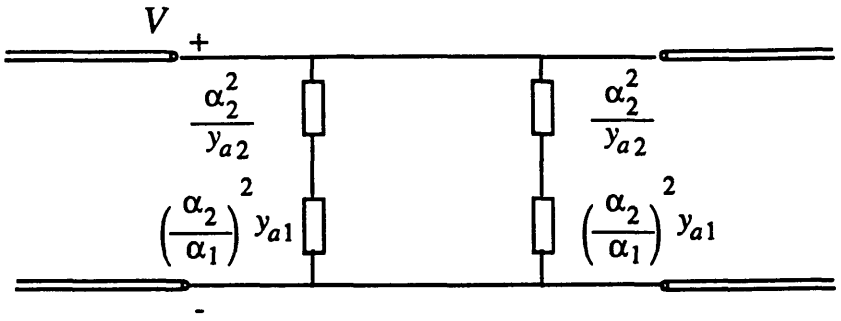

Figure 6-4: Equivalent Circuit for a Second-Order CDF viewed from the bus ports

Notice that $y_{ai} = \Delta_i + j\frac{\delta}{\kappa} \ll 1$ (for $\delta/\kappa \ll 1$) and is a first-order term. Also note that $\alpha_i^2 \equiv (\mu_{ij}/\kappa)^2$ is a second order term. $(\alpha_2^2\, y_{a1})$ is, thus, a third order term and can be ignored relative to the other terms in the denominator. With this approximation, we find that

$$\Gamma \simeq \frac{-\alpha_2^2\, y_{a1}}{y_{a1}y_{a2} + \alpha_1^2} \tag{6.4}$$

$$= \frac{-(\frac{\mu_{23}}{\kappa})^2 \left(\Delta_1 + j\frac{\delta}{\kappa}\right)}{\left(\Delta_1 + j\frac{\delta}{\kappa}\right)\left(\Delta_2 + j\frac{\delta}{\kappa}\right) + (\frac{\mu_{12}}{\kappa})^2} \tag{6.5}$$

The signal transmitted in the bus, T in the bus is given by

$$T = 1 + \Gamma$$

$$T = \frac{\alpha_1^2 + y_{a1}y_{a2}}{\alpha_1^2 + \alpha_2^2\, y_{a1} + y_{a1}y_{a1}} \tag{6.6}$$

In the case that $\alpha_2^2\, y_{a1} \ll y_{a1}y_{a2}$, the above equation reveals that $T \approx 1$ and the signal in the bus passes through essentially undisturbed. At resonance, this condition amounts to the requirement that $\left(\frac{\mu_{23}}{\kappa}\right)^2 \ll \Delta_2$.

6.1.1 Power Coupled to the Resonators

Having determined the reflected and transmitted signals in the bus, we turn our attention to finding the power coupled to resonators 1 and 2 respectively. These are

labelled by P_{r1} and P_{r2} respectively, and are defined as

$$\begin{aligned} P_{r1} &\equiv |A_1(l/2)|^2 \\ P_{r2} &\equiv |A_2(l/2)|^2 \end{aligned}$$

In terms of the circuit elements, these correspond to the power dissipated in the $1\Omega^{-1}$ conductance in the equivalent circuit of resonators 1 and 2 respectively of fig. (6-2). To calculate these power dissipations, however, we will consider the collapsed equivalent circuit, viewed from the bus ports (fig. (6-4)). Note that

$$Y = \left(\frac{1}{\alpha_2^2/y_{a2}} + \frac{1}{\left(\alpha_2^2/\alpha_1^2\right)^2 y_{a1}} \right)^{-1},$$

i.e Y is a series combination of $\frac{\alpha_2^2}{y_{a2}}$ and $\left(\frac{\alpha_2}{\alpha_1}\right)^2 y_{a1}$ as shown in the figure above. Recall that $y_{ai} = y_{ai}^{(1)} + 1$. The power coupled into resonator i is the power dissipated in the scaled $1\Omega^{-1}$ component of y_{ai} in the admittances $\frac{\alpha_2^2}{y_{a2}^{(1)}+1}$ and $\left(\frac{\alpha_2}{\alpha_1}\right)^2 \left(y_{a1}^{(1)} + 1\right)$. Consider one of the branches of fig. (6-4) as shown in fig. (6-5). The components of $\left(\frac{\alpha_1}{\alpha_2}\right)^2 y_{a1}$ have been drawn separately.

6.1.2 Power Coupled to Resonator 1

The power coupled into resonator 1, P_{r1}, is given by:

$$P_{r1} = \Re\{V_{r1} I_{r1}^*\}$$

where V_{r1} and I_{r1} are the voltage and current indicated in the fig. (6-5). From a voltage divider relation we have that

$$V_{r1} = \frac{\frac{\alpha_2^2}{y_{a2}}}{\frac{\alpha_2^2}{y_{a2}} + \left(\frac{\alpha_2}{\alpha_1}\right)^2 y_{a1}} V = \frac{\alpha_2^2}{\alpha_2^2 + \left(\frac{\alpha_2}{\alpha_1}\right)^2 y_{a1} y_{a2}} (1 + \Gamma) A_3 \tag{6.7}$$

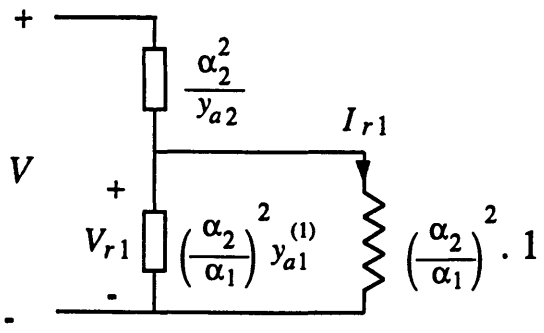

Figure 6-5: Calculating the power coupled to resonator 1

where we have used the fact that

$$V = (1 + \Gamma)A_3. \tag{6.8}$$

For a unity input on the bus (i.e $A_3 = 1$), assuming that $\alpha_2^2 \ll y_{a2}$, so that

$$T = (1 + \Gamma)A_3 \approx 1, \tag{6.9}$$

we have from eq. (6.7) that

$$V_{r1} = \frac{\alpha_1^2}{\alpha_1^2 + \alpha_2^2 y_{a1} + y_{a1}y_{a2}} \simeq \frac{\alpha_1^2}{\alpha_1^2 + y_{a1}y_{a2}} \tag{6.10}$$

Furthermore

$$I_{r1} = V_{r1}\left(\frac{\alpha_2}{\alpha_1}\right)^2 \tag{6.11}$$

Thus,

$$P_{r1} = \left|\frac{\alpha_1\alpha_2}{\alpha_1^2 + y_{a1}y_{a2}}\right|^2, \tag{6.12}$$

and The magnitude of the signal transmitted through resonator 1, $T_{r1} = |A_1(l/2)|$, is given by

$$T_{r1} \equiv \sqrt{P_{r1}} = \left|\frac{\alpha_1\alpha_2}{\alpha_1^2 + y_{a1}y_{a2}}\right|$$

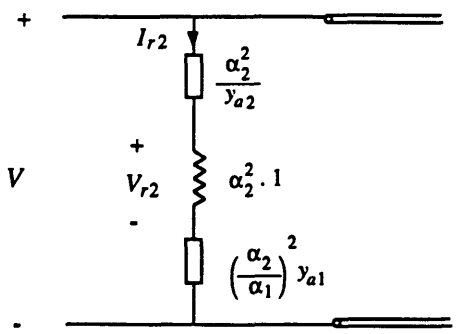

Figure 6-6: Calculating the power coupled into resonator 2.

$$= \left| \frac{\left(\frac{\mu_{12}}{\kappa}\right)\left(\frac{\mu_{23}}{\kappa}\right)}{\left(\frac{\mu_{12}}{\kappa}\right)^2 + \left(\Delta_1 + j\frac{\delta}{\kappa}\right)\left(\Delta_2 + j\frac{\delta}{\kappa}\right)} \right| \tag{6.13}$$

6.1.3 Power Coupled to Resonator 2

Consider the same branch again as shown in fig. (6-6). This time we have separately drawn each component of $\frac{\alpha_2^2}{y_{a2}}$. The power transferred to resonator 2, P_{r2}, is given by

$$P_{r2} = \Re\{V_{r2} I_{r2}^*\}$$

where V_{r2} and I_{r2} are indicated in the figure. We have that

$$\begin{aligned} V_{r2} &= \frac{y_{a1}}{y_{a1}y_{a2} + \alpha_1^2}(1+\Gamma)A_3, \\ &\simeq \frac{y_{a1}}{\alpha_1^2 + y_{a1}y_{a2}}, \end{aligned} \tag{6.14}$$

where use of eqs. (6.8) and (6.9) was made. Furthermore,

$$I_{r2} = \alpha_2^2 V_{r2} \qquad \Rightarrow \tag{6.15}$$

$$P_{r2} = \alpha_2^2 \left| \frac{y_{a1}}{\alpha_1^2 + y_{a1}y_{a2}} \right|^2 \tag{6.16}$$

The magnitude of the signal transmitted through resonator 2, $T_{r2} = |A_2(l/2)|$, is given by

$$\begin{aligned} T_{r2} &\equiv \sqrt{P_{r2}} = \alpha_2 \left| \frac{y_{a1}}{\alpha_1^2 + y_{a1}y_{a2}} \right| \\ &= \left| \frac{\left(\frac{\mu_{23}}{\kappa}\right)\left(\Delta_1 + j\frac{\delta}{\kappa}\right)}{\left(\frac{\mu_{12}}{\kappa}\right)^2 + \left(\Delta_1 + j\frac{\delta}{\kappa}\right)\left(\Delta_2 + j\frac{\delta}{\kappa}\right)} \right| \end{aligned} \tag{6.17}$$

6.1.4 Second-order Butterworth Filter

Let us consider the power coupled into resonator 1 for the special case when $y_{a1} = y_{a2}$ i.e $\Delta_1 = \Delta_2 \equiv \Delta$ and moreover $\frac{\mu_{12}}{\kappa} = \Delta$. In this case, use of eq. (6.18) gives that

$$\begin{aligned} P_{r1} &= \left| \frac{\left(\frac{\mu_{23}}{\kappa}\right)}{\Delta\left[1 + \left(1 + j\frac{\delta}{\kappa\Delta}\right)^2\right]} \right|^2, \\ &= \frac{\left(\frac{\mu_{23}}{\kappa}\right)^2 \Delta^2}{4\Delta^4 + \left(\frac{\delta}{\kappa}\right)^4} \end{aligned} \tag{6.18}$$

When $\left|\frac{\delta}{\kappa}\right| \ll \Delta$,

$$P_{r1} \simeq \left| \frac{\mu_{23}/\kappa}{2\Delta} \right|^2$$

which is independent of the frequency δ. However, for $\frac{\delta}{\kappa} \gg \Delta$,

$$P_{r1} \simeq \frac{\left(\frac{\mu_{23}}{\kappa}\Delta\right)}{\left(\frac{\delta}{\kappa}\right)^4}$$

The half power points, δ_{hp} can be found from eq. (6.18) and obey the following equation:

$$\begin{aligned} \left(\frac{\delta_{hp}}{\kappa}\right)^4 &= 4\Delta^4 \quad \Rightarrow \\ (\Delta\delta)_1 &\equiv 2\delta_{hp} = 2\sqrt{2}\kappa\Delta, \end{aligned} \tag{6.19}$$

where $(\Delta\delta)_1$ is the bandwidth of the signal coupled to resonator 1. Thus, we see that the power coupled into resonator 1 is maximally flat for low frequencies and falls off inversely as the fourth power of the normalized frequency for large deviations from the resonance condition. This is the characteristic response of a second order Butterworth filter. Therefore, we see that it is possible to shape the filter response for an appropriate choice of parameters as opposed to in a first-order CDF where the response is necessarily Lorentzian. However, we notice that once these parameters are chosen, we are forced to accept whatever response we get at the output port of resonator 2. Thus, in a sense resonator 2 only serves to provide an appropriate response at the output ports of resonator 1. For $y_{a1} = y_{a2}$ and $(\mu_{12}/\kappa) = \Delta$, the power coupled into resonator 2 is

$$\begin{aligned} P_{r2} &= \left| \frac{\left(\frac{\mu_{23}}{\kappa}\right)\left(\Delta + j\frac{\delta}{\kappa}\right)}{\Delta^2 + \left(\Delta + j\frac{\delta}{\kappa}\right)^2} \right|^2 \\ &= \frac{\left(\frac{\mu_{23}}{\kappa}\right)^2 \left(\Delta^2 + \frac{\delta^2}{\kappa^2}\right)}{4\Delta^4 + \left(\frac{\delta}{\kappa}\right)^4} \end{aligned} \tag{6.20}$$

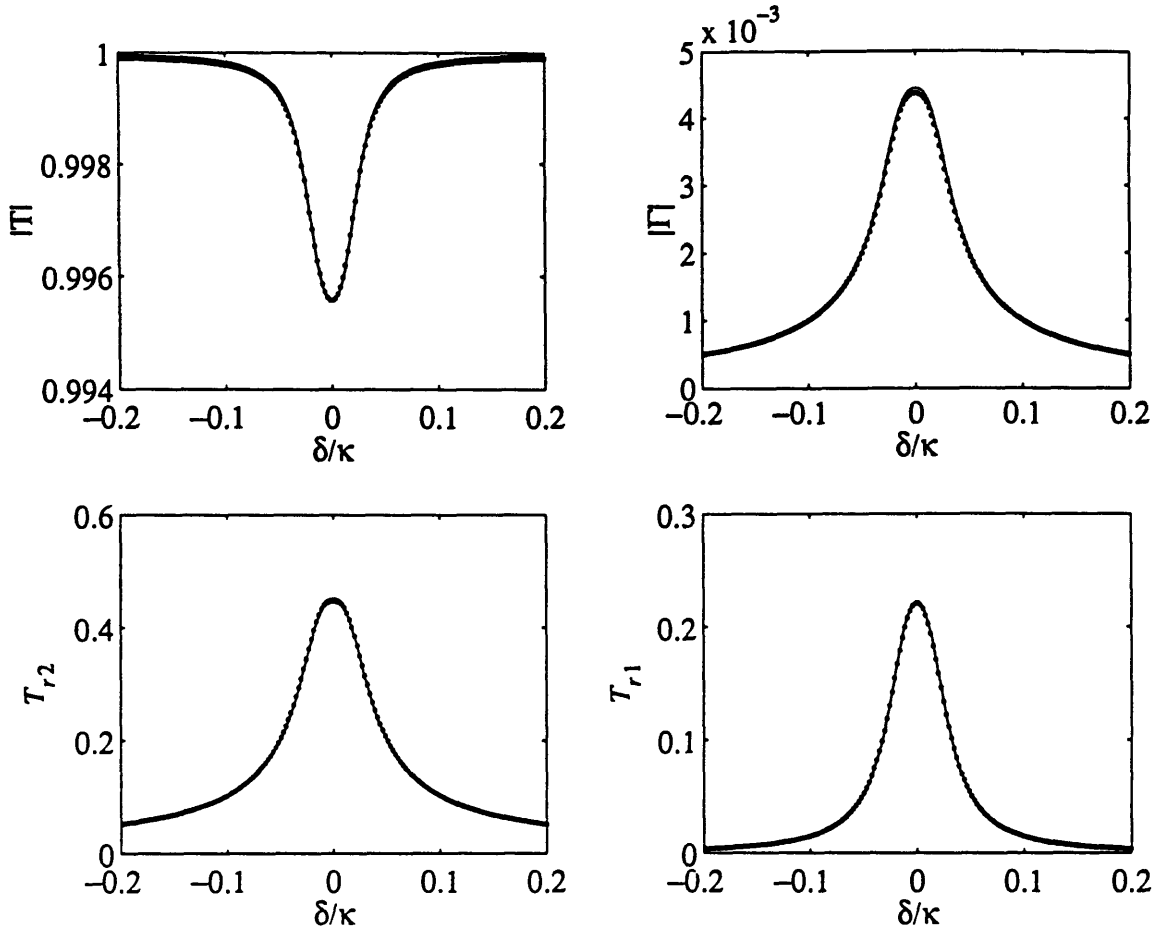

Figure 6-7: Responses computed using the circuit model (solid line) and the exact analysis (solid line). (a) Transmitted Signal, T, on the bus. (b) Reflected Signal Γ on the bus. (c) Signal Coupled to resonator 2, T_{r2}. (d) Signal Coupled to resonator 1, T_{r1}. $\mu_{12}/\kappa = 0.015$, $\mu_{23}/\kappa = 0.01$, $\Delta_1 = 0.03$, $\Delta_2 = 0.015$.

6.1.5 Comparison between Equivalent Circuit and Exact Coupled Mode Analysis

A comparison between the exact responses, found by numerically solving the full-coupled mode equations of the 2^{nd}-order CDF, and those computed using the expressions found from the equivalent circuit analysis of the previous section are shown in figures (6-7) and (6-8). Figure (6-7) shows the response using parameters for which the approximations made in deriving the equivalent circuit are strictly valid. The circuit model (solid line) provides an excellent fit to the exact analysis (dotted line).

Figure (6-8) shows the response of the second-order CDF for which the parameters were chosen so that the signal tapped off resonator 1 has a Butterworth response. For an assumed value of $\kappa = 35cm^{-1}$, the bandwidth of the filter is about 14 GHz. For channels spaced apart by 50 GHz, the cross-talk level is about -34 dB as compared to -17 dB for a first-order CDF with approximately the same bandwidth and peak power. We see that a considerable advantage in the cross-talk level is obtained in going to a second-order filter. This may be useful in a high density WDM system. Even though the value of the parameters used do not exactly obey the conditions for which the circuit model is strictly valid, the fit is reasonably good and equivalent circuits can be used to provide a first-cut design of channel-dropping filters.

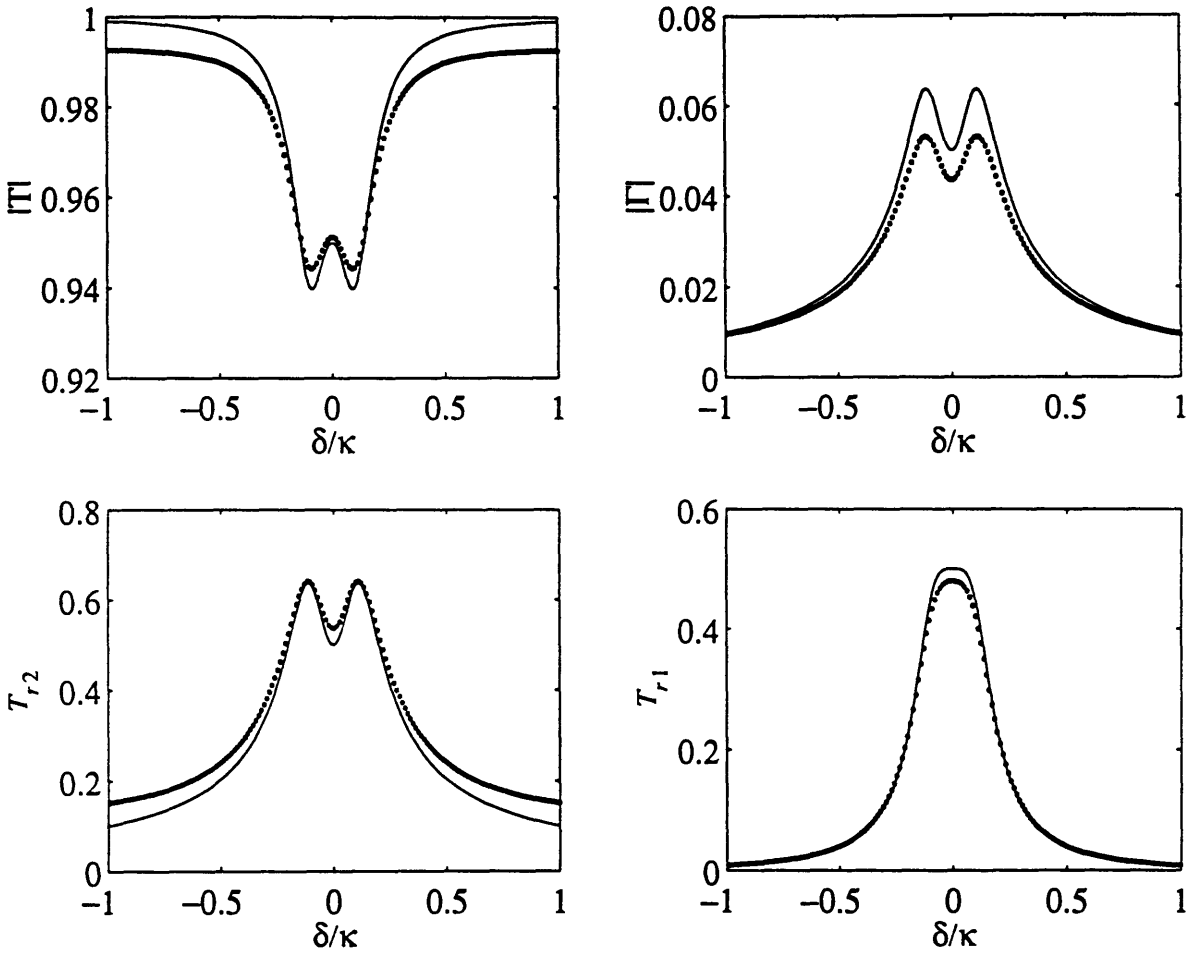

Figure 6-8: Responses computed using the circuit model (solid line) and the exact analysis (solid line). (a) Transmitted Signal, T, on the bus. (b) Reflected Signal Γ on the bus. (c) Signal Coupled to resonator 2, T_{r2}. (d) Signal Coupled to resonator 1, T_{r1}. $\mu_{12}/\kappa = 0.1$, $\mu_{23}/\kappa = 0.1$, $\Delta_1 = 0.1$, $\Delta_2 = 0.1$.

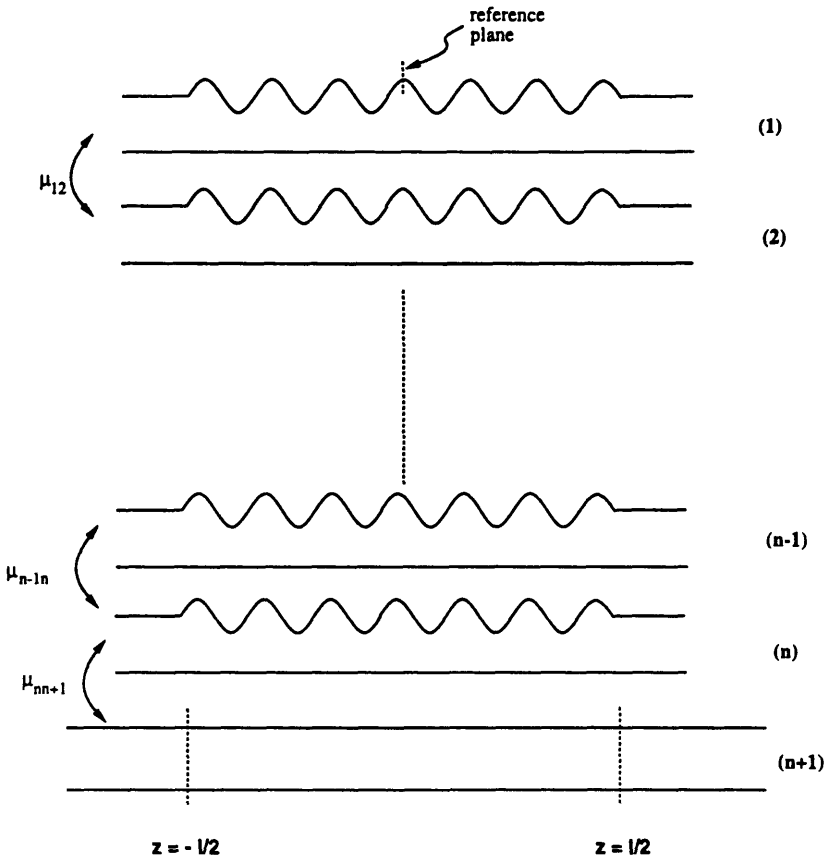

Figure 6-9: n^{th}-order channel dropping filter

6.2 n^{th}-order Channel Dropping Filter

An n^{th}-order channel dropping filter can be made by side-coupling n GDFB resonators, with n^{th} resonator evanescently coupled to a signal waveguide as shown in fig. (6-9). By sending a signal down the bus waveguide, it is possible to excite the modes of the n-coupled resonator system, transferring power to them and achieving filtering. The system of $2n+1$ equations describing the n^{th}-order CDF is given below.

$$\frac{dA_1}{dz} = -j\delta A_1 + \kappa B_1 - j\mu_{12}A_2 \tag{6.21}$$

$$\frac{dB_1}{dz} = -\kappa A_1 + j\delta B_1 + j\mu_{12}B_2 \tag{6.22}$$

$$\frac{dA_2}{dz} = -j\delta A_2 + \kappa B_2 - j\mu_{12}A_1 - j\mu_{23}A_3 \tag{6.23}$$

$$\frac{dB_2}{dz} = j\delta B_2 - \kappa A_2 + j\mu_{12}B_1 + j\mu_{23}B_3 \tag{6.24}$$

$$\vdots \qquad\qquad \vdots \tag{6.25}$$

$$\frac{dA_{n+1}}{dz} = -j\delta A_{n+1} - j\mu_{nn+1}A_n \tag{6.26}$$

$$\frac{dB_{n+1}}{dz} = j\delta B_{n+1} + j\mu_{nn+1}B_n \tag{6.27}$$

Even for modest values of n, it is difficult to analytically solve these equations exactly. Thus we resort to an equivalent circuit approach for the n^{th}-order CDF leaving the exact solutions of the above equations for the computer. The equivalent circuit of the n^{th}-order channel dropping filter is simply obtained by stacking the equivalent circuits of the isolated resonators (see fig. (3-12)). The coupling between adjacent resonators is represented by the quarter-wave section and transformer coils where the turns ratio of the coils in structure i to those in structure $i+1$ is $\mu_{ii+1} : \kappa$. Finally the last resonator couples to the bus as shown in fig. (6-10). Alternately, the circuit can be drawn as shown in fig. (6-11). The symmetric pi-circuit at the end of the quarter-wave section is the equivalent circuit of the n-coupled resonators. From the reasoning given earlier, it is clear that

$$y_b^{(n)} = y_b^{(1)} \simeq 1.$$

$y_a^{(n)}$ is found by transforming the total parallel admittances of the individual resonator, $(y_{ai}^{(1)} + 1)$, across the $\lambda/4$ sections and looking at the total parallel admittance at the n^{th} resonator of fig. (6-9). $y_a^{(n)}$ is given by a continued fraction of the form

$$y_a^{(n)} = y_{an}^{(1)} + \cfrac{\alpha_{n-1}^2}{\left(y_{an-1}^{(1)}+1\right) + \cfrac{\alpha_{n-2}^2}{\left(y_{an-2}^{(1)}+1\right) + \cdots \cfrac{\alpha_2^2}{(y_{a2}+1) + \cfrac{\alpha_1^2}{(y_{a1}+1)}}}} \tag{6.28}$$

$$y_a^{(n)} = y_{an} - 1 + \cfrac{\alpha_{n-1}^2}{y_{an-1}^{(1)} + \cfrac{\alpha_{n-2}^2}{y_{an-2}^{(1)} + \cdots \cfrac{\alpha_2^2}{y_{a2} + \cfrac{\alpha_1^2}{y_{a1}}}}} \tag{6.29}$$

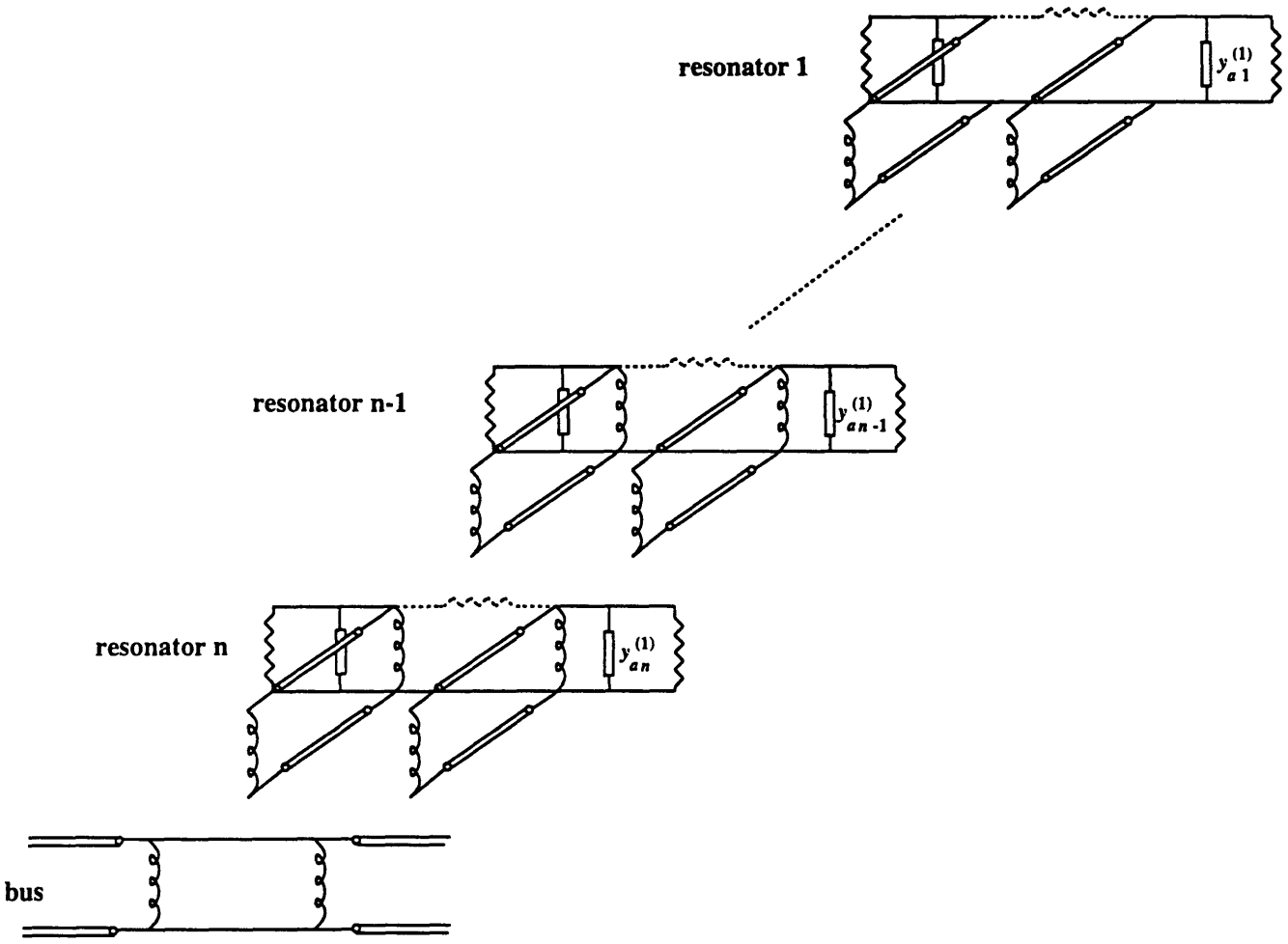

Figure 6-10: Equivalent circuit of the n^{th}-order channel dropping filter.

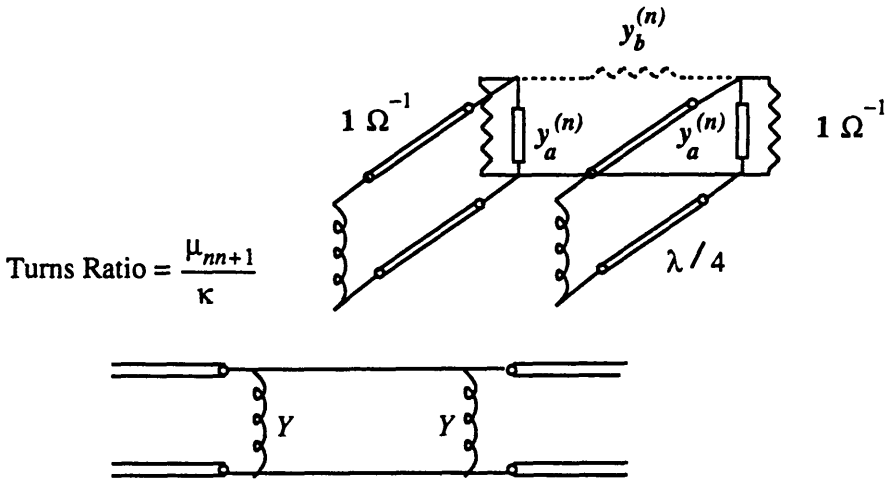

Figure 6-11: Alternate form of the equivalent circuit of a n^{th}-order channel dropping filter

where the previous expression follows from the definition, $y_{ai} \equiv y_{ai}^{(1)}+1$. The continued fraction is reminscent of the admittance of a LC ladder. However, the two are not equivalent as the admittance y_{ai} has a resistive component and is scaled by α_i. As a result it is not immediately possible to use conventional LC tables to design higher-order filters. All the same the signals at the output ports may be readily computed.

The admittance appearing across the coils of the bus is found simply by transforming $y_n \equiv (y_a^{(n)} + 1)$ across $\lambda/4$ wave section and is given by

$$Y = \frac{\alpha_n^2}{y_a^{(n)} + 1} \equiv \frac{\alpha_n^2}{y_n} = \cfrac{\alpha_n^2}{y_{an} + \cfrac{\alpha_{n-1}^2}{y_{an-1}+\cdots \cfrac{\alpha_2^2}{y_{a2}+\cfrac{\alpha_1^2}{y_{a1}}}}} \tag{6.30}$$

For a unity input, the reflected signal on the bus, Γ, is given by

$$\Gamma = \frac{-Y}{1+Y} = \frac{-\left(\frac{\mu_{nn+1}}{\kappa}\right)^2}{\left(\frac{\mu_{nn+1}}{\kappa}\right)^2 + y_n} \tag{6.31}$$

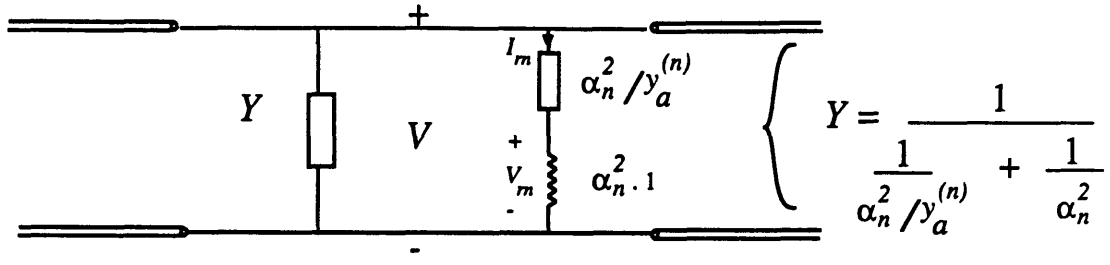

Figure 6-12: Calculating the power coupled to the n^{th} resonator.

If $|y_n| \gg \left(\frac{\mu_{nn+1}}{\kappa}\right)^2$,

$$\Gamma \simeq \frac{-\left(\frac{\mu_{nn+1}}{\kappa}\right)^2}{y_n}$$

$$T = 1 + \Gamma = \frac{y_n}{y_n + \frac{\mu_{nn+1}^2}{\kappa^2}} \simeq 1$$

Finally, since it is easy to calculate the power coupled to the n^{th} resonator, P_{rn}, (i.e the one closest to the bus), we will derive an expression for it. P_{rn} is the power dissipated in the $1\Omega^{-1}$ admittance of fig. (6-11). Alternately it the power dissipated in the α_n^2 admittance of fig. (6-12). From the fig. (6-12), we have that

$$V_{rn} = \frac{1}{1 + y_a^{(n)}} (1 + \Gamma) A_n \simeq \frac{1}{1 + y_a^{(n)}} \tag{6.32}$$

$$I_{rn} = \alpha_n^2 V_{rn} \qquad \Rightarrow \tag{6.33}$$

$$P_{rn} = \Re\{V_{rn} I_{rn}^*\} = \frac{\alpha_n^2}{\left|1 + y_a^{(n)}\right|^2} = \frac{(\mu_{nn+1}/\kappa)^2}{|y_n|^2} \tag{6.34}$$

Notice also that

$$|\Gamma|^2 = \left(\frac{\mu_{nn+1}}{\kappa}\right)^2 P_{rn}$$

analogous to the first-order CDF case. The reflected signal in the bus is due to the back coupling from the n^{th} resonator to the bus.

6.2.1 Comparison of Equivalent Circuit and Exact Analysis

The formalism discussed above was applied to the case of a 3^{rd}-order channel dropping filter. The results are shown in figure (6-13). The parameters of system were chosen rather arbitrarily. However, the response of resonator 2 is quite interesting and resembles a Chebyshev. Once these paramters have been selected, we have to accept whatever response is obtained at the output ports of the other two resonators. They only serve to provide the appropriate coupling to yield the desired response at the output of resonator 2. The equivalent circuit once again provides a reasonable fit to the exact analysis.

Thus far, we have only derived expressions for power coupled from the bus to the resonators in the forwards directions, for eg. P_{r1}, P_{r2} etc. We have not explicity derived expressions for the power coupled from the signal bus to the resonators in the backwards propagating direction. However, by looking at the equivalent circuit it is clear that since the admittances appearing across the two coils of the bus are symmetric, the power coupled into the i^{th} resonator in the backwards and forwards direction, to first order, is identical.

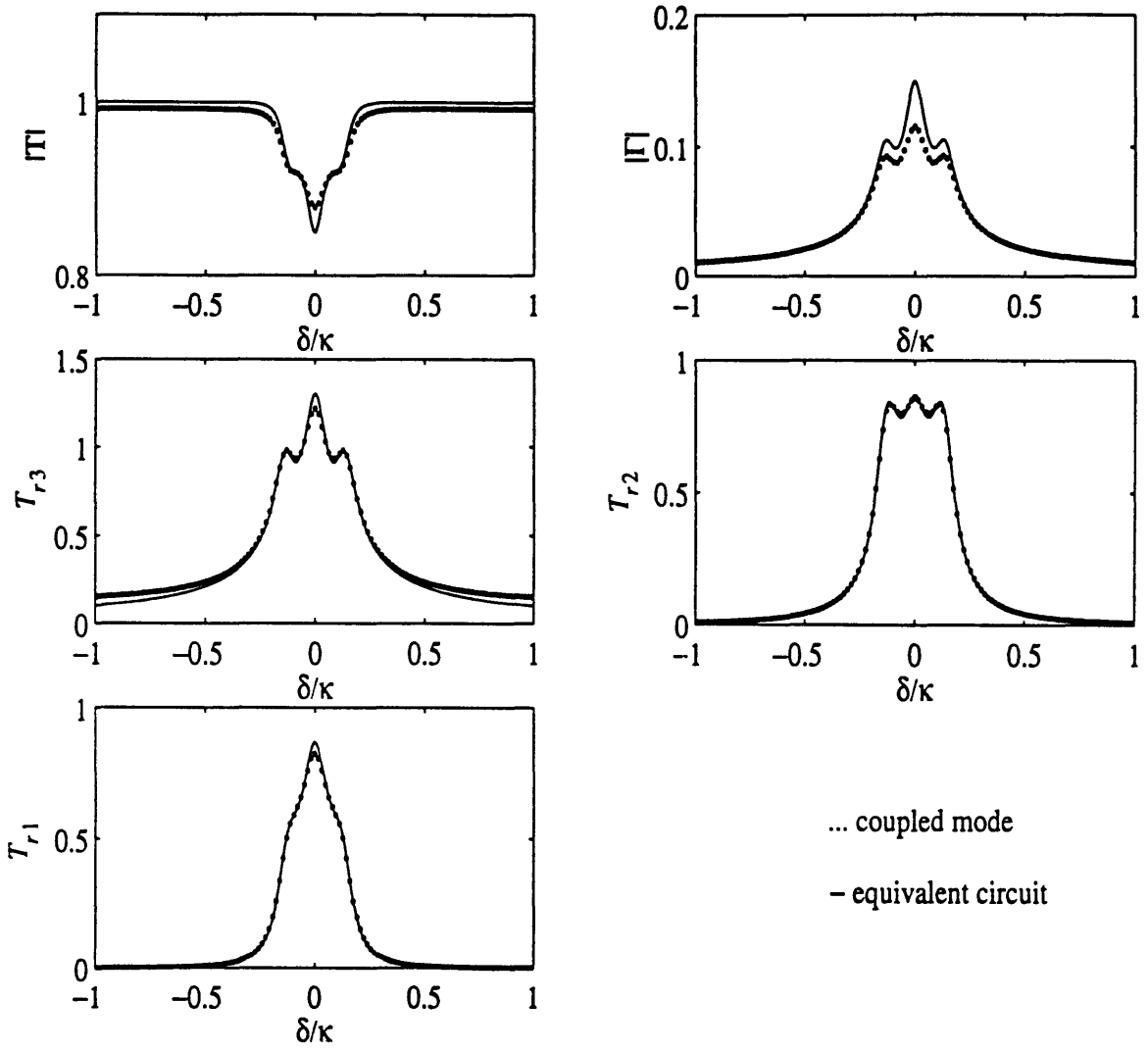

Figure 6-13: Comparing the equivalent circuit model with the exact analysis for a third-order channel dropping filter.(a) Transmitted Signal, T, on the bus. (b) Reflected Signal, Γ, on the bus. (c) Signal coupled to resonator 3, T_{r3}. (d) Signal coupled to resontor 2, T_{r2}. (e) Signal coupled to resonator 1, T_{r1}. $\mu_{12}/\kappa = \mu_{23}/\kappa = \mu_{34}/\kappa = 0.1$, $\Delta_1 = 0.1$, $\Delta_2 = 0.05$, $\Delta_3 = 0.01$

Chapter 7

Gain in Semiconductors

In the previous chapter we saw that evanescently coupled GDFB resonators excited from side-coupled signal waveguides form channel-dropping filters. The characteristic response of a filter of given order is determined by the choice of the device parameters, namely the DFB coupling coefficient κ, the coupling strength between structures i and j, μ_{ij}, and Δ_i. Δ_i is related to the κl_i product of the i^{th} resonator and is a measure of how close resonator i is to threshold. Some of the parameters, like the physical dimensions of the device and the spacing between the guides are obviously fixed at fabrication. Others like μ_{ij} and κ depend on the gain and can thus be controlled by adjusting the gain pumping mechanism. μ_{ij} depends weakly on gain via the dependence of the mode profile on the gain. To lowest order this dependence may be ignored provided the gain is not too large. κ on the other hand is directly dependent on the gain of the active region. Since the bandwidth of the filter response and the maximum power transferred to it are sensitive to the value of κ and Δ_i, use of GDFB resonators as viable CDFs relies on the ability to precisely control the gain/loss in the structure. In current injected systems, which is the type of gain pumping mechanism we are considering, this requirement translates to an accurate control of the gain by varying the current injected through the device. Therefore, to be able to design GDFB CDFs and evaluate their performance, an accurate characterization of the gain as a function of the current density and other material parameters is needed. This chapter is devoted to the study of optical gain and how it depends on the properties

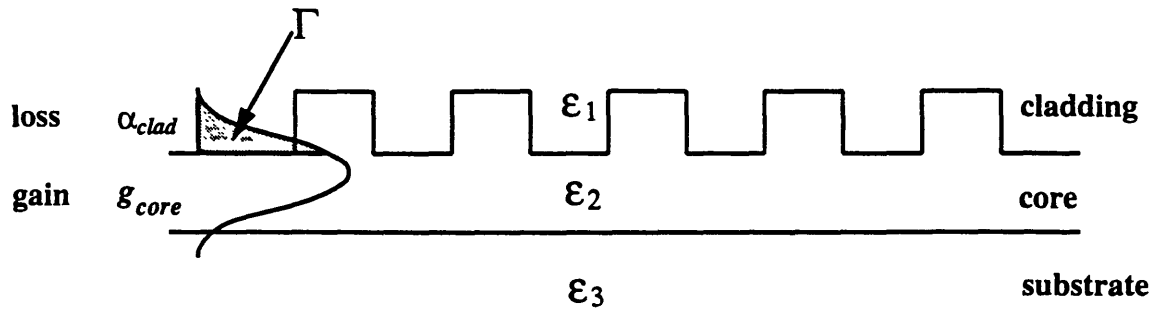

Figure 7-1: Schematic drawing of a gain grating

of a given material and the rate of carrier injection. We will consider the simplest case of an isotropic 3-D bulk medium. Some basic level of familiarity with electron Bloch wavefunctions and energy bands in semiconductors will be assumed. Using time dependent perturbation theory, the rate of transition of an electron from a discrete state in the conduction band to one in the valence band may be determined. Summing over all the electron states which obey energy conservation, will yield the total downward transition rate. A similar approach allows the upward transition rate, that is from the valence to the conduction band, to be obtained. Once these rates are known the gain of the active region may be found as a function of the carrier density which in turn can be related to the current density injected through the device, allowing a relation between current and gain to be obtained.

7.1 Electrons in Semiconductors

Consider the schematic representation of a gain grating shown in fig. (7-1). The figure shows a waveguide with the core region having gain and the cladding having loss. The substrate has neither gain nor loss. The patterned section of the guide provides alternate regions of gain/loss which cause DFB coupling, with the coupling coefficient, κ, given by

$$\kappa = \frac{\Delta g}{2\pi}\Gamma \tag{7.1}$$

as found in chapter 2. Γ is the overlap integral of the power in the field with the grating cross section, indicated shematically as the shaded region under the mode profile, and $\Delta g = g_{core} - g_{clad} = g_{core} + \alpha_{clad}$. We will assume that α_{clad} is chosen such that there is no net gain for a travelling wave in the guide. The gain, g_{core}, can be externally controlled via the pumping mechanism; i.e g_{core} is a function of the injected current density, j, through the device. Consequently, κ is a function of j via Δg (eq. (7.1)). By changing j, $\kappa(j)$ can be adjusted to give the desired value of $\Delta_i = \pi/2 - \kappa l_i$ and thus the appropriate filter response.

Before we can relate g_{core} and thus κ to j, we need a description of electrons in a semiconductor. Ignoring electron-electron interactions but allowing the electrons to interact with the periodic potential $V(\mathbf{r})$ of the crystal lattice, the equation describing the electronic wavefunction, Ψ_{nk}, in a semiconductor is [28]

$$H_o\Psi_{nk} = \left[\frac{\mathbf{p}^2}{2m} + V(\mathbf{r})\right]\Psi_{nk} = E_n(\mathbf{k})\Psi_{nk} \tag{7.2}$$

where H_o is the Hamiltonian describing the lattice. n and $\mathbf{k}$ are the band index and the crytal momentum or electron wavevector respectively. $E_n(\mathbf{k})$ is the energy of an electron in the n^{th} band with the wavevector $\mathbf{k}$. The interaction of the electron with the periodic lattice leads to a specific form of the Bloch wavefunction given by

$$\Psi_{nk}(\mathbf{r}) = e^{i\mathbf{k}.\mathbf{r}}u_n(\mathbf{k},\mathbf{r}) \tag{7.3}$$

where $u_n(\mathbf{k},\mathbf{r})$ is a periodic function with the periodicity of the lattice [28]. Accurately determining the Bloch functions and the energy band structures is an entire field in itself. We will assume presently that the Bloch functions are known. However, we will see later that they are not really needed; only the band structure is required. Moreover, we will not be concerned with the entire band structure of the solid but only be interested in the conduction and valence band $E_e(\mathbf{k})$ and $E_h(\mathbf{k})$ respectively.

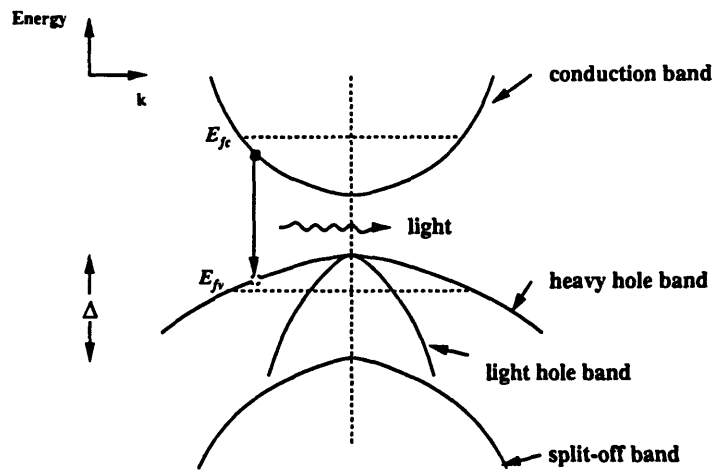

Figure 7-2: Schematic representation of the band structure of a direct gap semiconductor.

It will be assumed that these bands are parabolic, i.e

$$E_e(\mathbf{k}) = E_c + \frac{\hbar^2 k_e^2}{2m_c} \tag{7.4}$$

$$E_h(\mathbf{k}) = E_v - \frac{\hbar^2 k_h^2}{2m_v} \tag{7.5}$$

where m_c and m_v are the effective masses of the two bands and k_e and k_h are the magnitudes of the wavevectors of the electrons and the holes. The parabolic approximation is really a simplification. Away from the band edge this approximation is no longer valid. We have also assumed a lightly doped material so that there are no band-tail states [29] and the parabolic approximations is valid near the band edges. The energy versus wave-vector of a direct band gap semiconductor is shown schematically in fig. (7-2). Notice that there are three valence bands; the light-hole, heavy hole and the split off band which are twofold degenerate at $\mathbf{k} = 0$. Eq. (7.5) applies to each of these bands each with its respective E_v and m_v value.

Often we are interested in describing localized electron states in a given band, n_o. This may be done by using a linear superposition of the wavefunctions $\Psi_{n_o k}$ as follows

[28, 30]

$$\begin{aligned}\Psi &= \int A(\mathbf{k})\Psi_k(\mathbf{r})d^3\mathbf{k} \\ &= \int A(\mathbf{k})e^{i\mathbf{k}.\mathbf{r}}u(\mathbf{k},\mathbf{r})d^3\mathbf{k} \end{aligned} \tag{7.6}$$

where $A(\mathbf{k})$ are the expansion coefficients of the linear superposition. Since we are concerned with electrons in a specific band, the subscript n_o has been dropped. The subscripts will be re-introduced as needed. $u(\mathbf{k},\mathbf{r})$ is a slowly varying function of $\mathbf{k}$ and near the band edge may be approximated by its value at $\mathbf{k} = 0$, i.e $u(\mathbf{k},\mathbf{r}) \approx u(\mathbf{k}=0,\mathbf{r}) \equiv u(\mathbf{r})$ [31, 30]. Hence,

$$\Psi = \left[\int A(\mathbf{k})e^{i\mathbf{k}.\mathbf{r}}d\mathbf{k}\right] u(\mathbf{r}) \equiv F(\mathbf{r})u(\mathbf{r}) \tag{7.7}$$

The above description is called the envelope approximation where $F(\mathbf{r})$ is the envelope function [31, 28]. Since the electron wavepacket is strongly localized in reciprocal space, $F(\mathbf{r})$ is a slowly varying function of position and does not change much across a single unit lattice cell [30, 31]. According to convention, the two components of $\Psi(\mathbf{r})$ are independently normalized according to the following definition.

$$\langle F|F\rangle = \int_V F^*F\, d^3\mathbf{r} = 1, \tag{7.8}$$

$$\langle u|u\rangle = \frac{1}{V_{uc}}\int_{V_{uc}} u^*u\, d^3\mathbf{r} = 1, \tag{7.9}$$

where V is the volume of the entire crystal and V_{uc} is the volume of a single unit (or primitive) cell of the crystal. The eigen vectors of a Hermitian operator may be chosen to be orthonormal and therefore the periodic part of the conduction band and valence band Bloch functions, u_c and u_v, are orthogonal i.e

$$\langle u_c|u_v\rangle = 0 \tag{7.10}$$

For electrons in a bulk medium, the envelope function $F(\mathbf{r})$ takes a very simple

form, [31]

$$F(\mathbf{r}) = \frac{1}{\sqrt{V}} e^{i\mathbf{k}.\mathbf{r}}. \tag{7.11}$$

In more complicated structures, like quantum wells etc., however, $F(\mathbf{r})$ is obtained by using the effective mass theorm [31, 28, 30]. In this chapter we will be concerned with the simplest system i.e a 3D isotropic bulk medium.

7.2 Interaction of Photons and Electrons

Photons can interact with electrons in a solid causing transitions to occur between electrons in the conduction and valence band. Such transitions may lead to a growth or decay of photons in the optical mode. For example, a photon with energy greater than the bandgap energy, E_g, may be absorbed by an electron in the valence band causing it to make an upward transition to an unoccupied state in the conduction band. Such a process causes a depletion of photons in the optical mode, a mechanism leading to loss. On the other hand, a photon may excite a transition of an electron from an occupied state in the conduction band to an unoccupied electron state (or a hole) in the valence band resulting in a stimulated emission of a photon. The recombination of the hole and electron produces a photon and contributes to gain. In order to understand optical gain, we need to closely examine the electron-photon interaction.

Classically, the photon can be represented by an electromagnetic field. In the presence of an electric field, the Hamiltonian is modified through the introduction of the vector potential, $\mathbf{A}$ [32] i.e

$$\mathbf{p} \rightarrow (\mathbf{p} + e\mathbf{A}) \tag{7.12}$$

The vector potential is related to the electric field by the equation $\mathbf{E} = -\frac{\partial \mathbf{A}}{\partial t}$ and is given by

$$\mathbf{A} = \frac{\hat{\mathbf{e}}}{2}\left[\mathbf{A}(\mathbf{r})e^{-i\omega t} + \mathbf{A}^*(\mathbf{r})e^{i\omega t}\right] \tag{7.13}$$

where $\hat{\mathbf{e}}$ is the polarization vector. The Hamiltonian in the presence of a electromag-

netic field is, therefore,

$$\begin{aligned} H &= \frac{1}{2m_o}(\mathbf{p}+e\mathbf{A})^2 + V(\mathbf{r}) \\ &\simeq \frac{\mathbf{p}^2}{2m_o} + V(\mathbf{r}) + \frac{e}{m_o}\mathbf{A}.\mathbf{p} \equiv H_o + H'(\mathbf{r},t). \end{aligned} \tag{7.14}$$

m_o is the free-space mass of the electron. Notice that the $\mathbf{A}^2$ term has been dropped. The final result is, however, not affected by this approximation provided $\mathbf{A}(\mathbf{r})$ varies slowly over a unit cell [31]. Equation (7.14) has been written so as to separate the "unperturbed" Hamiltonian H_o, (eq. (7.2)), whose eigen-functions are the Bloch states, from the "perturbation", H' produced due to the field associated with $\mathbf{A}$. Written explicitly,

$$H'(\mathbf{r},t) = H'(\mathbf{r})e^{-i\omega t} + H'^*(\mathbf{r})e^{i\omega t} \tag{7.15}$$

where

$$H'(r) \equiv \frac{e\mathbf{A}(\mathbf{r})}{2m_o}\hat{\mathbf{e}}.\mathbf{p} \tag{7.16}$$

The effect of this time dependent perturbation as stated before is to cause transitions to occur between the valence and conduction band electron states. Using time dependent perturbation theory, it is straightforward to calculate the transition rate, $W_{e\to h}$, of an electron undergoing a transition from a conduction band state Ψ_e, with energy E_e, to a valence band state Ψ_h, with energy E_h [32]. It is given by

$$W_{e\to h} = \frac{2\pi}{\hbar}|H'_{eh}|^2\delta(E_e - E_h - \hbar\omega) \tag{7.17}$$

where

$$H'_{eh} \equiv \langle\Psi_h|H'(r)|\Psi_e\rangle = \int \Psi_h^* H'(r)\Psi_e\, d^3\mathbf{r} \tag{7.18}$$

Equation (7.17) is known as Fermi's Golden Rule. $|H'_{eh}|^2$ is the transition matrix element and represents the probability of the transition. The Dirac delta function ensures the fact that the energy, $(E_e - E_h)$, of the photon emitted due to the transition of the electron from an energy level E_e to E_h, is the same as the energy, $\hbar\omega$, of the photon which stimulated the transition. For upwards transitions the delta function

ensures that the energy absorbed by the electron, $\hbar\omega$, must be equal to the difference in energies between the final and initial states of the electron, thereby enforcing energy conservation. The transition matrix element may be simplified by substituting for the Ψ_e and Ψ_h, given by $\Psi_{e,h} = F_{e,h}\, u_{c,v}$. Thus,

$$\begin{aligned} H'_{eh} &= \langle \Psi_h | \left(\frac{e}{2m_o} \mathbf{A}.\mathbf{p} \right) | \Psi_e \rangle \\ &= \int F_h^* u_v^* \left(\frac{e}{2m_o} \mathbf{A}.\mathbf{p} \right) F_e u_c \, d^3\mathbf{r} \\ &= \int u_v^* u_c F_h^* \left(\frac{e}{2m_o} \mathbf{A}.\mathbf{p} \right) F_e \, d^3r + \int F_h^* F_e \, u_v^* \left(\frac{e}{2m_o} \mathbf{A}.\mathbf{p} \right) u_c \, d^3\mathbf{r}, \quad (7.19) \end{aligned}$$

where we have used the fact that

$$\mathbf{p}\,(F_e u_c) = u_c\,(\mathbf{p} F_e) + F_e\,(\mathbf{p} u_c)\,.$$

As mentioned previously, $F_e(\mathbf{r})$ and $F_h(\mathbf{r})$ vary slowly over a single unit cell. Moreover, we will also assume that $\mathbf{A}(\mathbf{r})$ does not vary appreciably over a primitive cell. This allows the integrals in eq. (7.19) to be approximated by considering their values at the unit cell j and summing over all unit cells. Thus,

$$\int_V u_v^* u_c F_h^* \left(\frac{e}{2m_o} \mathbf{A}.\mathbf{p} \right) F_e d^3\mathbf{r} \simeq \sum_j^{\text{unit cells}} \int_{V_{uc}^j} d^3\mathbf{r}\, u_v^* u_c \left\{ F_h^*(\mathbf{r_j}) \left(\frac{e}{2m_o} \vec{A}(\mathbf{r_j}).\mathbf{p} \right) F_e(\mathbf{r_j}) \right\}$$

However, $u_{c,v}$ are periodic functions with the periodicity of the lattice and can therefore be pulled out of the summation. Hence

$$\begin{aligned} \int_V u_v^* u_c F_h^* \left(\frac{e}{2m_o} \mathbf{A}.\mathbf{p} \right) F_e d^3\mathbf{r} &\simeq \int_{V_{uc}} u_v^* u_c d^3\mathbf{r} \left[\sum_j^{\text{unit cells}} \left\{ F_h^*(\mathbf{r_j}) \left(\frac{e}{2m_o} \vec{A}(\mathbf{r_j}).\mathbf{p} \right) F_e(\mathbf{r_j}) \right\} \right] \\ &= 0, \end{aligned}$$

by the orthogonality condition $\langle u_v | u_c \rangle = 0$. The second term can, likewise, be approximated by

$$\int F_h^* F_e u_v^* \left(\frac{e}{2m_o} \mathbf{A}.\mathbf{p} \right) u_c \, d^3\mathbf{r} = \frac{e}{2m_o} \sum_j F_h^*(\mathbf{r_j}) A(\mathbf{r_j}) F_e(\mathbf{r_j}) \int_{V_{uc}^j} u_v^*(\hat{\mathbf{e}}.\mathbf{p})\, u_c \, d^3\mathbf{r}$$

$$= \left(\frac{1}{V_{uc}}\int_{V_{uc}} u_v^*(\hat{\mathbf{e}}.\mathbf{p})u_c\, d^3\mathbf{r}\right)\frac{e}{2m_o}\sum_j F_h^*(\mathbf{r_j})\mathbf{A}(\mathbf{r_j})F_e(\mathbf{r_j})V_{uc}.$$

We have again used the periodicity of u_c and u_v to pull the integral out of the summation. Since the terms in the summation are fairly constant over each unit cell, the summation can be converted into an integral as

$$\sum_j^{\text{unit cells}} F_h^*(\mathbf{r}_j)A(\mathbf{r}_j)F_e(\mathbf{r}_j)V_{uc} \simeq \int_V F_h^*(\mathbf{r})A(\mathbf{r})F_e(\mathbf{r}\, d^3\mathbf{r}.$$

Therefore,

$$H'_{eh} = \frac{e}{2m_o}\langle u_v|(\hat{\mathbf{e}}.\mathbf{p})|u_c\rangle \int_V F_h^* A(\mathbf{r})F_e\, d^3\mathbf{r} \tag{7.20}$$

Consider a bulk medium, with $F = \frac{1}{\sqrt{V}}e^{i\mathbf{k}.\mathbf{r}}$, excited by a plane wave. In this case, $A(\mathbf{r}) = A_o e^{i\mathbf{k}_{ph}.\mathbf{r}}$ and we have that

$$\begin{aligned}\int F_h^* A(\mathbf{r})F_e &= A_o \int e^{-i\mathbf{k}_h.\mathbf{r}}e^{i\mathbf{k}_{ph}.\mathbf{r}}e^{i\mathbf{k}_e.\mathbf{r}} \\ &= A_o\delta(\mathbf{k}_h - \mathbf{k}_e - \mathbf{k}_{ph}) \\ &\simeq A_o\delta(\mathbf{k}_h - \mathbf{k}_e) \end{aligned} \tag{7.21}$$

The last expression follows from the fact that in general $\mathbf{k}_{ph} \sim \frac{\pi}{\lambda_{ph}} \ll \mathbf{k}_{e,h} \sim \frac{\pi}{a}$ where the wavelength of light, λ_{ph} is much larger than a which is the periodicity of the lattice and is generally on the order of angstroms . Thus, we see that wavevectors of the electrons are conserved in interband transitions and only vertical transitions are allowed. This is known as the **k**-conservation or **k**-selection rule [31] and applies to direct inter-band transitions. The **k**-selection rule does not apply to all transitions, for e.g. like phonon-assisted transitions etc. If the vector potential can be treated as a constant, i.e $A = A_o$, which is a good approximation in the case of quantum wells, we have that

$$H'_{eh} = \frac{eA_o}{2m_o}\langle u_v|(\hat{\mathbf{e}}.\mathbf{p})|u_c\rangle\langle F_h|F_e\rangle$$

which yields its own selection rules according to the value of $\langle F_h|F_e\rangle$.

Summarizing, for a 3D bulk material, excited by a plane wave, only vertical tran-

sitions are allowed and the transition matrix is given by

$$|H'_{eh}|^2 = \left(\frac{eA_o}{2m_o}\right)^2 |M_T|^2 \tag{7.22}$$

where $|M_T|^2 = |\langle u_v|(\hat{\mathbf{e}}.\mathbf{p})|u_c\rangle|^2$. At this stage, it seems that the functions u_c and u_v are needed to evaluate M_T. However, a second-order perturbation technique called the **k.p** theory [33] allows $|M_T|^2$ to be related to the band structure of the given material. Since this calculation is somewhat more involved and requires more familiarity with Bloch functions and band structures, the derivation of $|M_T|^2$ is not attempted. Here we present the key results [31].

$$|M|^2 = \left(\frac{m_o}{m^*} - 1\right) \frac{E_g + \Delta}{2\left(E_g + \frac{2}{3}\Delta\right)} m_o E_g \tag{7.23}$$

$$|M_T|^2 = \frac{2}{3}|M|^2 \tag{7.24}$$

where m^* is approximately the same as the effective mass, m_c, of the conduction band electron. E_g is the bandgap and Δ is the split-off energy (see fig. (7-2)). In relating $|M_T|^2$ to $|M|^2$, the factor of $\frac{1}{3}$ comes from averaging over all the **k**-vectors of the electrons and the factor 2 comes from taking the spin degeneracy into account. m_c can be measured quite accurately using cyclotron resonance techniques [28]. Assuming $m^* \simeq m_c$ allows $|M|^2$ to be evaluated by using eq. (7.23). Table (7.1) shows the most accurately reported value of $|M|^2$ for several commonly used material systems [31].

We now have the transition rate, $W_{e\to h}$, of an electron making a transition from a single occupied state in the conduction band to one in the valence band in terms of quantities that are either known or can be estimated.

$$W_{e\to h} = \frac{2\pi}{\hbar}|H'_{eh}|^2\,\delta(E_e(k_e) - E_h(k_h) - \hbar\omega)$$

Material system	$\frac{2\|M\|^2}{m_o}$ (in eV)	Reference
GaAs	28.8 ± 0.15	[34, 35]
$Al_xGa_{1-x}As$ $(x < 0.3)$	$29.83 + 2.85x$	[36]
$In_xGa_{1-x}As$	$28.8 - 6.6x$	[34, 35]
InP	19.7 ± 0.6	[34, 35]
$In_{1-x}Ga_xAs_yP_{1-y}$ $(x = 0.47y)$	$19.7 + 5.6y$	[35, 37]

Table 7.1: Magnitude of $|M|^2$ for various material systems.

For a bulk medium incorporating the **k**-selection rule and using eq. (7.22), we have

$$W_{e\to h} = \frac{2\pi}{\hbar}\left(\frac{eA_o}{2m_o}\right)^2 |M_T|^2\,\delta(E_e(\mathbf{k}) - E_h(\mathbf{k}) - \hbar\omega) \tag{7.25}$$

where $|M_T|^2$ is related to the band structure of the given material system, eqs. (7.23) and (7.24).

There are many states in the conduction and valence band of a given solid. In fact, from the periodic boundary conditions [28], we know that the number of **k**-states per unit volume per unit spin is given by

$$\#\ \text{states/vol} = \frac{\mathrm{d}^3\mathbf{k}}{(2\pi)^3}$$

To evaluate the total transition rate per unit volume from the conduction band to the valence band, $W_{c\to v}$, we must sum over all possible **k**-states which obey the energy relation imposed by the delta function. Since the **k**-selection imposes the condition that only vertical transitions take place (and we will assume that these are the only dominant transitions), we need only sum over the states in the conduction band to get $W_{c\to v}$. Thus, the total transition rate per unit vol. $W_{c\to v}$ is given by [31]

$$W_{c\to v} = \int W_{e\to h}\,\frac{d^3\mathbf{k}}{(2\pi)^3} \tag{7.26}$$

The spin degeneracy has been taken into account in $W_{e\to h}$ via $|M_T|^2$. Substituting

for $W_{e\to h}$, we have that

$$W_{c\to v} = \frac{2\pi}{\hbar}|H'_{eh}|^2 \int \delta(E_e(\mathbf{k}) - E_h(\mathbf{k}) - \hbar\omega)\,\frac{d^3\mathbf{k}}{(2\pi)^3} \tag{7.27}$$

The above integral is called the reduced or joint density of states, ρ_{red}, and is simply the total number of states per volume which obeys the energy relation imposed by the delta function.

$$\begin{aligned}
\rho_{red} &\equiv \int \delta(E_e(\mathbf{k}) - E_h(\mathbf{k}) - \hbar\omega)\,\frac{d^3\mathbf{k}}{(2\pi)^3} \\
&= \frac{1}{(2\pi)^3}\int \delta(E_e - E_h - \hbar\omega)\,\frac{d^2S\,dE}{\nabla_{\mathbf{k}}(E_e - E_h)} \\
&= \frac{1}{(2\pi)^3}\oint_{E_e-E_h=\hbar\omega} \frac{d^2S}{\nabla_{\mathbf{k}}(E_e - E_h)}
\end{aligned} \tag{7.28}$$

Using equations (7.4) and (7.5), we have that

$$E_{eh} \equiv E_e(\mathbf{k}) - E_h(\mathbf{k}) = \frac{\hbar^2k^2}{2m_r} + E_g \tag{7.29}$$

where $\frac{1}{m_r} = \frac{1}{m_c} + \frac{1}{m_v}$ and $E_g = E_c - E_v$. Using these expression in eq. (7.28), we get

$$\rho_{red} = \frac{1}{(2\pi)^3}\oint_{E_e-E_h=\hbar\omega} \frac{d^2S}{\nabla_{\mathbf{k}}(E_e - E_h)} = \frac{1}{(2\pi)^3}\left.\frac{4\pi k^2}{\frac{\hbar^2}{m_r}k}\right|_{E_e-E_h=\hbar\omega} \tag{7.30}$$

$$\rho_{red}(\hbar\omega) = \frac{1}{(2\pi)^2}\left(\frac{2m_r}{\hbar}\right)^{3/2}(\hbar\omega - E_g)^{1/2} \tag{7.31}$$

Physically $\rho_{red}(\hbar\omega)$ corresponds to the number of states per energy per volume that emit light of energy $\hbar\omega$ as a result of transitions between the conduction and the valence bands.

Thus far, we have assumed that the state in the conduction band is occupied and the state in the valence band that the electron is making a transition to is empty. However, for finite temperatures we can only associate probabilities for the occupancy of these states. f_c and f_v denote the probability of occupancy of a conduction band and valence band state respectively and are given by the Fermi-Dirac distribution

functions [38].

$$f_{c,v} = \frac{1}{1 + exp\left[\frac{(E_{e,h} - E_{fc,fv})}{k_B T}\right]}, \tag{7.32}$$

where E_{fc} and E_{fv} are the non-equilibrium Fermi levels [38, 31]. E_e and E_h are the energies of the electron and hole respectively and can be described in terms of E_{eh} and the effective masses $m_{c,v}$ as follows

$$E_e = E_c + (E_{eh} - E_g)\frac{m_r}{m_c}, \tag{7.33}$$

$$E_h = E_v - (E_{eh} - E_g)\frac{m_r}{m_v}. \tag{7.34}$$

Taking these probabilities into account, the transition rate per unit volume from the conduction to the valence band $W_{c\to v}$ is given by

$$W_{c\to v} = \overbrace{\frac{2\pi}{\hbar}|H'_{eh}|^2}^{\text{rate of transition}} \overbrace{\rho_{red}}^{\text{available states}} \overbrace{f_c}^{\text{occ. c-state}} \overbrace{(1 - f_v)}^{\text{unocc. v-state}} \tag{7.35}$$

As indicated, the first term represents the rate of transitions between discrete states in the conduction and valence band. The second term represents the density of states that can emit photons at the energy of interest. Finally the probability densities take into account that for downward transitions, the conduction band state must be occupied and the valence band state is unoccupied.

To find the transition rate per unit volume of electrons being excited from the valence band to the conduction band, $W_{v\to c}$, a similar analysis to the one above may be performed. However, we will find that the first two factors of $W_{v\to c}$ are the same as that of $W_{c\to v}$. The only difference is that we now require that the electron state in the valence band be occupied and the state in the conduction band that it is making the transition to be unoccupied. Thus the relevant probability is $f_v(1 - f_c)$ and

$$W_{v\to c} = \frac{2\pi}{\hbar}|H'_{eh}|^2 \rho_{red}(\hbar\omega) f_v(1 - f_c) \tag{7.36}$$

. We will use the transitions rates computed here to calculate the optical gain per

unit length in the following section.

7.3 Gain

As was mentioned earlier, the presence of photons in the form of an EM wave, causes electrons to make transitions between the conduction and the valence bands. Transition from the conduction to the valence bands lead to the generation of photons. Similarly transitions from the valence to the conduction band require energy and lead to the depletion of photons from the optical mode. Whether the net result is an increase or decrease of photons in the optical mode depends on which of the two types of transition processes dominates.

Let Φ represent the incoming photon flux in the optical mode. The rate of change of photon flux, Φ, along the direction of propagation of the EM wave (chosen as $\hat{z}$ for definiteness) is given by

$$\begin{aligned} \frac{d\Phi}{dz} &= W_{c\to v} - W_{v\to c} \\ &= \frac{2\pi}{\hbar}\left(\frac{eA_o}{2m_o}\right)^2 |M_T|^2 \rho_{red}\,(f_c - f_v)\,. \end{aligned} \tag{7.37}$$

The gain, g, is defined as the fractional increase in the photon flux per unit length, i.e

$$g \equiv \frac{1}{\Phi}\frac{d\Phi}{dz}. \tag{7.38}$$

The photons flux is given by

$$\Phi = \frac{\text{(energy density of the mode)(group vel.)}}{\text{energy per photon}}$$

The energy density of the optical mode is

$$\text{energy density} = \frac{1}{2}\overline{n}^2\epsilon_o E^2 = \frac{1}{2}\overline{n}^2\epsilon_o\omega^2 A^2$$

The group velocity, v_g is obtained from

$$\begin{aligned} v_g &\equiv \left(\frac{d\beta}{d\omega}\right)^{-1} = \left\{\frac{d}{d\omega}\left[\frac{\omega n(\omega)}{c}\right]\right\}^{-1} \\ &= \frac{c}{\left(n+\omega\frac{dn}{d\omega}\right)} \equiv \frac{c}{\overline{n}_g} \end{aligned} \tag{7.39}$$

where $\overline{n}_g$ is the group index. Substituting the above results in the expression for Φ we find that the photon flux is

$$\Phi = \frac{\left(\frac{1}{2}\overline{n}^2\epsilon_o\omega^2A^2\right)\left(\frac{c}{\overline{n}_g}\right)}{\hbar\omega} \tag{7.40}$$

Use of eqs. (7.37), (7.38) and the above expression allow the gain, g, to be calculated.

$$g = \left(\frac{1}{\hbar\omega}\right)\frac{\pi e^2\hbar\overline{n}_g}{\epsilon_o c\overline{n}^2 m_o^2}\left|M_T\right|^2\rho_{red}(\hbar\omega)\ (f_c - f_v) \tag{7.41}$$

It is clear from eqs. (7.31) and (7.41), that the gain is zero when $\hbar\omega = E_g$ and is positive when $f_c > f_v$. The latter condition implies that

$$\begin{aligned} \exp\left(\frac{E_e - E_{fc}}{k_BT}\right) &< \exp\left(\frac{E_h - E_{fv}}{k_BT}\right) \Rightarrow \\ \hbar\omega &< E_{fc} - E_{fv}. \end{aligned}$$

Combining the two conditions we see that $g > 0$ provided

$$E_g < \hbar\omega < E_{fc} - E_{fv}. \tag{7.42}$$

We see that the gain is function of frequency. Moreover, it depends on the quasi-fermi levels E_{fc} and E_{fv} via the Fermi-Dirac distribution functions, f_c and f_v. The fermi-levels are determined by the carrier densities in the active region and are related to the current injected through the device. In the following section, we will derive an expression for the current density, j, through the device and then relate j to g.

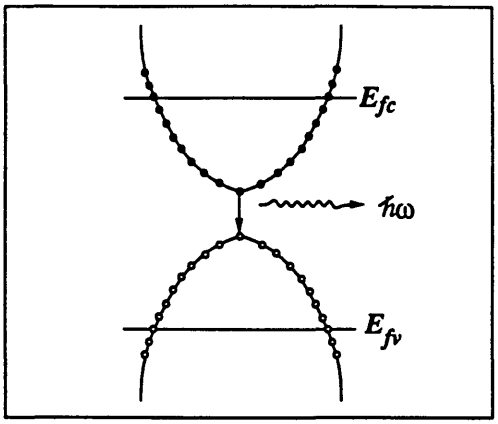

Figure 7-3: Schematic picture of a non-equilibrium situation which results in gain for some frequencies, ω

7.4 Current Density

Under equilibrium conditions, $E_{fc} = E_{fv}$ and according to eq. (7.42) none of frequencies experience gain. However, under non-equilibrium conditions, for eg. when carriers are injected into the active region, it is possible to have a situation in which $E_{fc} - E_{fv} > \hbar\omega$. In this case certain frequencies can experience gain. This situation is drawn schematically in fig. (7-3) which shows the conduction band and one of the valence bands of the active region. We see that in the active region, there is a large concentration of holes and electrons. The electron-hole pairs may either recombine via radiative mechanisms, giving rise to photons or via non-radiative processes which as the name implies does not result in the generation of photons. Radiative processes are of two types namely stimulated or spontaneous transitions. Non-radiative processes, on the other hand, may result from several mechanisms. Among these are bulk and interface recombination via defect states [29, 31], Auger recombination [29, 31] or leakage of carriers out of the active region [29, 31] etc. Each of the processes, radiative and non-radiative, is associated with its respective current densities, j_{rad} and $j_{non-rad}$. The current densities are functions of the carrier density in the active region and the rate of recombination of the carriers due to the two processes. The

total current density is the sum of the two contributions,

$$j_{tot} = j_{rad} + j_{non-rad}.$$

Non-radiative processes are undesireable since they do not contribute to gain and result in a larger current density through the device for the same gain. Below threshold, the radiative process is dominated by spontaneous recombination. To calculate j_{rad}, thus, we need to determine the spontaneous recombination rate which is discussed in the next subsection.

7.4.1 Spontaneous Recombination Rate

A complete quantum mechanical treatment of the optical processes which quantizes the electromagnetic field reveals that the rate of transitions from the conduction to the valence band is proportional to $(\langle n_{ph} \rangle + 1)\hbar\omega$, where $\langle n_{ph} \rangle$ is the average number of photons in the mode [31]. Thus, we see that the downward transitions are possible even in the absence of any photons. This decay of electrons from the conduction to the valence band in the absence of light corresponds to spontaneous emission.

The number of photons enters into the previously derived transition rate $W_{c \to v}$ through the A_o^2 term. Thus, to find the spontaneous emission rate the A_o^2 term in $W_{c \to v}$ must be replaced by relating the energy in the EM wave to the energy of single photon, i.e

$$\frac{1}{2}\overline{n}^2 \epsilon_o \omega^2 A_o^2 V = \hbar\omega \;\Rightarrow\; A_o^2 = \frac{2\hbar\omega}{\overline{n}^2 \epsilon_o \omega^2 V} \tag{7.43}$$

where V is the volume occupied by the optical mode. Spontaneous transitions can occur into any of the optical modes near the transition energy, $\hbar\omega \approx E_g$. Since there need not be photons in these modes for spontaneous emission to occur, the electron interacts with all the optical modes in this energy range. Thus, the quantity of interest is the rate of spontaneous emission per unit vol. at a given energy, $R_{sp}(\hbar\omega)$. $R_{sp}(\hbar\omega)$ is given by the product of $W_{c \to v}$, using the appropriate value of A_o^2, and the number of optical modes, N_{opt} available at $\hbar\omega$. The number of optical modes at a

given energy may be found using the density of optical modes, ρ_{opt}.

$$N_{opt}(\hbar\omega) = \rho_{opt}(\hbar\omega)V$$

where $\rho_{opt}(\hbar\omega)$ is given by

$$\rho_{opt}(\hbar\omega)\, d(\hbar\omega) = 2\frac{d^3\mathbf{k}_{opt}}{(2\pi)^3} \tag{7.44}$$

$$k_{opt} = \frac{\overline{n}(\omega)}{\hbar c}(\hbar\omega) \quad \Rightarrow \quad dk = \frac{\overline{n}_g}{\hbar c}\, d(\hbar\omega) \tag{7.45}$$

$$\rho_{opt}(\hbar\omega) = \frac{1}{\pi^2}\frac{\overline{n}^2\,\overline{n}_g}{(\hbar c)^3}(\hbar\omega)^2 \tag{7.46}$$

The factor of 2 in eq. (7.44) takes into account the fact that for each plane wave there exist two polarization states. $\overline{n}_g$ is the group index defined by eq. (7.39). From the above discussion, it is clear that the equation defining $R_{sp}(\hbar\omega)$ is

$$R_{sp}(\hbar\omega)\, d(\hbar\omega) = W_{c\to v}\left(A_o^2 = \frac{2\hbar\omega}{\overline{n}^2\epsilon_o\omega^2}\right)\rho_{opt}\, V\, d(\hbar\omega). \tag{7.47}$$

Substituting for $W_{c\to v}$ and ρ_{opt} into the above equation, we find that

$$R_{sp}(\hbar\omega) = \left(\frac{1}{\hbar\omega}\right)\frac{\pi e^2\hbar}{\overline{n}^2\,\epsilon_o m_o^2}\,|M_T|^2\,\rho_{red}(\hbar\omega)\,\rho_{opt}(\hbar\omega)\,f_c(1-f_v) \tag{7.48}$$

for an isotropic bulk medium. In general, $|M_T|^2$ must be replaced by an appropriately averaged quantity $|M_{ave}|^2$ which takes into account the anisotropy of the medium, i.e

$$|M_{ave}|^2 = \frac{1}{3}\sum_{\text{all 3 polarizations}}|M_T|^2$$

The radiative component of the current density, j_{rad}, is simply given by the integral of $R_{sp}(\hbar\omega)$ over the spontaneous emission spectrum, i.e

$$j_{rad} = e\int R_{sp}(\hbar\omega)\, d(\hbar\omega) \tag{7.49}$$

We now have an expression for the radiative current density, j_{rad}, and are in a position

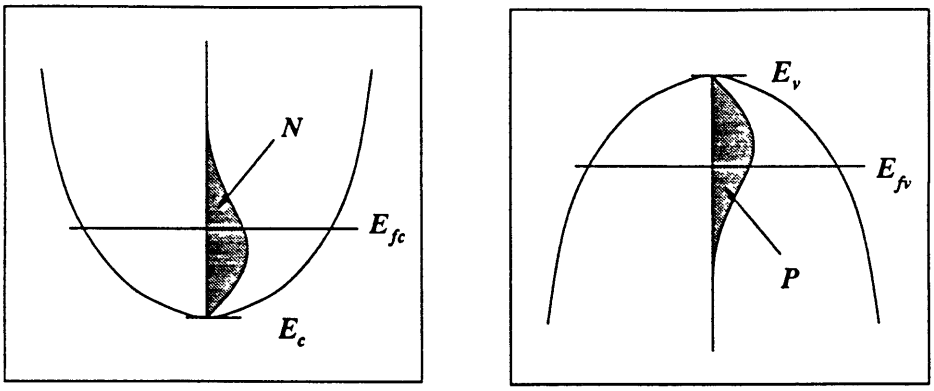

Figure 7-4: Calculating the quasi-fermi levels $E_{fc,fv}$ by relating them the carrier density in the active region, N ($\simeq P$).

to relate it to the gain. The expression for the optical gain is rewritten here.

$$g = \left(\frac{1}{\hbar\omega}\right) \frac{\pi e^2 \hbar}{\epsilon_o c m_o^2} \frac{\overline{n}_g}{\overline{n}^2} |M_T|^2 \rho_{red}(\hbar\omega) \, (f_c - f_v)$$

Looking at the above expression, we see that all quantities are either known like the physical/optical constants or can be estimated; for eg. $|M_T|^2$ is related to the band structure. The only quantities which are undetermined are the quasi-fermi levels, E_{fc} and E_{fv} in the distribution functions f_c and f_v. Likewise, it is clear from eqs. (7.49) and (7.48) that the only quantities that are not known in j_{rad} are the quasi-fermi levels. The quasi-fermi levels can be related to the carrier density in the active region via the following equations:

$$N = \int_{E_c}^{\infty} \rho_c(E) f_c(E) \, dE \tag{7.50}$$

$$P = \int_{-\infty}^{E_v} \rho_v(E)(1 - f_v(E)) \, dE \tag{7.51}$$

where N and P are the density of electrons and holes respectively (see fig. (7-4)). $\rho_{c,v}(E)$ are the density of states in the conduction and valence band which are found using the dispersion relation, eqs. (7.4) and (7.5), and the periodic boundary

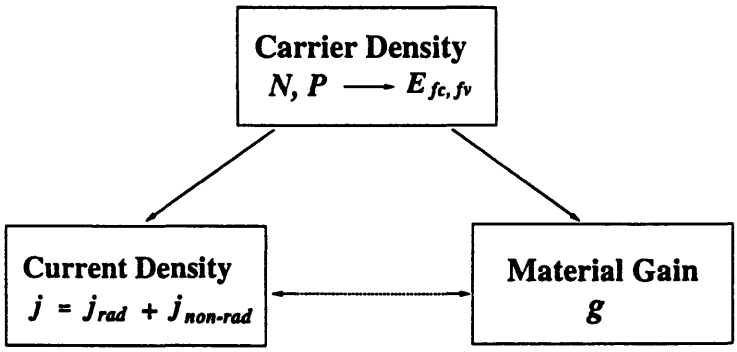

Figure 7-5: Relating the current injected to the gain

conditions [28].

$$\rho_{c,v} = 2\frac{d^3\mathbf{k}}{(2\pi)^3} \Rightarrow$$

$$\rho_c = \frac{1}{2\pi^2}\left(\frac{2m_c}{\hbar^2}\right)^{3/2}(E - E_c)^{1/2} \tag{7.52}$$

$$\rho_v = \frac{1}{2\pi^2}\left(\frac{2m_v}{\hbar^2}\right)^{3/2}(E_v - E)^{1/2} \tag{7.53}$$

To relate the gain, g, to the current density , we follow the following operations. This approach is very similar to that of reference [31].

(i) For a given density N and P of carriers in the active region, the quasi-fermi levels E_{fc} and E_{fv} are calculated by using eqs. (7.50) and (7.51). E_{fc} and E_{fv} are related by imposing the condition of charge neutrality which is

$$N \simeq P.$$

(ii) Once quasi-fermi levels are known, use of eqs. (7.41), (7.48) and (7.49) allows the gain, g, and the radiative current, j_{rad}, to be calculated as a function of the carrier density, N ($\simeq P$). By eliminating the carrier density a relation between g and j_{rad} may be obtained. To relate the gain to the total current density, j_{tot}, an expression for the non-radiative component of the current density needs to be determined. As

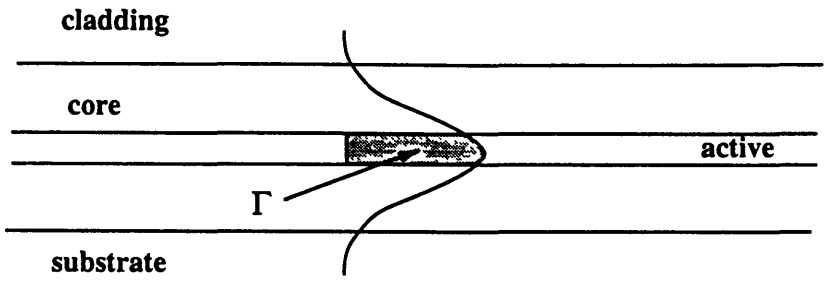

Figure 7-6: Waveguide with gain in its central region.

mentioned earlier, there are several mechanisms which contribute to $j_{non-rad}$. Each has its characteristic dependence on the carrier density N in the active region. For eg. for the Auger process, the recombination rate is proportional to N^3 [29] and for surface and defect recombination, the rate is proportional to N [29]. A rigorous derivation of the total non-radiative component of the current density is beyond the scope of the present discussion. The interested reader is referred to some references on this topic. Suffice it to say that an expression for $j_{non-rad}$ as a function of the carrier density N may be obtained. For the given carrier density in (i), the total current density $j_{tot}(N) = j_{rad}(N) + j_{non-rad}(N)$, and the gain may be obtained as functions of N. Eliminating N, between them allows a relation between g and j_{tot} to be obtained. The steps followed are shown diagramatically in fig. (7-5).

7.5 Material Gain and Modal Gain

In the previous sections we found the optical gain, g, of an infinite 3-D bulk medium excited by a plane wave of the form $\mathbf{A}(\mathbf{r}) = A_o e^{i\mathbf{k}.\mathbf{r}}$. g is the material gain and as is clear from eq. (7.41) it is only depends on the material and optical properties and on the pumping levels. Typically, in semiconductor devices, however, the excitations are not plane waves but are rather optical modes of waveguides. Moreover, the active region is finite and is often smaller compared to other features of the device. Figure (7-6) shows a waveguide which has gain in the central region of its core. The optical modes supported by the waveguides stimulate transitions which lead to

gain if condition (7.42) is satisfied. Only the field overlapping with the active region contributes to the gain as the field outside this regions does not give rise to stimulated emission, thus not contributing to gain. As a result, the net gain experienced by the optical mode, or the modal gain, γ, is smaller than the material gain, g. Since the medium is not uniform in the transverse dimension, instead of considering the photon flux, Φ, and the transition rate per unit volume, $W_{c\to v}$, we are concerned with the number of photons, n_{ph} passing through the guide per unit time, and the transition rate per unit length denoted by $w_{c\to v}$. The modal gain, γ, is defined as the change in the number of photons per unit length per unit time along the guide normalized to the number of photons per unit time passing the guide, i.e

$$\gamma = \frac{1}{n_{ph}} \frac{dn_{ph}}{dz} \tag{7.54}$$

but n_{ph} is related to the rate of transitions per unit length by the equation

$$\frac{dn_{ph}}{dz} = w_{c\to v} - w_{v\to c}$$

where $w_{c\to v}$ may be related to rate of transitions per unit volume $W_{c\to v}$ by

$$w_{c\to v} = \int_{\text{active region}} W_{c\to v}\, d\rho \tag{7.55}$$

where ρ denotes the transverse coordinate and the integral is over the transverse cross-section of the gain region. A similar expression relates $w_{v\to c}$ to $W_{v\to c}$. Provided $\mathbf{A}(\mathbf{r})$ varies much more slowly than the envelope functions $F_e(\mathbf{r})$ and $F_h(\mathbf{r})$ and we assume that $\mathbf{k}$-conservation holds, the previous expression derived for $W_{c\to v}$ for a plane wave excitation, is valid with A_o simply replaced by $\mathbf{A}(\mathbf{r})$ i.e

$$W_{c\to v} = \left(\frac{2\pi}{\hbar}\right) |M_T|^2 \left(\frac{e\mathbf{A}(\mathbf{r})}{2m_o}\right)^2 \rho_{red}\, f_c(1 - f_v)$$

Moreover,

$$n_{ph} = \int_{-\infty}^{\infty} \Phi(\mathbf{r}) d\rho$$

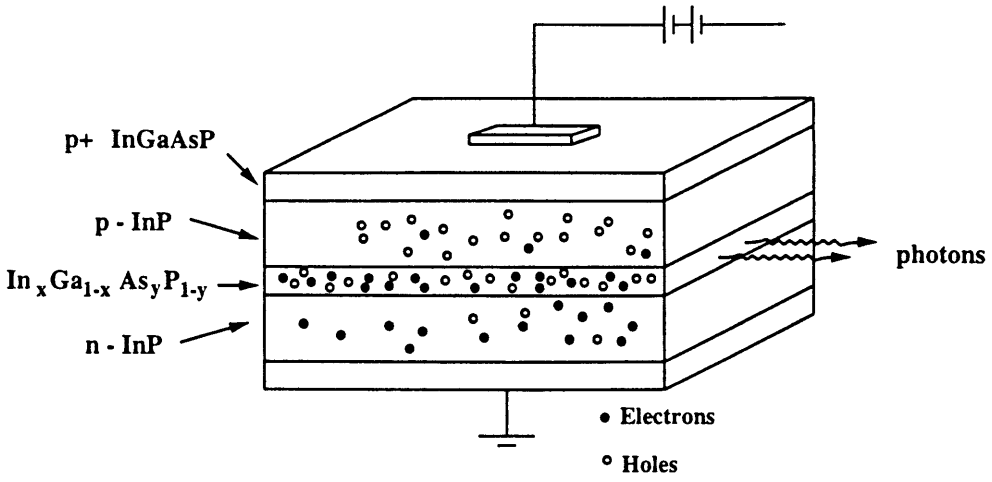

Figure 7-7: Double-Heterojunction Laser Diode

where Φ is the photon flux found earlier with A_o replace by $\mathbf{A}(\mathbf{r})$. Thus,

$$n_{ph} = \frac{\frac{1}{2}\overline{n}^2 \epsilon_o \omega^2 \frac{c}{\overline{n}_g}}{\hbar\omega} \int_{-\infty}^{+\infty} |\mathbf{A}(\mathbf{r})|^2 \, d\rho. \tag{7.56}$$

Substituting the above expressions in eq. (7.54), we find that

$$\gamma = g \frac{\int_{\text{active}} |\mathbf{A}(\mathbf{r})|^2 \, d\rho}{\int_{-\infty}^{+\infty} |\mathbf{A}(\mathbf{r})|^2 \, d\rho} \tag{7.57}$$

$$= g \frac{\int_{\text{active}} |\mathbf{E}(\mathbf{r})|^2 \, d\rho}{\int_{-\infty}^{+\infty} |\mathbf{E}(\mathbf{r})|^2 \, d\rho} \equiv g\,\Gamma \tag{7.58}$$

where Γ is called the mode confinement factor and is the fraction of the power in the mode overlapping with the active region. i.e

$$\Gamma = \frac{\int_{\text{active}} |\mathbf{E}(\mathbf{r})|^2 \, d\rho}{\int_{-\infty}^{+\infty} |\mathbf{E}(\mathbf{r})|^2 \, d\rho}$$

Physically this makes sense as we expect only the field interacting with active region to contribute to the gain. In the limit that the active region fills the entire space, Γ approaches unity and $\gamma \to g$.

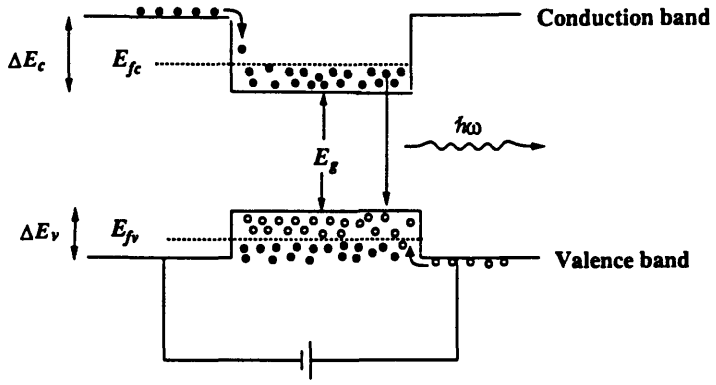

Figure 7-8: Band diagram of a DH diode

7.6 Double Heterojunction Laser Diode

A convenient way of obtaining gain in a semiconductor is by using a p-i-n heterostructure of the type shown in fig. (7-7). The choice of the material systems is determined by the lasing frequency. In the $1.1\,\mu m$ - $1.6\,\mu m$ wavelength range, the material of choice is InGaAsP. The adjacent n and p regions must be lattice matched to the active region to avoid defects arising due to stress. Defects can produce a continuum of states in localized regions [29] which serve as sites of non-radiative recombination. This lattice match restrictions constrains the n and p regions to be InP. For $x \simeq 0.45y$, $In_xGa_{1-x}As_yP_{1-y}$ is lattice matched to InP. This kind of a p-i-n structure is called a double heterojunction (DH) diode. Figure (7-8) shows the energy band edges (i.e $\mathbf{k} = 0$) as a function of position in the DH diode under forward bias conditions. The bandgap of InGaAsP is less than that of the adjacent InP regions. As a result, a potential well of height ΔE_c is formed for the electrons and a corresponding well of height ΔE_v is formed for the holes. These potential wells can trap electrons and holes respectively, allowing them to recombine. Under forward bias conditions electrons from the n-side and holes from the p-side are injected into the active region. This non equilibrium condition is characterized by the quasi-fermi levels, $E_{fc,fv}$. The carriers injected into the active region are confined by the potential well and eventually recombine resulting in net gain for frequencies satisfying condition (7.42). The modal gain, γ, depends on the material gain g and the optical

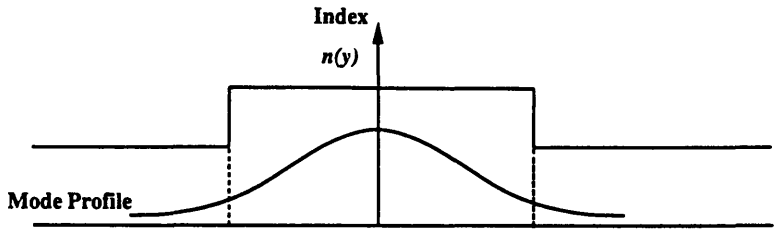

Figure 7-9: Index distribution of DH diode; mode profile is also shown schematically.

confinement factor Γ. Thus, for a maximum modal gain, it is desired to confine the light as tightly as possible in the active region. Fortuitously, $In_xGa_{1-x}As_yP_{1-y}$ has a higher refractive index than the adjacent InP regions. The refractive index, n, is given by $n(y) \simeq 3.4 + 0.256y - 0.095y^2$ at a wavelength corresponding to the bandgap energy. This produces a waveguiding effect resulting in the confinement of light. Additional confinement in the other transverse dimension, may be effected by creating a rib waveguide structure. Figure (7-9) shows the index distribution and the mode profile in the InP/InGaAsP DH diode. The net modal gain, γ, is given by

$$\gamma = g\Gamma_a - \alpha_p\Gamma_p - \alpha_n\Gamma_n$$

where Γ_a, Γ_p and Γ_n are the field confinement factors in the active, p and n regions respectively. g is the gain of the active region and α_p and α_n are the losses of the p and n regions respectively.

Chapter 8

Non-Ideal Gain Gratings

In this chapter we will discuss a simple gain grating design. This example will allow us to highlight some basic issues that one must contend with in making these devices. We will see that a simplistic approach is not optimal as it results in non-ideal device behavior. Some of the "non-idealities" are due to a lack of precise control of the fabrication process which results in achieved parameter values being different from those designed for. Others, however, as we shall see are more inherent and overcoming them requires a more sophisticated fabrication sequence which will be discussed. This chapter will primarily focus on two non-idealities in gain gratings namely index coupling and d.c modal gain and their effect on device performace.

8.1 A Simple Gain Grating

Figure (8-1 (a)) shows a schematic picture of a gain grating. The waveguide core has alternating regions of gain and loss which produce DFB coupling. A schematic longitudinal cross-section of a device which possesses the features of fig. (8-1 (a)) is shown in fig. (8-1 (b)). This device is a DH diode (see section 7.6) in which the active region has been patterned by using a lithographic step followed by etching. The upper cladding layer is then overgrown epitaxally. If organometallic vapor phase epitaxy (OMVPE) is used to perform the overgrowth, the growth conditions may be controlled to avoid transferring the corrugation to the upper cladding [39]. As

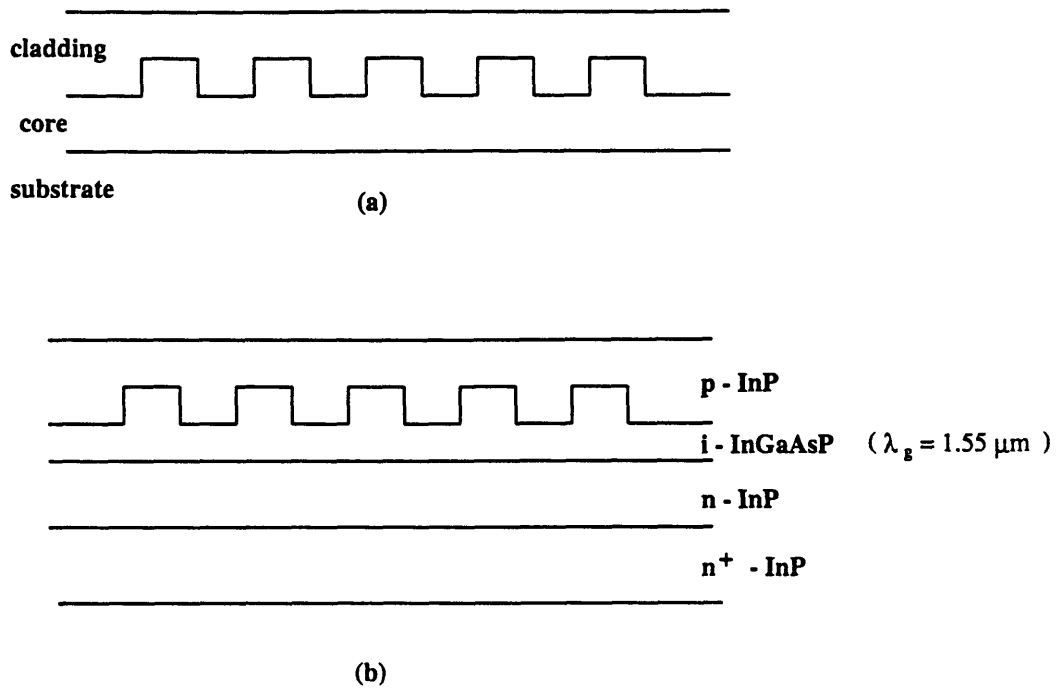

Figure 8-1: (a) Schematic representation of a gain grating. (b) Longitudinal cross-section of a simple gain grating device

discussed in chapter 4, when the device is forward biased, the carrier population in the intrinsic InGaAsP can be inverted giving rise to gain in that region. Due to free carrier absorption, the cladding regions have loss. Thus, the patterned section of the device provides a region of modulated gain giving rise to DFB coupling.

Each tooth of the corrugation demarkates a boundary between regions of different gain and refractive index. As a result at each interface, reflections occur both due to the difference in the index of cladding and core, n_{core} and n_{clad} and also due to the difference in the gain of these two regions, $g_{core} = g$ and $g_{clad} = -l$. Consequently, we expect both index coupling and gain coupling, characterized by κ_{index} and κ_{gain} respectively, to be present in the device. The variation of the index or the real part of the dielectric constant due to changes in the gain or the imaginary part of the dielectric constant is, in fact, an inherent characteristic of physical systems and is predicted by the Kramers-Kronig relation. It is independent of the device design and thus we expect gain coupling to always be accompanied by index coupling even if the gain modulation is produced by a scheme other than patterning.

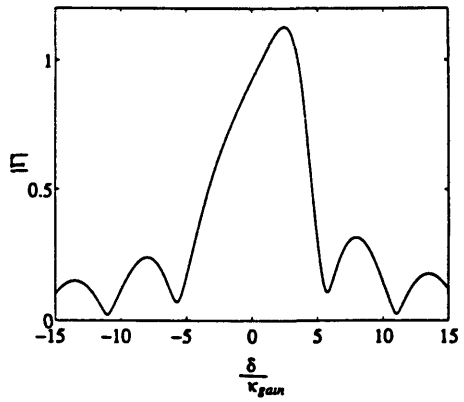

Figure 8-2: Effect of κ_{index} on the response of a gain grating. $\frac{\kappa_{index}}{\kappa_{gain}} = 2$

8.2 Index coupling in a gain grating

The presence of index coupling is gain-coupled systems is undesirable. Recall, index gratings do not support a mode at the Bragg frequency [7, 10] (i.e at $\delta = 0$) or within the stopband. Therefore, index coupling distorts and asymetrizes the gain grating response and causes the center frequency of the laser to drift. For an arbitrary $\kappa_{gain}/\kappa_{index}$ value, the response of the system must be computed using the computer (see fig. (8-2)). However, for small values of κ_{index} it is possible to predict the effect on the response. We will see that for $\kappa_{index}/\kappa_{gain} \ll 1$, to lowest order, the center frequency of the GDFB resonator is shifted by an amount related to this ratio.

The total DFB coupling coefficient, κ, is the sum of its contribution due to the gain and index coupling and is given by

$$\kappa = \kappa_{gain} + j\kappa_{index} \equiv \kappa' + j\kappa''$$

The 90° phase difference between κ_{gain} and κ_{index} is due to the difference in the phase of the waves reflected from index and gain boundaries. We know from chapter 2 that the oscillation condition for a matched grating is given by

$$\frac{\kappa - j\delta}{\beta} \tan\frac{\beta l}{2} = 1 \tag{8.1}$$

where

$$\beta^2 = \delta^2 + \kappa^2$$

When $\kappa'' = 0$, lasing occurs at the Bragg frequency, $\delta = 0$, for $\beta l = \kappa l = \pi/2$. For the case that $\kappa''/\kappa' \ll 1$, we have that

$$\beta^2 \simeq (\beta')^2 + 2j\beta'\beta'' \simeq \delta^2 + (\kappa')^2 + 2j\kappa'\kappa'' \tag{8.2}$$

where we have made use of the fact that $\beta'' \ll \beta'$. Since by assumption $\kappa'' \ll \kappa'$, we expect the lasing frequency, δ, will be close to zero and in this limit,

$$\beta' \simeq \kappa' \tag{8.3}$$

$$\beta'' \simeq \kappa'' \tag{8.4}$$

At threshold $\kappa' l \simeq \pi/2$. Therefore,

$$\beta'' l \simeq \frac{\kappa''}{\kappa'}\frac{\pi}{2} \ll 1.$$

Use of the above gives that

$$\tan\left(\frac{(\beta' + j\beta'')l}{2}\right) \simeq \tan\frac{\beta' l}{2}\left[1 + j\frac{\beta'' l}{2}\left(\cot\frac{\beta' l}{2} + \tan\frac{\beta' l}{2}\right)\right] \approx 1 + j\beta'' l$$

where the approximation that $\exp(j\frac{\beta'' l}{2}) \simeq 1 + j\frac{\beta'' l}{2}$ and that $\beta' l \simeq \frac{\pi}{2}$ have been used. Substituting this into eq. (8.1) we get

$$(\kappa' + j\kappa'' - j\delta)(1 + j\beta'' l) = \beta' + j\beta'' \simeq \kappa' + j\kappa'' \tag{8.5}$$

which simplifies to

$$\frac{\delta}{\kappa'} = \kappa'' l \tag{8.6}$$

and can be rewritten as

$$\frac{\delta}{\kappa'} \simeq \frac{\pi}{2}\frac{\kappa''}{\kappa'} \tag{8.7}$$

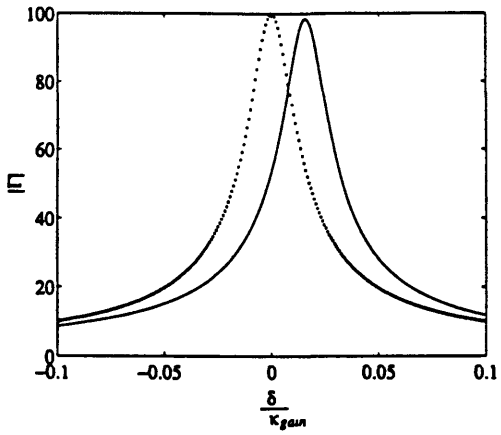

Figure 8-3: Response of a gain grating with $\frac{\kappa_{index}}{\kappa_{gain}} = 0.01$. The dotted line is the response of an identical grating but with $\kappa_{index} = 0$. The shift in the lasing frequency is evident and is given by eq. (5.7)

We see that the lasing frequency of the structure is no longer at $\delta = 0$ as for a pure gain grating but has shifted to a new position related to $\frac{\kappa''}{\kappa'}$ as asserted earlier, (see fig. (8-3)).

To understand this, let us see what is the effect of an index grating on the waves inside the resonator. As we know an index grating reflects waves within the stopband. The reflectivity at the Bragg frequency, $\delta = 0$, of an index grating of coupling strength κ'' that is matched at one end is given by [7]

$$\begin{aligned} \Gamma\left(\frac{-l}{2}\right) &= \tanh \kappa'' l \\ &\simeq \kappa'' l \qquad\qquad \text{for } \kappa'' l \ll 1 \end{aligned} \tag{8.8}$$

for $\kappa'' l \ll 1$. From chapter 2 we know that if a reflection coefficient Γ_o is placed at one end of the GDFB resonator it causes the lasing frequency to be shifted from $\delta = 0$ to the location δ governed by the equation

$$\Gamma_o = \frac{\beta}{\kappa} \cot \beta l + j\frac{\delta}{\kappa}. \tag{8.9}$$

To lowest order, $\beta l \simeq \kappa' l \simeq \frac{\pi}{2}$. In this case

$$|\Gamma_o| = \frac{\delta}{\kappa'}$$

The above equation suggests that the lasing frequency can be shifted to $\delta/\kappa' = \kappa'' l$ by a lumped reflector of reflectivity $|\Gamma_o| = \kappa'' l$. Notice that this is exactly the reflectivity of an index grating of length l and $\kappa_{index} = \kappa''$, (eq. (8.8)). Thus, for $\frac{\kappa''}{\kappa'} \ll 1$, the effect of an index grating is equivalent to that of a lumped reflector placed at one end of the resonator, which causes its lasing frequency to be shifted to $\frac{\delta}{\kappa} = \kappa'' l$.

Generally, differences in the real part of the dielectric constant are much larger than those in the imaginary part. This is due to the fact that even for very high values of material gain, the gain per wavelength is small and consequently the $\Re\{n\}$ is much larger than $\Im\{n\}$ where n is the complex refractive index of the active material. Consequently, $\kappa_{index} = \frac{2\Re\{\Delta\epsilon\}}{\lambda_o n_e}$ may be significantly larger than $\kappa_{gain} = \frac{\Delta g}{2\pi}\Gamma = \frac{2\Im\{\Delta\epsilon\}}{\lambda_o n_e}$. As mentioned earlier and is clear from fig. (8-2), this is undesirable as the advantages obtained from gain-coupling are then lost. Ideally, κ_{index} should be zero. However, according to the previous discussion, gain-coupling is inevitably accompanied by index-coupling.

8.2.1 Pure Gain Grating

An elegant scheme to eliminate index-coupling to yield a purely gain-coupled system was proposed by Tada et al. [39]. This, is however, achieved at the expense of a more complicated structure with stricter design constraints. A schematic longitudinal cross-section of the device proposed by Tada et al. is shown in fig. (8-4). This device used a GaAs/AlGaAs material system with $\lambda_o = 870\,nm$. However, the scheme should be generalizable to InP/InGaAsP systems. Notice that there are two gratings in this device. One of the gratings is between the buffer and the pattern providing layer and the other is between the active region and the buffer. The former grating provides only index coupling as the pattern providing layer and the buffer have minimal, if any, gain/loss. The latter grating, that is the one between the active layer and the

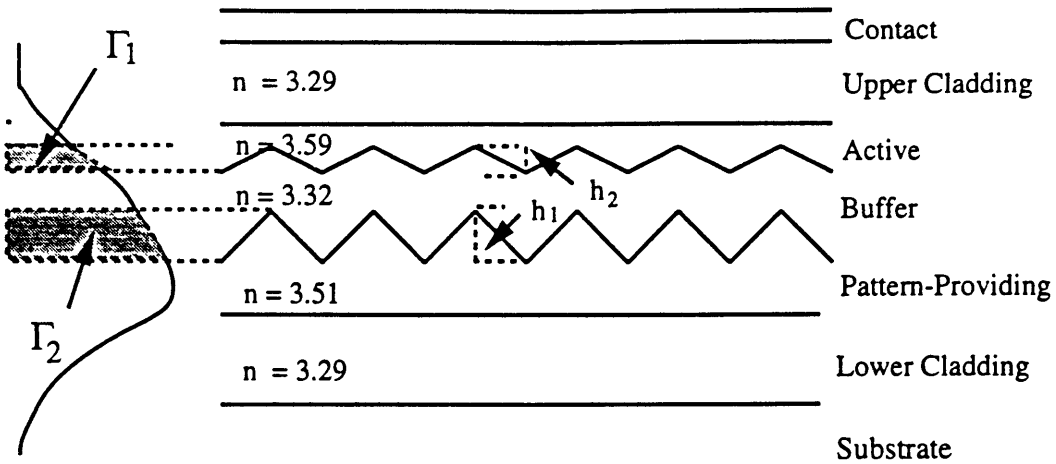

Figure 8-4: Pure gain grating as proposed by Tada et al.

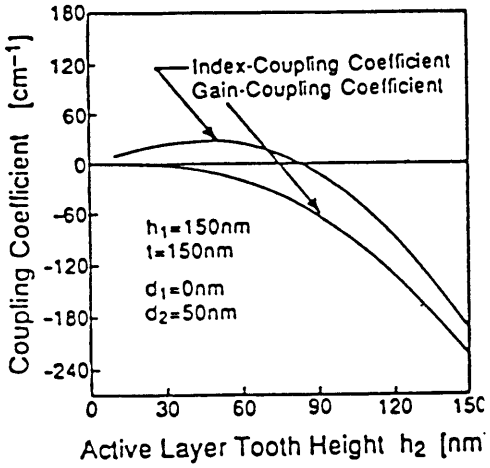

Figure 8-5: Variation of the coupling coefficient vs. h_2. (Courtesy of [39].)

buffer, by the previous argument provides both index and gain coupling. The net index coupling coefficient, κ_{index} is given by the sum of the contributions from either grating, i.e

$$\begin{aligned} \kappa_{index} &= \kappa_{act-buf} + \kappa_{buf-p.p} \\ \kappa_{index} &= \frac{2\Delta\epsilon_1}{\lambda_o n_e}\Gamma_1 + \frac{2\Delta\epsilon_2}{\lambda_o n_e}\Gamma_2 \end{aligned}$$

Notice that $\Delta\epsilon_1 = (n_{act}^2 - n_{buf}^2)\epsilon_o > 0$ whereas $\Delta\epsilon_2 = (n_{buf}^2 - n_{p.p}^2)\epsilon_o < 0$. Once h_1 is chosen, the growth conditions can be adjusted to yield the desired active region corrugation depth, h_2. By appropriately designing for h_1 and h_2, it is possible to

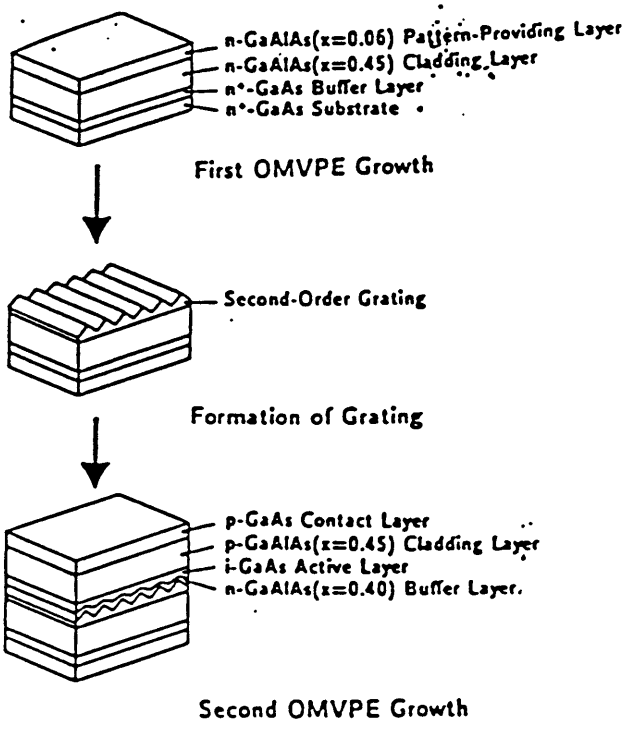

Figure 8-6: Fabrication sequence of a pure gain grating. (Courtesy of [39].)

engineer the overlap integrals so as to drive κ_{index} to zero [39]. Figure (8-5) shows the variation of κ_{index} as a function of the active corrugation height, h_2. The $\kappa_{index} = 0$ design constrains the values of Γ_1 and Γ_2 and thus,

$$\kappa_{gain} = \frac{g_{act} - g_{buf}}{2\pi} \Gamma_1 = \frac{\Delta g}{2\pi} \Gamma_1$$

may only be increased by increasing Δg or having a higher gain in the active region.

A fabrication procedure of Tada's device is shown in fig. (8-6). The first OMVPE growth grows the n+ GaAs buffer layer, the lower cladding and the pattern providing layer. Next a second-order grating is etched in the pattern providing layer. The second OMVPE process grows the buffer, the active layer, the upper cladding and the contact layers. The growth parameters are chosen so that the underlying pattern of the pattern providing layer is conveyed to the buffer layer but is lost in the growth of the active region. This results in only one side of the active region having corrugations as desired. The ability to propagate patterns or extinguish them relies on the fact

that the orientation dependence of OMVPE is a function of the temperature. Thus by controlling the temperature conditions during growth it is possible to achieve a device with pure gain coupling, however, it is at the expense of a more complicated fabrication process.

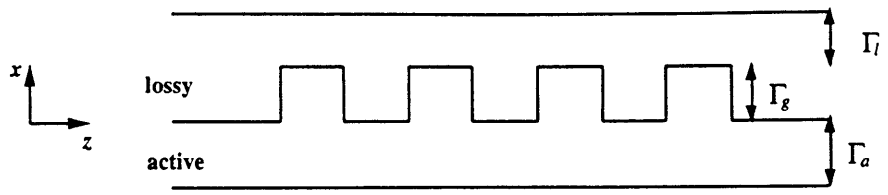

Figure 8-7: Focussing on the region with the gain and loss in a simple gain grating

8.3 D.C Gain

The grating structures discussed thus far have had no travelling wave (or d.c) gain or loss. Even though there are alternating regions of gain, g, and loss, l, these are assumed to be centered about an average gain value of zero. The advantage of gratings with an average gain value of zero is that they exhibit better suppression of other resonant (lasing) longitudinal modes [22], a point which will be discussed later in more detail. In any practical device, however, we do not expect the condition or no travelling wave gain to be precisely met, if at all. There will always be some residual net gain/loss in the structure. Consider the simple device of fig. (8-7). As stated earlier, the active region has a material gain, g which is a function of the current through the device. The cladding has material loss, l, due to free carrier absorption. For simplicity we will assume that the rest of the regions in the device have no gain or loss. As indicated in the fig. (8-7), Γ_g, Γ_a and Γ_l are respectively the mode overlaps with the corrugated region, and the active and the loss regions excluding the corrugation. The net modal gain, γ is given by

$$\gamma = \Gamma_a g - \Gamma_l l + \Gamma_g \frac{(g-l)}{2}, \tag{8.10}$$

where the first two terms correspond to the net gain of the active region and the upper cladding, minus the corrugation. The last term is the contribution to the modal gain due to the d.c gain of the patterned region as indicated in the fig. (8-8).

We expect the material gain, g, to be significantly larger than l, under forward bias conditions. Thus, we see from eq. (8.10) that we have a net modal gain γ. One way to minimize γ could involve growing a lossy region in the device so as to compensate

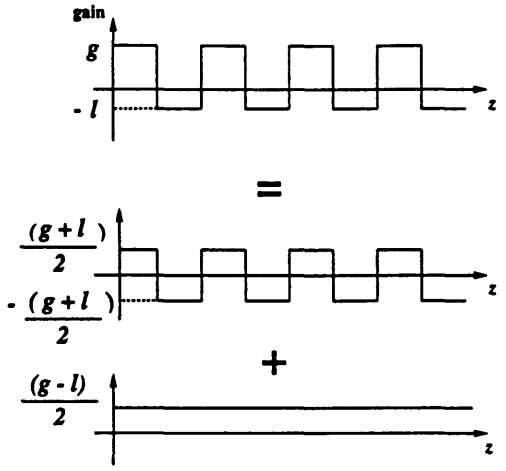

Figure 8-8: Contribution to the modal gain due to the d.c gain offset of the grating.

for the net modal gain. The disadvantage of such an approach is an increase in the injection current density required to achieve the same material gain, g. Since it is expected that $g \gg l$, another method may be to design a grating with $\Gamma_a = 0$, i.e the grating depth is equal to the active region thickness. For a given loss value, l, it is then possible to design for a Γ_l such that the value of γ is minimized or ideally driven to zero.

Why do we want a d.c gain value of zero ? To answer this question let us see how the performance of the gain grating is affected due to a net modal gain, γ. The equations describing the forward and backwards propagating waves, A and B, in a grating with a finite γ are

$$\frac{dA}{dz} = -j\delta A + \kappa B + \gamma A \tag{8.11}$$

$$\frac{dB}{dz} = j\delta B - \kappa B - \gamma B \tag{8.12}$$

For $\delta = \kappa = 0$ it is clear from the above equations that A grows exponentially in the $+z$ direction and B increases exponentially in the $-z$ direction as expected. Rewriting the above equations we have

$$\frac{dA}{dz} = -j(\delta + j\gamma)A + \kappa B \tag{8.13}$$

$$\frac{dB}{dz} = -\kappa A + j(\delta + j\gamma)B \tag{8.14}$$

Notice that these equations are of the same form as those describing a gain grating with no modal gain but with $\delta \rightarrow (\delta + j\gamma)$. For an assumed solution of the form $e^{j\beta z}$, we find that the eigen values are

$$\beta^2 = \kappa^2 + (\delta + j\gamma)^2 \tag{8.15}$$

Generalizing the oscillation condition obtained in chapter 2 to the case of a grating with a finite γ, we have that this structure lases provided

$$\frac{\kappa - j(\delta + j\gamma)}{\beta} \tan\frac{\beta l}{2} = 1. \tag{8.16}$$

This is a complex transcendental equation which may be solved numerically for the resonant mode spectrum of the gain grating. For a given length and coupling coefficient, the threshold modal gain, γ, required for the N^{th} mode to lase may be calculated using the above equation. Figure (8-9 (a)) shows spectrum of resonant modes. Figure (8-9 (b)) shows the relation between the threshold gain, γl and κl for the N^{th} laser mode. $N = 0$ corresponds to the mode at $\delta = 0$ as indicated in the figure. In the notation of the reference from which the plot has been obtained, α represents the net modal gain, γ and $\kappa = \alpha_1/2$. Notice that for $\alpha = 0$, or in other words with no travelling wave gain, there is a larger difference between the threshold gain value of the higher order modes and the $N = 0$ mode, resulting in a better side mode suppression ratio than for a case of a non-zero modal gain (α) value. Physically, this is due to the fact that in the absence of average gain, only the field profile of the $N = 0$ mode can effectively conform itself to the gain distribution in the guide, resulting in this mode experiencing net gain even though there is no average gain. The higher order modes require d.c gain to lase.

Let us assume that

$$\frac{\gamma}{\kappa} = a$$

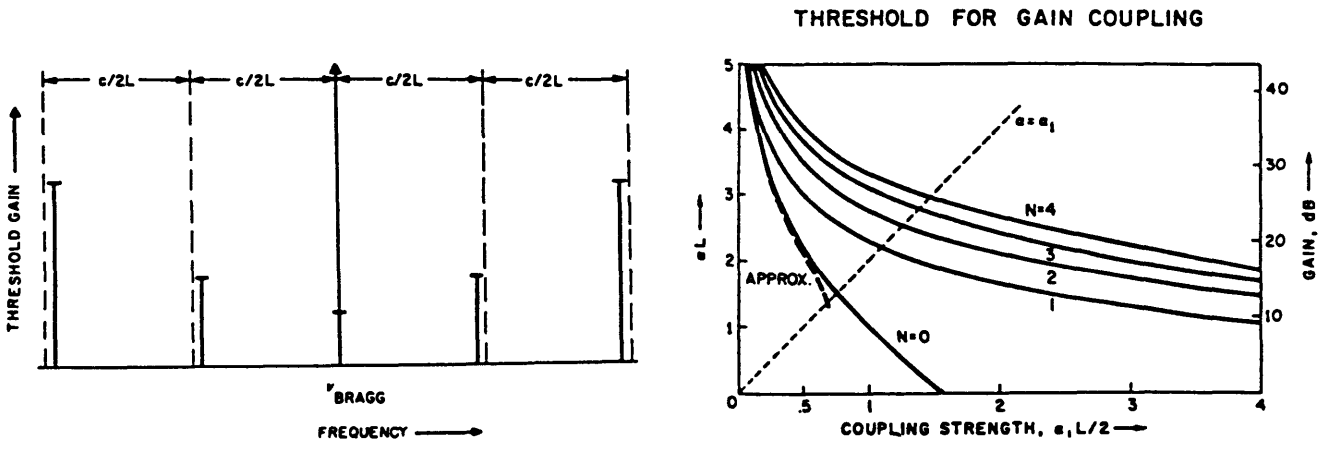

Figure 8-9: (a) Spectrum of the GDFB laser against threshold modal gain values. (b) Relation between the modal gain, α in the notation of [22] and the coupling coefficient, $\kappa = \alpha_1/2$. (Courtesy of [22].)

and concentrate on the mode at the Bragg frequency. A lasing mode exists at Bragg frequency or $\delta = 0$ provided

$$\frac{\kappa + \gamma}{\beta} \tan \frac{(\beta l)_o}{2} = 1$$

or

$$(\kappa l)_o = \frac{2}{\sqrt{1-a^2}} \arctan\left(\frac{\sqrt{1-a^2}}{1+a}\right). \tag{8.17}$$

where the subscript o indicates the threshold value of the parameters. For $a > 0$ it can be shown that $\kappa l < \frac{\pi}{2}$, (see fig. (8-9 (b))). The above equation is solvable for any value of a which means that a laser mode always exists at the Bragg frequency. Notice, however, that for $\gamma > \kappa$ or equivalently $a > 1$, the eigen values, β are purely imaginary, (eq. (8.15)). We will make a change of variables such that the eigen values are real for $a > 1$, i.e $\beta \rightarrow -j\beta$. In this case, the assumed solutions are of the form $e^{\beta z}$ and

$$\beta^2 = \gamma^2 - \kappa^2 - \delta^2 - 2j\delta\gamma \qquad \text{for } a > 1 \tag{8.18}$$

At $\delta = 0$, $\beta^2 = \kappa^2(a^2 - 1)$. In the new variable, the oscillation condition for a mode

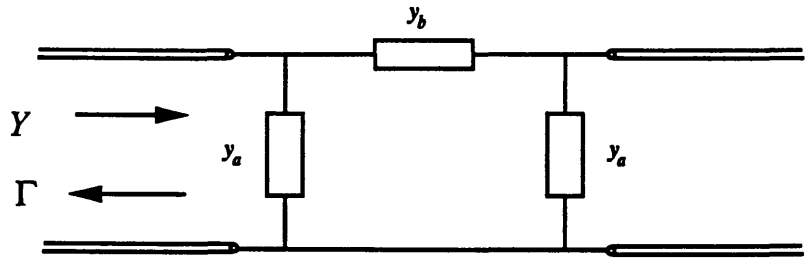

Figure 8-10: Pi-circuit representation of a gain grating with net modal gain, γ

at the Bragg frequency becomes

$$(\kappa l)_o = \frac{2}{\sqrt{a^2-1}} \operatorname{arctanh}\left(\frac{\sqrt{a^2-1}}{a+1}\right) \qquad \text{for } a > 1. \tag{8.19}$$

It can also shown that for $a > 1$, $\kappa l < 1$. (fig. (8-9 (b))).

An equivalent circuit of the gain grating with net modal gain, γ, near resonance, i.e $\delta = 0$, can be found by considering the symmetric and antisymmetric excitations of the system. From the symmetry of the structure we expect a pi-circuit representation, shown in fig. (8-10). As in chapter 2, the device is tuned slightly below threshold and we are interested in the response of the grating close to resonance, i.e

$$\begin{aligned} (\beta l)_o - \beta l &\equiv \Delta \\ \frac{\delta}{\kappa} &\ll 1 \end{aligned}$$

where

$$(\beta l)_o = \begin{cases} (\kappa l)_o\sqrt{1-a^2} & \text{for } a < 1 \\ (\kappa l)_o\sqrt{a^2-1} & \text{for } a > 1 \end{cases} \tag{8.20}$$

where $(\kappa l)_o$ satisfies either eq. (8.17) or eq. (8.19) depending on the value of a. The parallel admittance y_a of the pi-circuit is given by

$$y_a = \begin{cases} -\frac{[\kappa - j(\delta + j\gamma)]}{\beta} \tan\frac{\beta l}{2} & \text{for } a < 1 \\ -\frac{[\kappa - j(\delta + j\gamma)]}{\beta} \tanh\frac{\beta l}{2} & \text{for } a > 1 \end{cases} \tag{8.21}$$

where

$$\beta = \beta' + j\beta'' \simeq \begin{cases} \kappa\sqrt{1-a^2} + j\frac{a\delta}{\sqrt{1-a^2}} & \text{for } a < 1 \\ \kappa\sqrt{a^2-1} - j\frac{a\delta}{\sqrt{a^2-1}} & \text{for } a > 1 \end{cases} \tag{8.22}$$

Proceeding as in chapter 2 and realizing that $\beta'' l \ll 1$, provided a is not too close to unity, we find that for $a < 1$

$$\begin{aligned} y_a &\simeq \Delta' - 1 + j\left(\frac{\delta}{\kappa}\right)' \qquad \text{where} \qquad (8.23) \\ \Delta' &\equiv \frac{\Delta}{\sqrt{1-a^2}} \\ \left(\frac{\delta}{\kappa}\right)' &\equiv \left(\frac{1-a\kappa l}{1-a^2}\right)\frac{\delta}{\kappa} \\ y_b &\simeq \frac{1}{1-a} \qquad (8.24) \end{aligned}$$

and for $a > 1$, we have that

$$\begin{aligned} y_a &\simeq \Delta' - 1 + j\left(\frac{\delta}{\kappa}\right)' \qquad \text{where} \qquad (8.25) \\ \Delta' &\equiv \frac{\Delta}{\sqrt{a^2-1}} \\ \left(\frac{\delta}{\kappa}\right)' &\equiv \left(\frac{a\kappa l - 1}{a^2-1}\right)\frac{\delta}{\kappa} \\ y_b &\simeq -\frac{1}{a-1} \qquad (8.26) \end{aligned}$$

Notice, y_b is negative for $a > 1$ which means that the antisymmetric excitation also experiences gain unlike in the case of a gain grating with $\gamma = 0$. The reflection coefficient of the grating Γ as shown in fig. (8-10) is given by

$$\Gamma = \frac{1-Y}{1+Y} \tag{8.27}$$

where Y is the net admittance seen in the port indicated in fig. (8-10) and is given by

$$Y = y_a + \frac{(1+y_a)y_b}{1+y_a+y_b}$$

Note that $y_b = \frac{1}{1-a}$ is the same for both $a > 1$ or $a < 1$. Substituting in eq. (8.27), we find that

$$\Gamma = \frac{(1-a)(1-y_a^2) - 2y_a}{(1-a)(1+y_a)^2 + 2(1+y_a)} \tag{8.28}$$

Now

$$\begin{aligned} y_a &= \Delta' - 1 + j\left(\frac{\delta}{\kappa}\right)', \\ y_a^2 &\simeq 1 - 2(1+y_a), \\ (1+y_a)^2 &= \left(\Delta' + j\left(\frac{\delta}{\kappa}\right)'\right)^2 \approx 0, \end{aligned}$$

where we have made use of the fact that Δ', $j(\frac{\delta}{\kappa})' \ll 1$ and have only retained terms to first order. Use of the above in eq. (8.28) gives,

$$\Gamma = \frac{1 - a(1+y_a)}{(1+y_a)} \simeq \frac{1}{(1+y_a)}$$

$$\Gamma = \frac{1}{\frac{\Delta}{\sqrt{1-a^2}} + j\frac{(1-a\kappa l)}{1-a^2}\frac{\delta}{\kappa}} \qquad \text{for } a < 1 \tag{8.29}$$

$$\Gamma = \frac{1}{\frac{\Delta}{\sqrt{a^2-1}} + j\frac{(a\kappa l-1)}{a^2-1}\frac{\delta}{\kappa}} \qquad \text{for } a > 1 \tag{8.30}$$

Notice that for $0 < a < 1$, $1 < \kappa l < \frac{\pi}{2}$ and the prefactor of $\frac{\delta}{\kappa}$ is less than unity, i.e

$$\frac{1 - a\kappa l}{1 - a^2} < 1$$

Likewise for $a > 1$, $\kappa l < 1$ and

$$\frac{a\kappa l - 1}{a^2 - 1} < 1$$

Since $\left(\frac{\delta}{\kappa}\right)' < \frac{\delta}{\kappa}$, both for $a > 1$ and $a < 1$, this frequency scaling causes the response of the gain grating to be broadened. For $a >> 1$ this can result in a very broad bandwidth of the laser, which is undesireable.

Figure (8-11) shows a plot of Γ normalized to its peak value versus $\frac{\delta}{\kappa}$ for a gain grating with $a = 0.3$. The dotted line is the exact solution obtained by solving the eqs. (8.13) and (8.14). The solid line is the approximate response using the equivalent

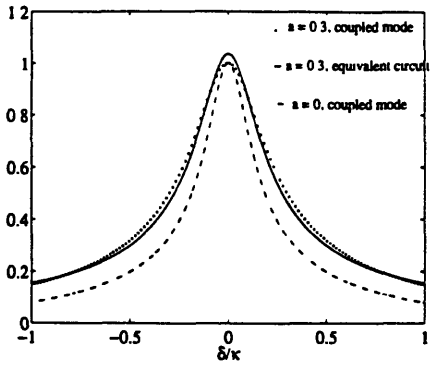

Figure 8-11: Normalized Γ vs. $\frac{\delta}{\kappa}$. Dotted line is the exact response of a grating with $a = 0.3$ and $\Delta = 0.1$. Solid line is the equivalent circuit approximation. Dashed-dot line is the response of a grating with $a = 0$ and $\Delta = 0.1$.

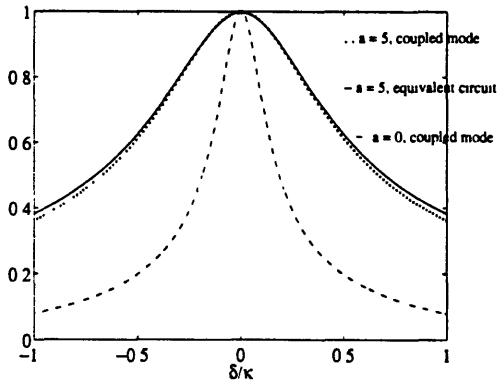

Figure 8-12: Normalized Γ vs. $\frac{\delta}{\kappa}$. Dotted line is the exact response with $\Delta = 0.1$ and $a = 5$. Solid line is the equivalent circuit approximation. Dashed-dot line is the response of a grating with $a = 0$ and $\Delta = 0.1$.

circuit response, (eq. (8.29)). The dashed-dot line represents the response of a gain grating with $\gamma = 0$ that has been detuned by the same amount Δ, (i.e $(\beta l)_o - \beta l \equiv \Delta$) as the grating with net modal gain $\gamma = a\kappa$. The frequency broadening is evident. Figure (8-12) show the same three responses but with $a = 5$. The broadening is much more evident. For large a, the half power frequency points, $\left(\frac{\delta}{\kappa}\right)_{hp} \simeq \Delta\frac{\sqrt{a^2-1}}{a\kappa l-1}$ as compared to $\left(\frac{\delta}{\kappa}\right)_{hp} = \Delta$ for a grating with no dc gain. The reason why the normalized reflection coefficient was plotted was to enable the bandwidths to be visually compared. However, this conceals the fact that the peak magnitudes of Γ are not same for a grating with a finite dc gain and one for which $\gamma = 0$. This can easily be

seen by comparing $\Gamma(\delta = 0, a)$ using eqs. (8.29) and (8.30) with $\Gamma(\delta = 0, a = 0) = \frac{1}{\Delta}$.

Bibliography

[1] M. J. N. Sibley, *Optical Communications*, Macmillan New Electronics Series, 1990.

[2] John Gowar, *Optical Communication Systems*, Prentice-Hall International Series in Optoelectronics, 1984.

[3] J. E. Midwinter and Y.L. Guo, *Optoelectronics and Lightwave Technology*, John Wiley and Sons, 1992.

[4] Edited by Chinlon Lin, *Optoelectronic Technology and Lightwave Communications Systems*, Van Nostrand Reinhold, 1989.

[5] R. G. Hunsperger, *Integrated Optics: Theory and Technology*, Springer Series in Optical Sciences, Second Edition, 1984.

[6] Jean-Pierre Laude, *Wavelength Division Multiplexing*, Prentice Hall International Series in Optoelectronics, 1993.

[7] H. A. Haus, *Waves and Fields in Optoelectronics*, Prentice-Hall, 1984.

[8] H. A. Haus and Y. Lai, *Narrow-Band Optical Channel-Dropping Filter*, Journal of Lightwave Technology, vol. 10, No. 1, Jan. 1992.

[9] H. A. Haus and M. J. Khan, *Gain Distributed Feedback Structures*, Journal of Lightwave Technology, vol. 13, No. 2, Feb. 1995.

[10] J. N. Damask, *Master's Thesis*, Massachussetts Institute of Technology, May 7, 1993.

[11] M. J. Khan, *Bachelor Thesis*, Massachussetts Institute of Technology, May 1994.

[12] H.A. Haus, J.N. Damask, M.J. Khan, "DFB Channel-Dropping Filters," editor T. Tamir et. al. *Guided-Wave Optoelectronics: Device Characterization, Analysis and Design*, Plenum Press, pp 299-311. 1995.

[13] H. F. Taylor, "Optical switching and modulation in parallel dielectric waveguides," *J. Appl. Phys., 44* pp 3257-3262, July 1973.

[14] R. C. Alferness and P. S. Cross, "Filter characteristics of codirectionally coupled waveguides with weighted coupling," *IEEE J. Quantum Electron., QE-14*, no. 11, pp 843-847, Nov. 1978.

[15] A. Yariv, *Optical Electronics*, Holt, Rinehart and Winston, Inc., New York (1985)

[16] D. Staelin, A. Morgenthaler, J. A. Kong, *Electromagnetic Waves*, Prentice Hall, Englewood Cliffs, New Jersey 1994.

[17] D. Marcuse, *Theory of Dieletric Optical Waveguides*, Academic Press, New York, 1991.

[18] H. A. Haus and W. Huang, "Couple-Mode Theory", *Proceedings of the IEEE*, vol. 79, pp 1505 - , 1991.

[19] W. Louisell, *Coupled Mode and Parametric Electronics*, Wiley, New York, 1960.

[20] E. A. J Marcatili, "Dielectric Rectangular Waveguides and Directional Coupler for Integrated Optics," *Bell System Technical Journal*, pp. 2071-2012, Sept. 1969.

[21] H. A. Haus et. al., "Coupled-Mode Theory of Optical Waveguides," *J. Lightwave Technol.*, vol. 5, pp 16-23, 1987.

[22] H. Kogelnik and C. V. Shank, "Coupled-wave theory of distributed feedback lasers," *J. Appl. Phys., 43*, no. 5, 2328-2335, May 1972.

[23] H. A. Haus and Y. Lai, "Narrow-band Optical Channel-Dropping Filter," *J. Lightwave Technol.*, vol. 10, pp. 57-62, 1992.

[24] H. A. Haus and Y. Lai, "Theory of cascaded quarter wave shifted distributed feedback resonators," *IEEE J. Quantum Electronics.*, vol. 28, pp 205-213, Jan. 1992.

[25] A. Yariv, "Coupled-Mode Theory for Guided-Wave Optics", *IEEE J. of Quantum Electron.*, vol. 9, pp. 919-933, 1973.

[26] William Siebert, *Circuits, Signal and Systems*, McGraw-Hill Edition, 1986.

[27] Y. Luo, Y. Nakano, K. Tada, T. Inoue, H. Hosomatsu, and H. Iwaoka, *Integrated Optics and Optical Fiber Communication (IOOC '89)* (Kobe, Japan, July 18-21, 1989, post-deadline paper 20PDB-2, pp. 39-42).

[28] N.W. Ashcroft and N.D. Mermin, *Solid State Physics*, Saunders College, 1976.

[29] Agarwal and Dutta, *Long Wavelength Semiconductor Lasers*, Van Nostrand Electrical/Computer Science and Engineering Series, Von Nostrand Reinhold Company, 1986.

[30] T.P. Orlando, S.D. Senturia, H.I. Smith, and P.F. Bagwell *Physics for Solid State Applications*, Department of Electrical Engineering and Computer Science, Massachussetts Institute of Technology, 1992.

[31] Edited by Peter S. Zory, *Quantum Well Lasers*, Academic Peress, Inc. Harcourt Brace Jovanovich, Publishers, 1993.

[32] Claude Cohen-Tannoudji, Bernard Diu, Frank Laloe, *Quantum Mechanics, Volume 1*, John Wiley and Sons, 1977.

[33] Mildred Dresselhaus, *Solid State Physics, 6.732*, Massachussetts Institute of Technology.

[34] C. Hermann and C. Weisbuch, *Phys. Rev. B* **13**, 4466, 1977.

[35] V.M Agranovich, A.A. Maradudin, *Modern problems in condensed matter sciences*; vol 8: *Optical orientation*, pp. 463-508. North-Holland Physics Publishing Co. 1984.

[36] B. Jani, P. Gilbart, J.C. Portal, and R.L. Aulombard, *Journal of Appl. Phys.* **58**, 3481, 1985.

[37] R.J. Nicholas, J. C. Portal, C. Houlbert, P. Perrier, T.P. Pearsall, *Applied Physics Letters* **34**, 492, 1979.

[38] K. Huang, *Statistical Mechanics* Second Edition, John Wiley and Sons, 1987.

[39] Y. Luo, Y. Nakano, K. Tada, et. al. *Fabrication and Characteristics of Gain-Coupled Distributed Feedback Semiconductor Lasers with a Corrugated Active Layer.* IEEE Journal of Quantum Electronics, vol. 27, No. 6, June 991.

[40] H. A. Haus and Y. Lai, *Theory of Cascaded Quarter Wave Shifted Distributed Feedback Resonators*, IEEE Journal of Quant. Elec., vol 28, No. 1, Jan. 1992.